THE ROLE OF POLYMER COMPATIBILITY IN CERAMIC PROCESSING

BY

UNGSOO KIM

A THESIS
SUBMITTED TO THE FACULTY OF

ALFRED UNIVERSITY

IN PARTIAL FULFILLMENT OF THE REQUIREMENTS
FOR THE DEGREE OF

DOCTOR OF PHILOSOPHY

IN

CERAMICS

ALFRED, NEW YORK

SEPTEMBER, 2002

THE ROLE OF POLYMER COMPATIBILITY IN CERAMIC PROCESSING

BY
UNGSOO KIM

B.S. KYONGGI UNIVERSITY, KOREA (1995)

M.S. ALFRED UNIVERSITY (1998)

SIGNATURE OF AUTHOR (Signature on file)

APPROVED BY (Signature on file)
WILLIAM M. CARTY, ADVISOR

(Signature on file)
DAVID A. EARL, ADVISORY COMMITTEE

(Signature on file)
MICHELE M. HLUCHY, ADVISORY COMMITTEE

(Signature on file)
REBECCA L. DEROSA, ADVISORY COMMITTEE

(Signature on file)
ALASTAIR N. CORMACK, CHAIR, ORAL THESIS DEFENSE

ACCEPTED BY (Signature on file)
RONALD GORDON, DEAN,
SCHOOL OF ENGINEERING

ACCEPTED BY (Signature on file)
ALASTAIR N. CORMACK,
DIRECTOR OF THE GRADUATE SCHOOL,
ALFRED UNIVERSITY

Acknowledgements

I would like to thank members of my thesis committee, Dr. William M. Carty, Dr. David A. Earl, Dr. Michelle M. Hluchy, and Dr. Rebecca DeRosa for their sincere discussions on this project. In particular, I would like to thank my advisor, Dr. William M. Carty. His endless energy for work always amazed me, his knowledge and insight in colloidal processing inspired me, and his thoughtful care for students has shown me the role of teacher. Also, financial support from WRC on this project is deeply appreciated.

I would like to thank all the former and current members of Dr. Carty's research group for sharing the great memories at Alfred. I would especially thank Brett Schulz for reading my dissertation and giving all the good comments. Also, Mrs. Jeannette Harris and Marion Smith deserve a great deal of thanks for their help in dealing with all the matters related to computers and business. I would like to thank Ju-Youn Byun. Her existence made my life in Alfred blissful and valuable. She has always been on my side and supported me through the years.

I would like to thank my parents, Jae-Sun Kim and Soon-Ok Bae, my sister, brother in law, and my nephew, Jung-Hoon Lee. I would say that my parents have made it possible for me to come all this way. Everything I have accomplished so far is meaningless without them. Their reckless support and love, encouragement and patience, and vision are the great lessons that I should carry on. My family has been through difficult times in the past years. We have lost my baby brother, Hyun-Soo Kim, during my stay at Alfred. He was always proud of me and another big supporter of mine. We will always miss him. During the difficult time my sister and brother in law successfully filled the gap that I left. They have made me to feel the warm love from family.

Table of Contents

List of Tables

Chapter II.

Chapter III.

Chapter IV.

List of Figures

Chapter II

Chapter III

Chapter IV

Abstract

The proper use of multiple polymeric additives in ceramic processing is discussed. First, the use of a polyelectrolyte as a dispersant is studied by looking at the adsorption of various molecular weight PAAs on clay and the effect on suspension rheology. The adsorption of PAA on clay particles is not influenced by molecular weight, but there exists an optimal chain length for minimum viscosity. Secondly, the interactions between polymeric additives in suspensions and during drying are investigated. The phase behavior of polymer systems is studied by Flory-Huggins theory and the interactions in polymer solutions are examined using light scattering and optical microscopy. The results are used to explain the PVA migration behavior. PVA can be stained and its location within the spray dried granule can be observed, verifying the effect of other polymers on binder migration. It is shown that phase separation of polymer systems is the primary reason for the PVA migration. The chain length and functional groups of polymers determine the phase behavior of polymers and in turn the degree of binder migration.

I. INTRODUCTION

Polymeric additives are frequently used in ceramic processing for a variety of purposes. In the processing of advanced ceramics the use of polymers becomes more significant. However, the selection method of polymers has not changed with recent progress in process development and is mostly dependent on trial and error. A polymer is selected for a specific purpose, whether desirable control of slurry properties or of the green body, and little consideration is given to the global consequences of the polymer addition. This will result in a time consuming process for a polymer selection in a new process. In addition, the use of multiple polymers in the process makes the selection more difficult. Normally, the interaction between polymers is assumed to be negligible when multiple polymers are used. However, polymers in a dilute system are forced into close proximity with the loss of solvent during drying process and the polymeric interaction becomes considerable. Negative interactions between polymers can lead to defects in the final product. Therefore, depending on the desired properties of the product, the interactions between polymers should be carefully considered. In the spray drying process multiple polymers are used; including a dispersant, a binder, a plasticizer to control the slurry property and to give green strength to the pressed body. It is necessary to ensure that each polymer acts as expected and all polymeric additives are compatible.

A polyelectrolyte is commonly used to disperse ceramic particles in an aqueous medium. The polyelectrolyte is known to adsorb on particles and forms electrostatic and steric barriers. This leads to the electrosteric stabilization of particles. The charge of particle surface and polymer directly influences the adsorption behavior of polyelectrolytes, and the charge formed by polymer adsorption and the thickness of the steric barrier determine the degree of stabilization of suspension, which is manifested as the suspension viscosity. Therefore, the slurry property can be controlled by changing the polymer charge and configuration as well as polymer chain length and adsorption amount.

A binder is used to give strength to the pressed body for handling. Many studies were performed to examine the effect of binder on the slurry properties and the resulting pressed body. However, the interaction between multiple polymers has never been suitably addressed even though there exists interactions between polymers. The negative interactions between polymeric additives can cause variations in suspension rheology, enhance the case hardening in spray-dried granules, or promote polymer-generated porosity in the dried granule. In the process of spray drying the relative polymer concentrations increase and the interactions between polymers can be altered with the removal of solvent.

The goal of this study is to understand the behavior of multiple polymers in ceramic system during processing. It is also intended potentially to make recommendation for the selection of polymers. In this study the problems in dry pressing are addressed in Chapter II by analysis of the surface properties of dry pressed plates from an industrial production line. The effect of polymer molecular weight is studied in Chapter III, where the relationship between polymer adsorption and suspension rheology is investigated. Several different molecular weight PAAs are used for the investigation. The compatibility between the polymers used in the spray drying process is examined in Chapter IV. Four commonly used dispersants are chosen to study the interaction between the dispersants and PVA binder. The PVA migration behavior during spray drying is explained based on the compatibility of the polymers. This study covers the polymer use in aqueous processing and the results are applicable to any process using multiple polymers.

II. SURFACE ROUGHNESS CHARACTERIZATION OF DRY PRESSED BODIES AND RELATIONSHIP TO OPERATION PARAMETERS OF SEMI-ISOSTATIC DRY PRESS

1. Introduction

Dry pressing is the most energy efficient and commonly used forming process within the ceramic industry, with applications ranging from dinnerware and tile to electronic capacitors and thread guide bushings. The process begins by spray drying an aqueous suspension of ceramic powders and polymeric additives (used to control the viscosity of the suspension and to impart high green strength to the pressed part) to make a granular feedstock. The feedstock is fed into a die and then pressed to the desired shape. Dry pressing can produce up to 900 pieces per hour, and allows for larger pieces to be manufactured. When properly implemented, losses should be lowest of any forming process due to the high degree of automation. Potentially, dry pressing technology could replace other forming techniques as the primary forming process for a variety of ceramic products. However, there are several problems that need to be solved before dry pressing becomes an efficient alternative. These are surface roughness, warping and cracking during firing, poor fired strength, and low density (i.e. relatively high porosity). Dinnerware requires a thin glaze and a decoration layer that cannot accommodate a rough surface finish. The warping, cracking, and poor strength result in a 20 % loss of the bisque-fired pieces.[1,2]

There are numerous variables encountered in the dry pressing process that can cause these problems. All the variables can be classified into two groups for evaluation, (1) press operation related and (2) granular feedstock related variables. Inappropriate pressing cycle and operation parameters result in low production rates and defective pressed pieces, leading to loss. Properties of the granular feedstock govern the process behavior of the granules such as flow rate and filling behavior and the properties of the green and fired bodies such as density, strength, and morphology. It would be ideal to operate a press at the highest production rate while producing flawless pressed pieces.

In this chapter press operation related variables are examined with regard to the properties of pressed bodies. Most of published works in this area were limited to studies

of compaction properties with pressing variables at the laboratory scale.[3-5] This study is carried out on the industrial scale by collecting samples from production lines in industry and making samples using an industrial scale dry press. It is intended to clarify the problems currently existing in the dry pressing process in industry and provide a reference for operating a dry press. Surface roughness of dry pressed plates from a whiteware company (Buffalo China, Buffalo, NY) was quantitatively analyzed using an optical interferometer. The change in roughness at each process step was observed. Also, the effect of press operation parameters on dry pressed plates was studied. Dinnerware plates were produced at different press operation parameters and the surface and mechanical properties of plates were characterized including surface roughness, density, and strength.

2. Background Information

2.1 Dry Pressing

Dry pressing is a forming technique, which simultaneously compacts and shapes a powder or granular material confined in a rigid die or a flexible mold.[6] The history of development of dry pressing has traced back to early 1800s. What led to the development of pressing at the beginning is not clear whether it was for dimensional accuracy (and consequently reduced water content) or to address problems associated with shaping of non-plastic raw materials.[7] Dry pressing is the most widely used forming process today because of the technical and economical advantages. Dry pressing is applicable to all ceramic systems, shortens or eliminates the drying process and exhibits essentially no drying shrinkage, produces parts ranging widely in size and shape, and allows high production rate. Therefore, dry pressing can be applied to the production of a wide variety of electronic ceramics, structural ceramics, refractories, and ceramic tile and porcelain products.[2,6-8]

Uniaxial pressing and isostatic pressing can be distinguished among the dry pressing techniques by the way pressure is applied. In uniaxial pressing the pressure is applied by a punch in metal dies. The control of green dimensions is better than in the

isostatic case. This process allows the fabrication of rather complicated shapes. In isostatic pressing pressure is uniformly transmitted over a rubber mold, which surrounds the feed material, by means of liquid. This process ensures uniform compaction, even in protruding areas. It is used for producing shapes with extreme aspect ratio such as rods and tubes and very massive products with large thickness differences. Dry pressing and isostatic pressing are combined to produce large flat pieces such as dinnerware. This will be called as semi-isostatic pressing for a convenience since isostatic pressure is applied on one side of die.

The dry pressing process consists of several stages; (1) granulation of the powder, (2) filling of the die, (3) pressing to a compact, and (4) ejection. For industrial operations these stages are continuous and automatic.

Fine powders can stick to the hopper and the die as well as each other, resulting in clogging and non-uniform filling of the mold. Granulation of the powder is necessary in an industrial process to give good flowing ability.[9] Spray drying is an ideal process that forms spherical powder agglomerates of controlled size and deformability from the fine powder particles. For the spray drying process slurry is atomized into the drying chamber and forms droplets, which quickly achieve a spherical shape due to surface tension. The droplet size can be adjusted by changing the slurry properties such as surface tension and viscosity or the atomization parameters such as feed rate and wheel speed or nozzle pressure. The extensive surface area of the droplets provides ideal conditions for heat and mass transfer, and thus drying is accomplished very quickly. Following established drying theory evaporation rates during the initial period are very high and there is a fall-off during the subsequent period.[9,10] The resulting dry granules are separated from the exhaust gas and dust and stored for future use.

In the dry pressing process granulation is a critical step since it determines the granule properties and consequently the compact properties. Spherical dense granules with low granule strength will be ideal for successful compaction. Granules with spherical shape flow freely, and the packing in a die is more efficient. Homogeneous high-density granules are often desired for efficient compaction, but too high-density granules can also be a disadvantage. During the compaction granules should be easily

broken, leading to completely homogeneous compact without voids. If granules are too hard, much of the structure of the granules are preserved in the pressed body, resulting in the formation of strength limiting flaws in the fired body.[11-19] The properties of granules are greatly influenced by the slurry characteristics, and accordingly much attention has to be paid on the preparation of the slurry.[20-24]

To obtain granules with the desired properties the slurry for spray drying should be well dispersed and contain a high concentration of solids. This also reduces the problem of hollow granules. A slurry with a high solids content is desirable for technical reasons as well as to increase the energy efficiency in drying and the product yield. Dispersant is usually used to prepare a stable slurry of high solids content. In spray drying polymeric additives such as binders, plasticizers, and lubricants are added into the dispersed slurry. The binder gives adequate cohesive strength and flowing properties to the spray dried granules. Moreover, binders affect granule strength, the green body strength, and the density of the compact. The addition of a binder into the dispersed slurry often increases the viscosity. A compromise often has to be made between the viscosity of the slurry and the amount of binder needed to increase the green body strength. It is necessary to ensure that any dispersants and other polymeric additives are compatible. When multiple polymers are used in a suspension, negative interactions between polymers can lead to defects in final products. Therefore, depending on the desired properties of products, the interactions between polymers should be considered.[13,23-27]

During compaction granules are compressed and form a well-defined shape of high density. In uniaxial pressing the force applied by the moving punch is transmitted through the interaction forces at granule contacts. The force is transferred into normal and shear forces at contacts, and imbalance of these forces can lead to sliding and multiple particle rearrangement and deformation. The reaction forces of neighboring granules in contact restrict sliding and translation. As the applied force increases, stresses at contacts increases, and consequently both normal and frictional forces are increased. Since the force concentrates on the contact areas, which are only a small fraction of the total cross section of the granules, the contact stresses can cause elastic

deformation and perhaps plastic flow or fracture at local contacts for relatively low applied pressure.[28] The increase in the number of contacts per unit volume and a greater deformation at contacts would tend to diminish the stress multiplication at the contact points. In isostatic pressing due to the mode of pressure application a very small amount of shear force takes place between particles. This makes it more difficult to break granules and eliminate all traces of granules during compaction.[6,13,29,30]

Major pressing parameters, which influence the pressure/density relationship for a given powder and polymer system, are punch speed, pressure, and dwell time. Punch speed is the most important parameter from an industrial aspect to maximize the number of pieces made. An increase in punch speed will reduce the time for granules to rearrange and will be detrimental to density.[31] Moreover, it will not give enough time for entrapped air to escape, which will result in pore pressure buildup and possible fracture upon unloading and ejection. The density of pressed body is non-linearly dependent on the pressure. The density can increase to a limiting maximum with pressure. Dwell time at the maximum pressure is important not only for density improvement but also for microstructure improvement.[3,31]

On ejection elastic energy stored in the compact is relieved and increases the dimensions of the pressed piece, called springback. During the compaction the movement among the granules and inter-granule forces are not homogeneous. Thus, upon unloading stress relaxation is not a simple isotropic elastic deformation. It necessarily involves some plastic sliding due to the high elastic energy stored under loading compared with the weak energy of adhesion between particles. Springback increases with the applied pressure on compaction. Granules of high aspect ratio or highly agglomerated granules store more elastic energy during compaction, and lead to a greater amount of deformation on unloading. In isostatic pressing the relaxation of the rubber mold and its sliding against the pressed body may cause tensile stresses on the body, leading to fracture. The unloading rate needs to be carefully controlled with the mold design.[6,31]

2.2 Surface Roughness Measurement

The available techniques for surface roughness measurement may be generally divided into contact or non-contact methods based on whether the scanning probe touches the sample surface or not. The most common contact method is a mechanical profiler, also called a profilometer, where a mechanical stylus crosses over the surface of interest and the height variations are converted into an electrical signal. It is a robust technique well suited for measuring line profiles. Optical interferometry, scanning electron microscopy (SEM), optical microscopy (OM) belong to the non-contact methods. An optical interferometer scans the surface using white light and records the height variations as an interference pattern in an image plane. Scanning electron microscopy (SEM) is useful for qualitative visualization of a rough surface with high slope angles, in which the surface is probed by an electron beam. A shadowing effect occurs from the back-scattered electrons depending on the relative slope of the surface.[32]

Figure II-1 is a photograph of the complete optical interferometer system used in this study (Newview Model 5032, Zygo Corporation, Middlefield, CT). A schematic of the optical interferometer is shown in Figure II-2. Surface morphology is imaged and measured by the interference pattern of reflected white light, and surface structure analysis is provided without contacting the surface. Light from the microscope divides within the objective; one portion reflects from the sample surface and another portion reflects from an internal reference surface in the objective. These two reflected beams are then recombined at the beam splitter, creating an interference pattern due to the path length difference, and directed onto a solid-state camera. Interference between the two light wavefronts results in an image of light and dark bands, called fringes, which indicate the surface structure of the surface being tested.[33-36] The surface is scanned by vertically moving the objective with a piezoelectric transducer (PZT). As the objective scans, a video system captures intensities at each camera pixel. These intensities are converted into a three dimensional image by a mathematical method.[37]

The optical interferometer scans up to 100 μm in z-axis using a bipolar scan, which starts in the center of the scan envelope and moves the objective down and then up, with 0.1 nm resolution and 0.4 nm rms repeatability, which are independent of

objective magnification. The extended scan option extends the standard scan range up to 5000 μm. This option provides increased range for all objectives, limited only by the objective working distance. The software operating the optical interferometer (MetroPro™, Zygo Corporation, Middlefield, CT) has a "stitching" option, which allows collecting multiple images in a sequence and combining the images together for the analysis of a larger surface area.

The software provides filters that can modify the original data to remove noise or block unwanted data. Table II-I lists the filters and summarizes the effect of filtering. Filtering separates the collected roughness information into waviness, roughness, and high frequency components. Figure II-3 shows schematic description of each component. The roughness or waviness of the data can be adjusted by setting the filter frequency. The filter type and the window size used with the filter determine the overall effect and amount of filtering. The filter types are listed in Table II-II with a brief description. The window size is selected by the operator and can range from 3 to 49 pixels in increments of two. The window is a square grid of data points surrounding the data point that is being analyzed, i.e. a window size of 3 is a three by three grid of data points with the results being applied to the data point in the center of the grid. The larger the window size the greater the effects of the filtering and the longer the computer processing time to calculate the roughness of the surface.

Table II-I. List of the Filters Available with the MetroPro™ Software and Their Effects on the Surface Roughness Analysis.

Filter	Effect on the roughness measurement
Off	Disables filtering of the data
Low Pass	Data above a set frequency is rejected
High Pass	Data below a set frequency is rejected
Band Pass	Only data with a set range of frequencies is analyzed, filter must be used with a FFT (Fast Fourier Transform) filter mode.
Band Reject	Data within a set range of frequencies is rejected during analysis, filter must be used with a FFT filter mode.

Table II-II. List of the Filter Methods, or Algorithms, in the MetroPro™ Software Application.

Filter Method	Resulting Effect on the filtered data point
Average	Averages all valid data points in the filter window and applies the result to the central point
Median	Applies the "middle" value of all valid data points to the central data point
2-Sigma	Uses data points that are only within two times the root mean square (rms) value in each filter window and disregards values outside of this range.
FFT Auto	Fast Fourier Transform – automatic. A Fourier transform is applied to the data points and the filter window size is not used. The frequency settings for the Fourier transform are automatically selected. This algorithm should only be used as a starting point for selecting the frequency settings.
FFT Fixed	A Fast Fourier Transform that uses fixed frequency settings, determined by the operator, for the frequency cutoffs.

The mechanical profiler operates on a principle that is similar to a record player. The stylus is traced across a specified sampling length under an applied load. As the tip follows the contours and topography of the surface, the deflection of the stylus is translated into an electrical signal. This electrical signal is amplified and then typically converted into a digital format for use in a computer software package. The stylus tip is usually made of diamond, and can possess a number of geometries. Despite the strength of diamond, the stylus tip is quite fragile, owing largely to its small size. The bevel of the tip allows the stylus to traverse sharp steps, but when it encounters a feature, which extends beyond the bevel, the tip or sample can both be damaged.[38]

Figure II-4 shows the mechanical profiler used for this study. The mechanical profiler (Tencor P-10, Tencor Instruments, Santa Clara, CA) characterizes a surface by using a diamond stylus of 60° angle. Vertical scan length ranges up to 300 μm with 5 nm vertical resolution. The applied force on stylus can be varied from 1 to 50 mg. Scan speed also can be changed to preselected value ranging from 1 to 25000 mm/sec. The software used with the profiler also provides filters which can control the range of wavelengths collected in the scanned data to remove unwanted noise.[40]

Both techniques have advantages and limitations. If the load applied to the stylus on a mechanical profiler is too high, surface damage can occur. For the measurement of soft materials the load on stylus should be sufficiently low (0.2-2 mg depending on the material) or the largest acceptable tip must be used. Optical interferometry is free from the problem of surface damage. The stylus is calibrated with a standard for height variations whereas the optical interferometer is automatically calibrated because they are measured in terms of a known wavelength of the light. The measured profile by a mechanical profiler is an interpretation of the stylus radius/shape on the true surface profile. Sometimes, the shape of the surface interferes with the analysis of the surface roughness. Although the surface is flat, the variations of optical constants in the surface can be misinterpreted as height variations for optical interferometer. In addition, with steep local slopes light is not reflected enough and leaves an unmeasured spot in the graph.[40,41]

3. Experimental Procedure

3.1 Surface Roughness of Dinnerwares

The surface finish of dinnerware was quantitatively characterized using an optical interferometer. All the samples used for this study were generously provided by Buffalo China (Buffalo China Inc., Buffalo, NY). Samples were collected at each stage of dry press production line where the surface was altered, i.e. green, bisque fired, after vibratory finishing, and glazed. Several samples were taken at each stage in the process to provide statistically significant measurements for the surface roughness. Table II-III lists the number of samples analyzed. The results were compared to the qualitative results obtained from the scanning electron microscope and the optical microscope.

Table II-III. Number of Samples Tested from Each Manufacturing Process at Buffalo China.

Process	Green	Bisque Fired	Processed	Glazed
Dry Pressing	20	24	24	23

For this study the interferometer was set up using the 5x Michelson type objective lens and a 1x zoom setting. This arrangement allowed the lateral resolution of 2.72 μm and the analysis of a 1.44 x 1.07 mm area for a single scan of the surface. The stitching technique was applied to gather statistically significant results from a large area. For unglazed samples a total of 48 scans over a randomly selected area on the surface of the plate were performed and compiled. The scanned area for each sample was 6.85 x 6.76 mm. Two smaller areas, comprised of six scans each, were analyzed for the glazed samples. Each of the smaller areas analyzed was 2.52 x 2.70 mm. Depending on the curvature of the sample, an extended scan was performed to assure the collection of the data from the surface. The data collected from the bisque fired and processed samples showed the most noise. To reduce this source of error in the roughness measurement, the F2 filter was used for the incident radiation.

Three roughness values are reported; the peak-to-valley distance (PV), the root-mean square (rms) roughness, and the average roughness (R_a). The PV is the distance between the highest and the lowest points within the analyzed surface. PV is the maximum roughness height and is the worst case point-to-point error in the data set. It is possible that PV value is not representative of the overall surface since PV compares the two most extreme points on the surface. The rms roughness is the root-mean-square deviation from the reference surface. The rms is calculated as the standard deviation of the height (or depth) of the test surface relative to the reference plane for all the collected data points. The average roughness is the arithmetic average deviation from the reference surface.

The roughness of the dinnerware was also analyzed using secondary electrons in the SEM. The image taken from the SEM is a qualitative measurement of the surface roughness and is shown as a comparison to the data collected from the interferometer. There were differences in the surface analyzed using the SEM and the interferometer. To determine the source of these variations optical microscopy, using either diffuse or reflected light, was used to view the surface.

3.2 Semi-Isostatic Pressing and Surface Roughness

The effect of dry press operation parameters on the properties of pressed bodies was analyzed. An industrial scale semi-isostatic press (Model PI550G, Dorst Maschinen and Anglagenbau, Kochen, Germany) relocated to Alfred University was used to make dinnerware plates. The photograph of the press is shown in Figure II-5. The press has vertical piston motion and generates 600 tons maximum closing force. Granules are fed into the mold horizontally assisted by vacuum. The mold is made of polyurethane and the pressure is transmitted through oil existing between the membrane and upper piston. The operation of the press is fully automated. All the spray dried granules used in this study were provided by Pfaltzgraff China (Pfaltzgraff China Co., York, PA) out of production dry press material. The spray dried granules were characterized before pressing. Granule size distribution was determined by sieve analysis as ranging from 30 to 500 μm as shown in Figure II-6. The residual water content of granules was measured as 2.71% by heating the granules at 110°C for 24 hours. Thermogravimetric analysis (TGA) showed that most of the adsorbed water and organic materials decomposed below 600°C in Figure II-7.

Dinnerware plates were produced using different press setups, which were generated using the adjustable parameters on the press, and the properties of the plates were characterized. There are many adjustable parameters on the press. Some of the parameters are set initially during installation and not recommended for adjustment. Parameters controlling the application and release of the pressure behind mold and dwell time for those processes are mostly chosen for this study. Table II-IV lists the selected parameters. The experimental parameters with high and low levels are listed. K2 is given as a percentage of K1. The diagram in Figure II-8 explains the application and release of the isostatic pressure behind the mold as a function of time.[42] Parameter A is the isostatic pressure applied to the mold and symbolized as K1. The period of time held at the pressure, T4, is parameter D. After the time T4 the pressure drops rapidly down to the pressure K2, which is parameter B. At the pressure K2, the pressure release speed decreases, and second stage of isostatic pressure release begins. The flow control (Parameter C) changes the rate that the pressure is released. Another parameter (End T5)

can be set to tell the system how long to follow the rate set by the flow control. If the timer reaches the value set by End T5 and the pressure is greater than zero, the pressure rapidly drops to zero. One further parameter is the time T6, which allows the piston to remain closed on the plate without any isostatic pressure for a given time before releasing. It should be noted that for this time only the weight of the cylinder itself is applying pressure to the plate.

Table II-IV. Press Parameters and Ranges Selected for the Experiment.

Parameter	Variable	Symbol	Tested low and high levels
A	Isostatic Pressure	K1	250 /300 bar
B	Initial Fast Isostatic Release Pressure	K2	40 /80 %
C	Flow Control	Flow rate	0.5 / 2.5
D	Time at pressure	T4	0 / 3 sec
E	Time to follow Flow control after K2	End T5	40 / 80 bar
F	Time closed after press at 0 Isostatic	T6	5 / 20 sec

Following the previous study, statistical experimental design software (Design Expert Version 5.07, Stat-Ease Corporation, Minneapolis, MN) was used to generate a series of experimental conditions of pressing using the six parameters.[42] The design is a ¼ fractional factorial for six factors at two levels, which provides a Resolution IV design with 16 experiments as listed in Table II-V. Fifteen plates were pressed at each set of experimental conditions and fettled on the fettling machine. This statistical design generates aliases, which are discussed in Appendix. The details of the alias structure are explained in Appendix.

Pressed plates were characterized for bulk density, fracture strength, and surface roughness. To determine the density gradient in different areas of the plate the plate was sectioned and broken into five areas, Front, Back, Left, Right, and Center. The front side of the plate was marked during the pressing. Three pieces from the center and four pieces from the rest of areas for each plate were collected from three plates. The test

outlined in the ASTM C830-88 was followed with substituting kerosene for water. The measured density of the kerosene used was 0.781 g/cm^3.

Table II-V. Press Operation Setups for the Experiment Generated by Design Expert.

Std #	Run #	Block	K1 (Bar)	K2 (%)	Flow Control	T4 (sec)	End T5 (Bar)	T6 (sec)
10	1	Block 1	300	40	0.5	3	80	20
3	2	Block 1	250	80	0.5	0	80	20
1	3	Block 1	250	40	0.5	0	40	5
11	4	Block 1	250	80	0.5	3	80	5
4	5	Block 1	300	80	0.5	0	40	20
8	6	Block 1	300	80	2.5	0	80	5
9	7	Block 1	250	40	0.5	3	40	20
14	8	Block 1	300	40	2.5	3	40	5
5	9	Block 2	250	40	2.5	0	80	20
15	10	Block 2	250	80	2.5	3	40	20
2	11	Block 2	300	40	0.5	0	80	5
13	12	Block 2	250	40	2.5	3	80	5
7	13	Block 2	250	80	2.5	0	40	5
12	14	Block 2	300	80	0.5	3	40	5
6	15	Block 2	300	40	2.5	0	40	20
16	16	Block 2	300	80	2.5	3	80	20

To measure the strength of the plates a device was constructed to center the plate on a set of three ball bearings arranged in a ring with a diameter of approximately 133 mm. Another ball bearing was used to apply the load on the opposite side of the plate in the center of the ring. Testing was conducted on a universal testing machine (Model 8562, Instron, Canton, MA). Figure II-9 shows the device attached to the testing machine. Five plates for each setup were tested and the results were averaged. The geometry of the plate due to the rim and foot would make an actual calculation of strength complicated and inaccurate. This test was used only for comparison of maximum load obtained.

The surface roughness was measured using a stylus profilometer, Tencor P-10. Both top and bottom sides of three plates were tested. The applied force on the stylus

was 5 mg, scanning speed was 50 μm/sec, and the scanning length was 6000 μm. Before the test proceeded it was determined if the diamond stylus tip caused any damage or change to the surface of the plate. The scanned area of some samples was observed by SEM. Also, two 3D images obtained by running a sample twice were compared. It was concluded that there is no morphology change at this test condition.

4. Experimental Results and Discussions

4.1 Surface Roughness of Dinnerwares

The results of the surface roughness from the optical interferometer are listed in Table II-VI. The optical interferometer provides roughness information and scanned images of the surface in several different plots such as contour, oblique, 3D, and solid. Images obtained by optical interferometer are shown in Figure II-10. All the bisque fired pieces go through a finishing process in the vibratory mill to improve the surface finish. These samples are named "processed." Glazes are then applied onto the processed samples after drying and the glaze is fired at a temperature below that of the bisque process.

Corrections were made to eliminating the unrealistic roughness or waviness, resulting from the presence of noises, from the raw data. The origin of the noise can be from the rough surface that scatters the light away from the objective or regions on the surface that are transparent to the wavelength of the incident light.[40] In addition, differences in the refractive index of the area being profiled can lead to differences in the phase change upon reflection, resulting in height differences.[43] Filters were used to remove certain frequency ranges from the roughness calculations. The dinnerware samples in the green state were filtered using a low pass, median filter with a window size of 5 (each data point is the median of the surrounding 25 data points). The bisque fired and processed samples were filtered using a low pass filter with a fixed Fourier transform set between 8 and 15 mm^{-1}. For the glazed samples a band reject filter with a fixed Fourier transform, set at 110 mm^{-1} and 2.5 mm^{-1} for the high and low frequencies, was used to remove the subsurface bubbles from analysis.

Table II-VI. Results of the Surface Roughness Measurement for the Dinnerware Samples from Buffalo China.

Forming Technique	Sample Treatment	Area (mm^2)	Filter Type, Method (Window size)	PV (μm)	rms (μm)	R_a (μm)
Dry press	Green	46.306	Low pass, median (5)	91.8	8.5	6.7
	Bisque	46.306	Low pass, fixed FFT	94.3	9.1	7.1
	Processed	46.306	Low pass, fixed FFT	86.7	8.5	6.6
	Glazed	6.804	None	3.41	0.4	0.3

The surface roughness of plates increases upon firing while there is a slight improvement after vibratory milling. Since the same filter was applied to both the bisque body and the processed samples, the extent of filtering should be the same. The average roughness of processed samples is slightly lower than that of the bisque samples. It is found that milling process reduces the surface roughness of bisque samples by 7 %. The average roughness of the dry pressed samples after glazing is 0.3 μm, which tells that glazing covers most of surface texture from granules. The PV distance also decreases to 3.41 μm from 86.7 μm of processed sample. The smooth glassy surface increases the reflectance at the surface and improves data collection.

4.2 Comparison to Images obtained by SEM and OM

Images from the optical interferometer were compared to images obtained by SEM and OM. The images from the green dry press surface are shown in Figure II-11. The images of the surface from the interferometer and the SEM were taken in the approximately the same region. The optical microscope image is shown only for comparison purposes and is taken from a different section of the sample. The light source for the optical image is parallel to the surface to provide shadowing in the image.

The presence of irregularly shaped granules can be seen in all three of the images. The images from the SEM and optical microscope are qualitative measurements of the surface roughness, which is imaged by creating “shadows” on the surface of the sample. The SEM image provides more detail of the surface texture, but roughness on the image seems to be obscured by the difference of scale in X-Y and Z directions.

Figure II-12 shows the images from the bisque fired dry press surface. The images show that the shape of granules used to manufacture the dinnerware has persisted through the firing process. The image from the optical microscope shows the presence of bright grains in the surface of the sample. These grains are transparent and allow light transmission through the surface. Therefore, without filtering any data from these regions result in unreliable information.

The images from the glazed dry press surface are shown in Figure II-13. The images from the interferometer and the SEM are taken in approximately the sample region of the sample surface. The image from the optical microscope is taken using reflected light, which replicates the process used by the interferometer to collect data. The reflected light source also allows for the internal analysis of the glazed sample. When the optical microscopy is focused on the surface of glazed sample, only smooth surface is seen. The focal plane is lowered down below the surface, and bubbles appear in the image. The image of the surface from the interferometer shows the presence of depressions in the surface of the glaze. These depressions are believed to be the bubbles that are present beneath the glaze surface. Since the interferometer works with visible white light and the glaze is a "clear, gloss" glaze, the light from the interferometer is able to penetrate through the surface and collect data from interfaces within the glaze, i.e. the concave bottom of the bubbles. Since these surfaces focus and reflect the light, the interferometer records the bottom surface of the bubbles as the external surface of the glaze. The roughness information due to the bubbles in the glaze can be filtered from the image and roughness calculations using a "Band Reject" filter with a Fourier transform. This process allows only the long-range roughness or the waviness to be used in calculating the roughness of the sample.

4.3 The Effect of Pressing Parameters on Green Body Properties

The bulk density of pressed plates made at different operational parameters was measured. Small pieces from five different areas of a plate were analyzed for density gradients. The sample size was smaller than that recommended by ASTM standard C830-88.

Table II-VII lists the measured density values for the samples studied. The density gradient between different areas of a plate at each setup is insignificant. There is no trend of density gradient in different areas of a plate. The highest density is 1.858 g/cm^3 and the lowest is 1.794 g/cm^3 for all of the samples tested.

The density gradient is usually caused by stress and deformation variations in the pressed compact. In dry pressing the stress variation is caused by the friction against the mold or die walls. The polymeric additives used in granules serve as a lubricant during compaction and minimize the die wall friction. Another origin of stress variations is high aspect ratio of the compact. Since the shape of pressed compact in this study has very low aspect ratio, axial density distribution should be minimal. The press used in this study applies isostatic pressure to the granulates allowing pressure to be evenly transmitted to granules filled in the mold. Compression is achieved over the entire surface of the compact. The variation in radial density is also expected to be minimal.

Table II-VII. Measured Density of Plates at Different Areas.

	Front (g/cm^3)	Right (g/cm^3)	Left (g/cm^3)	Back (g/cm^3)	Center1 (g/cm^3)	Center2 (g/cm^3)	Center3 (g/cm^3)	Std. Dev.
Set 1	1.848	1.846	1.852	1.851	1.847	1.847	1.850	0.002
Set 2	1.816	1.818	1.817	1.817	1.813	1.818	1.812	0.002
Set 3	1.816	1.813	1.828	1.815	1.809	1.810	1.815	0.006
Set 4	1.825	1.818	1.817	1.819	1.819	1.823	1.823	0.003
Set 5	1.830	1.828	1.821	1.833	1.823	1.828	1.829	0.004
Set 6	1.831	1.826	1.831	1.829	1.829	1.829	1.837	0.003
Set 7	1.831	1.831	1.832	1.838	1.828	1.832	1.830	0.003
Set 8	1.858	1.854	1.854	1.845	1.845	1.848	1.851	0.005
Set 9	1.803	1.804	1.796	1.797	1.801	1.805	1.799	0.004
Set 10	1.810	1.807	1.816	1.814	1.809	1.813	1.811	0.003
Set 11	1.818	1.831	1.822	1.819	1.823	1.821	1.817	0.005
Set 12	1.812	1.802	1.804	1.805	1.809	1.812	1.796	0.006
Set 13	1.797	1.794	1.805	1.799	1.800	1.805	1.799	0.004
Set 14	1.832	1.844	1.831	1.843	1.835	1.844	1.834	0.006
Set 15	1.834	1.828	1.836	1.828	1.834	1.830	1.829	0.003
Set 16	1.830	1.843	1.836	1.836	1.834	1.837	1.853	0.008
Average	1.824	1.824	1.825	1.824	1.822	1.825	1.824	
Std. Dev.	0.016	0.017	0.016	0.016	0.015	0.014	0.018	

Due to the minimal density variations in different areas of a plate all the density values for each setup were averaged and used as a response for statistical analysis. Analysis of variance (ANOVA) shows that 3 factors, K1, T4, and interaction between K1 and flow rate, have the most significant effect on the density for the factorial model as indicated in Table II-X. However, these parameters have aliases as denoted in Appendix. As a consequence of alias structure in the design it is impossible to separate the effects of aliased interactions. Figure II-14 shows the density change with K1 and T4. The pressure has a greater impact than does the time at the pressure. Density change is shown with factors, K1 and flow rate, in Figure II-15. Maximum density is obtained with K1 and flow rate. Density change seems to be independent of the individual variable. However, when the interaction of K1 and flow rate is considered, the density change becomes significant.

The strength analysis was done using the maximum load applied to the plates. Table II-VIII lists the measured strengths. The highest was 7.31 kg and the lowest was 4.44 kg. Interestingly, the first half of the experimental parameters was higher than the second half. It is not clearly shown what caused the difference, but most of the first half have slow flow rate.

Table II-VIII. Strength of Dry Pressed Plates.

SET#	Average (kg)	Std. Dev.	SET#	Average (kg)	Std. Dev.
1	6.92	0.46	9	4.44	0.25
2	5.93	0.14	10	4.84	0.24
3	6.06	0.43	11	4.70	0.56
4	6.33	0.40	12	4.89	0.37
5	6.82	0.51	13	4.71	0.44
6	6.60	0.30	14	4.58	0.42
7	6.51	0.37	15	4.70	0.18
8	7.31	0.17	16	5.11	0.29

Factors K1, flow rate, and T4, have the most significant effect on the strength as shown in Table II-X. Figures II-16 and II-17 show that strength increases with K1, flow rate, and T4. One interesting fact is that an increase in flow rate slightly increases strength. The strength is also influenced by the interactions between K1 and flow rate and between K1, K2, and flow rate; interactions between K1 and flow rate decrease strength while interactions between K1, K2, and flow rate increase strength. However, the effects of these two interactions are relatively small. It is again noted that these parameters have aliases.

Surface roughness of both sides of a pressed plate was measured. Three samples for each setup were measured and averaged. Table II-IX lists the surface roughness of both surfaces. The bottom surface, where the isostatic pressure is applied, exhibits higher roughness values than the top surface for all the setups. Roughness ranges from 14.0 to 17.0 μm on top surface and from 15.9 to 21.6 μm on bottom surface.

Table II-IX. Results of Surface Roughness Measurement by Mechanical Profiler.

	Top surface (μm)	Std. Dev.	Bottom surface (μm)	Std. Dev.
1	14.4	6.0	21.2	3.7
2	15.1	3.0	19.5	2.4
3	12.6	1.1	21.6	2.9
4	15.5	1.5	19.3	2.3
5	16.3	2.8	19.5	2.9
6	16.4	4.1	19.1	4.4
7	13.7	1.6	17.8	2.0
8	15.4	4.5	20.0	2.7
9	14.6	1.4	15.9	2.0
10	13.7	2.6	17.0	1.6
11	17.0	2.4	17.8	0.9
12	14.0	0.5	18.4	4.8
13	14.8	0.3	18.2	1.9
14	15.3	1.3	18.6	5.3
15	17.0	1.1	16.4	1.4
16	15.2	1.3	17.3	0.7
Average	15.1		18.6	
Std. Dev.	1.2		1.6	

During compaction pressure is transmitted through the plate from one side of the plate to the other. The moving punch applies pressure to the granules, and the pressure propagates through the granulate bed. The degree of granule deformation is directly governed by the forces at the granule contacts and determines surface roughness. It was expected that granule deformation would be more severe near the moving punch than near the fixed plate at the bottom. However, this result was reversed. The surface near the moving punch showed higher surface roughness. It is believed that this is mainly influenced by the way pressure was applied on both surfaces. Due to the dimension of a pressed plate the axial density gradient is very small, which indicates that pressure is evenly distributed between granules. For the semi-isostatic press used in this study isostatic pressure, which applies no shear force, is applied on the bottom surface of a plate by the moving punch while top surface follows an uniaxial pressing mechanism. The granule deformation is mostly induced by the shear force, therefore the roughness on the bottom surface is higher.

From the statistical analysis the factors affecting the roughness of top surface were found as shown in Table II-X. Many factors influence the roughness of the top surface, but four factors K1, T4, interaction between K1 and T4, and interaction between K1 and End T5 have the most of effect. Aliases of the two interaction parameters are found in Appendix. Figure II-18 shows the roughness change with K1 and T4. Contrary to the expectation, the surface roughness increases with applied pressure. The roughness increase with applied pressure is higher at zero dwell time. This seems to be related to the springback effect of pressed pieces. All the tested plates were pressed at between 250 and 300 bar, which corresponds to 25 and 30 MPa, respectively. At this pressure range the deformation of the granules is very small and most granules retain their shapes, which allows the granules to store elastic energy. The springback of pressed pieces mostly occurs in axial direction and increases with applied pressure.[44] Therefore, plates pressed at high pressure with no dwell time have high roughness values. Roughness seems to be indirectly related to dwell time at the applied pressure. Roughness decreases with T4 at the applied pressure. This suggests that the dwell time at the pressure gives more time for granules to deform under pressure. The roughness change was plotted with K1 and

End T5 in Figure II-19. The opposite trend is shown at the two ends of the K1. Roughness increases with End T5 at the lowest K1 while decreases at the highest K1.

Again, several of parameters influence the roughness of the bottom surface. In the case of roughness on the bottom surface T6 has the most significant effect. Figure II-20 shows that roughness decreases with the time that piston remains without any isostatic pressure before releasing. Even though the isostatic pressure is zero at this stage, the load of the piston is still applied to the plate and must be able to decrease the roughness.

Table II-X. Results of Statistical Analysis.*

Properties	Coded Factors	R^2	Std. Error	F Value	p-value
Density	1.82431+(0.011438xK1)+(0.006688xT4)+(0.002875xK1xFlow Rate)	0.93	4.463×10^{-3}	48.67	<0.0001
Strength	5.65218+(0.188656xK1)+(0.2065xFlow Rate)+(0.158556xT4)-(0.12029xK1xFlow Rate)+(0.088694xK1xK2xT6)	0.91	0.13	17.42	<0.0002
Roughness of top surface	15.0639+(0.80315xK1)+(0.221837xK2)-(0.43244xT4)+(0.206612xT5)-(0.29351xK1xK2)-(0.37601xK1xT4)-(0.34959xK1xT5)+(0.245262xK1xK2xT6)	0.96	0.41	16.21	<0.0016
Roughness of bottom surface	18.6019+(0.147269xK1)-(0.2061xFlow Rate)+(0.111006xT4)-(0.53407xT6)-(0.32064xK1xFlow Rate)+(0.437456xK1xT4)+(0.153269xK1xT5)+(0.394481xK1xT6)+(0.293456xK2xT6)-(0.38462xK1xK2xT6)	0.99	0.20	44.61	<0.0012

* This gives information of the factors that influence the properties of dry pressed plates. R^2 gives an indication of the fraction of the variation in the response that is explained by the model. The p-value is used to calculate the confidence level (CL) that a model term is significant based upon the F test from ANOVA (analysis of variance). The p-value is probability of stating a factor, is significant, when it is not. The CL is calculated as CL=(1-p)x100. All model terms have >95% confidence levels.

5. Conclusions

5.1 Surface Roughness Characterization

The surface roughness measurement by optical interferometer reveals that there is a change in roughness at each stage of dry pressing process. During the compaction granules do not break down, preserve their shapes, and result in high surface roughness. The high surface roughness is retained after firing process while there is a slight improvement after vibratory milling process. The milling process is found to be inefficient. After glazing most of surface texture is covered and produces a smooth surface. However, the measurement of the surface roughness does not account of the aesthetic quality of the surface that is visible through the glazed surface.

5.2 Dry Press Operation Parameters

It is found that isostatic pressure and dwell time at pressure have most effect on the properties of pressed plates including density, strength and surface roughness. The density and strength of pressed plates increase with isostatic pressure and dwell time. The surface roughness of plates is influenced by many parameters and interactions between the parameters. Due to the relatively low pressure and lack of shear force, granules do not efficiently deform. Therefore, dwell time at the pressure and the holding time at the end of the pressing cycle have a major impact on the roughness of top and bottom surfaces, respectively. However, due to the alias structure in the design, statistical analysis of the data is not able to differentiate the effects of aliased interactions.

Figure II-1. Photograph of the optical interferometer and analysis system (Newview Model 5032, Zygo Corporation, Middlefield, CT). Interferometer microscope is on the left, the controller for the microscope is in the middle, and the computer monitor is on the right on the table.

(a)

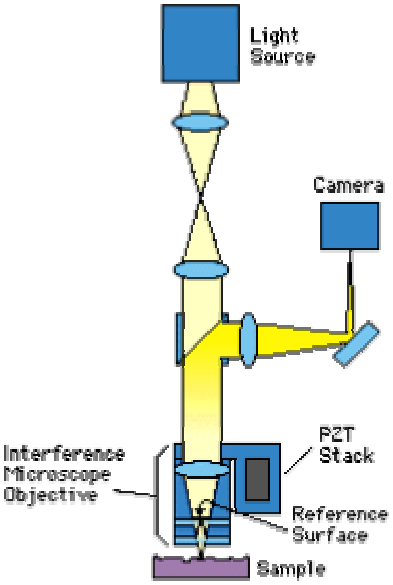

(b)

Figure II-2. (a) Photograph and (b) schematic of the Michelson interferometer, upon which the optical interferometer is based. Light from the microscope divides within the objective; one portion reflects from the sample surface and another portion reflects from an internal reference surface in the objective. These two reflected beams are then recombined at the beam splitter, creating an interference pattern and directed onto a solid-state camera.

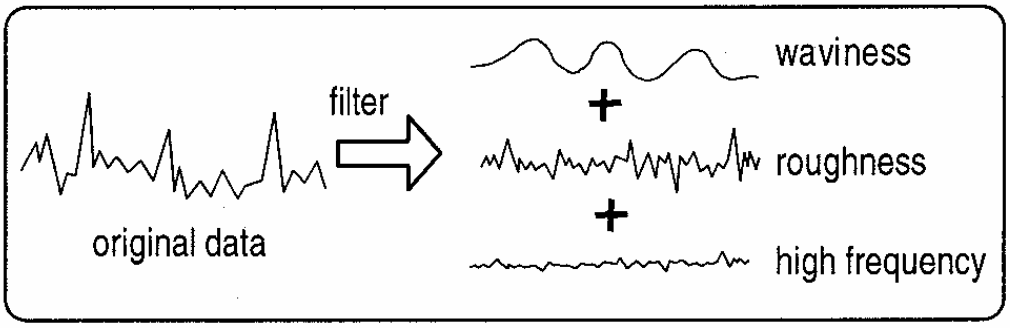

Figure II-3. The effect of filtering on the collected data. Filtering separates the collected roughness information into waviness, roughness, and high frequency components. Filters are used to analyze only the pertinent data and to block the noise from the analysis.

(a)

(b)

Figure II-4. (a) Photograph of mechanical profiler system (Tencor P-10, Tencor Instruments, Santa Clara, CA) and (b) close-up picture of sample stage and stylus head house.

Figure II-5. Photograph of semi-isostatic press (Model PI550G, Dorst Maschinen and Anglagenbau, Kochen, Germany). The press has vertical piston motion and generates 600 tons maximum closing force.

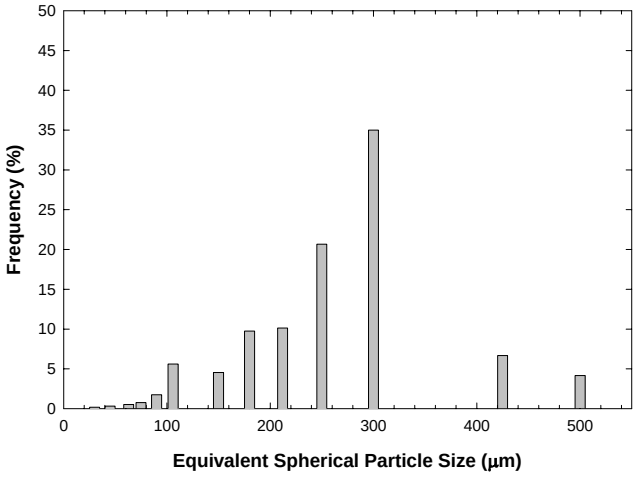

Figure II-6. Size distribution of spray dried granules provided by Pfaltzgraff China (York, PA). Size of granules ranges from 30 to 500 μm.

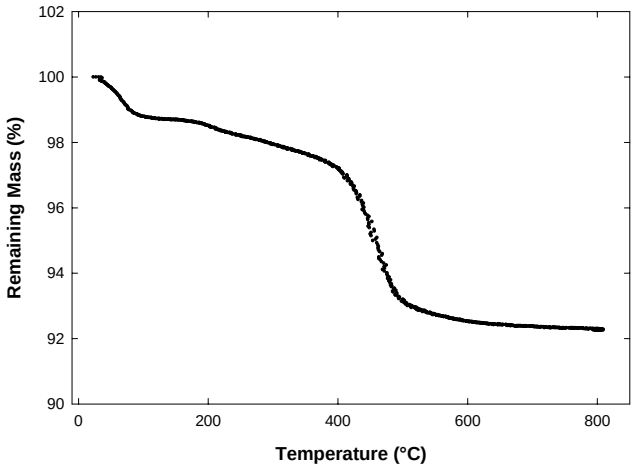

Figure II-7. Thermogravimetric analysis of spray dried granules of whiteware batch. Adsorbed water and added organic materials decompose below 600°C.

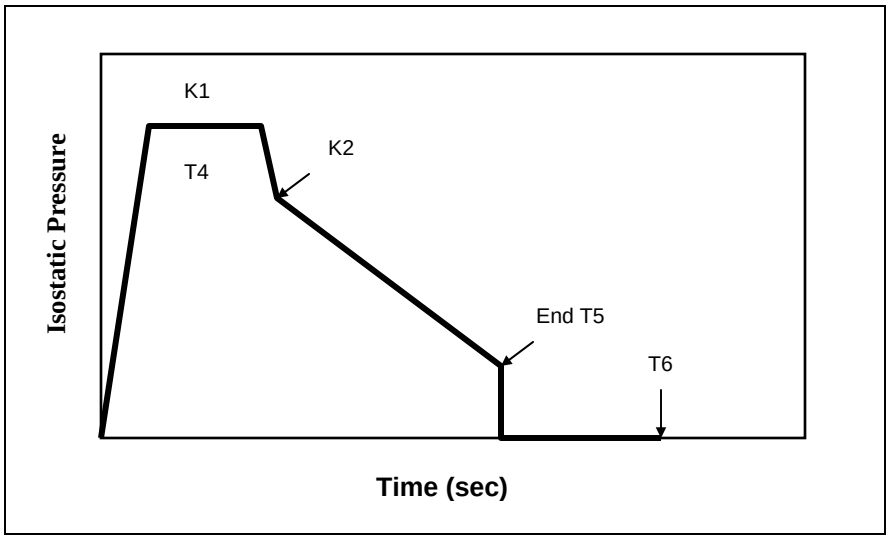

Figure II-8. Isostatic pressure change behind the membrane with time in semi-isostatic press (Model PI550G, Dorst Maschinen and Anglagenbau, Kochen, Germany). K1 is the isostatic pressure applied to the mold. The period of time held at the pressure is T4. After the time T4 the pressure drops rapidly down to the pressure K2. If the timer reaches the value set by End T5, the pressure rapidly drops to zero. T6 allows the piston to remain closed on the plate without any isostatic pressure for a given time before releasing.

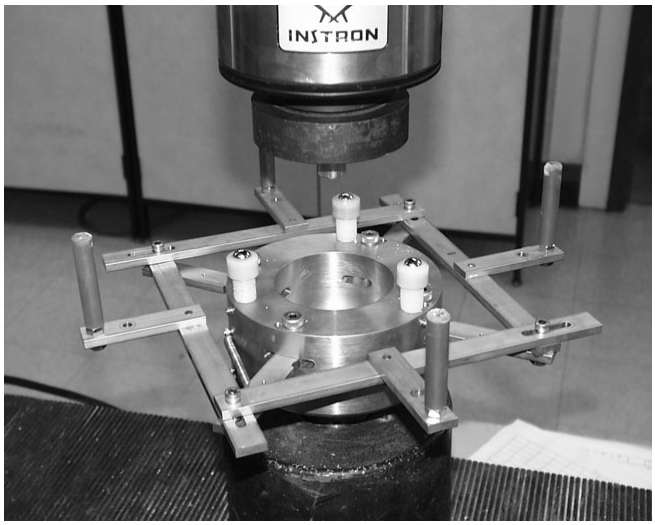

(a)

(b)

Figure II-9. The picture of the strength testing device; (a) close-up picture of the device and (b) the device with a plate. Device is based upon a "ball on ring" test method.

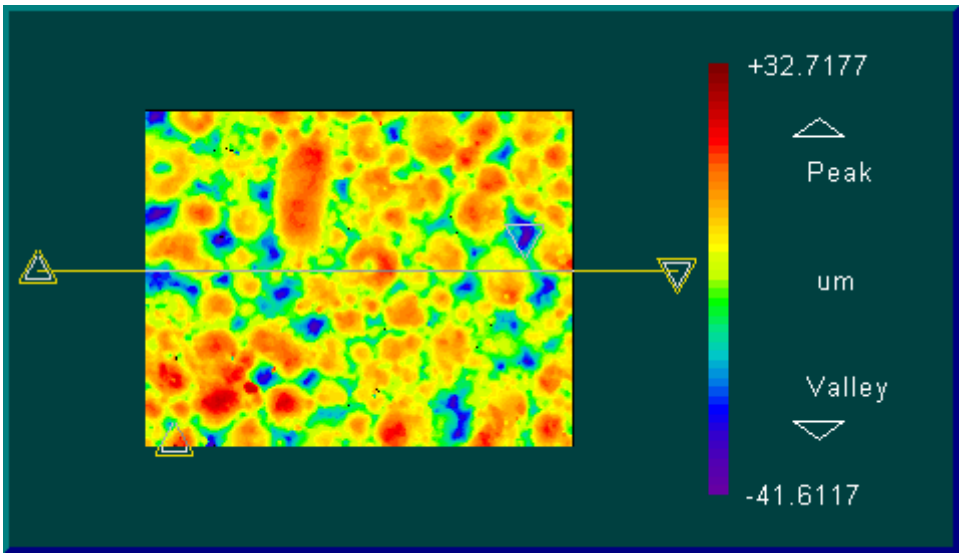

(a)

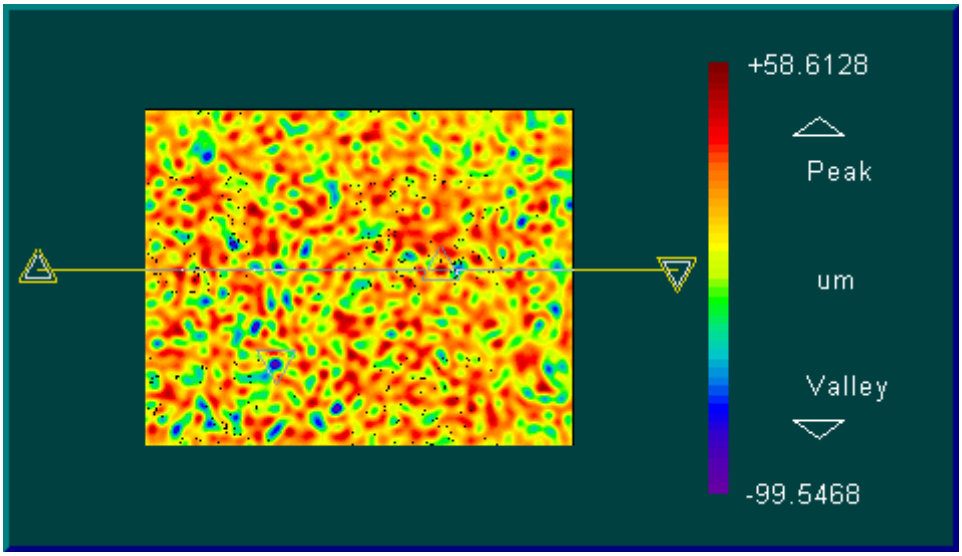

(b)

Figure II-10. Images obtained by optical interferometer from dry press sample; (a) green; (b) bisque fired, (c) processed, and (d) glazed samples. Images (c) and (d) are continued on the next page.

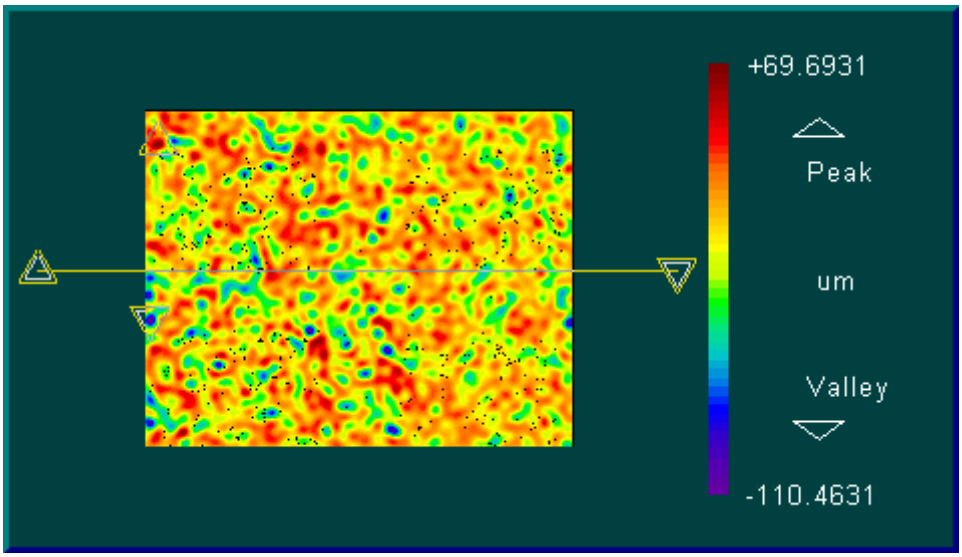

(c)

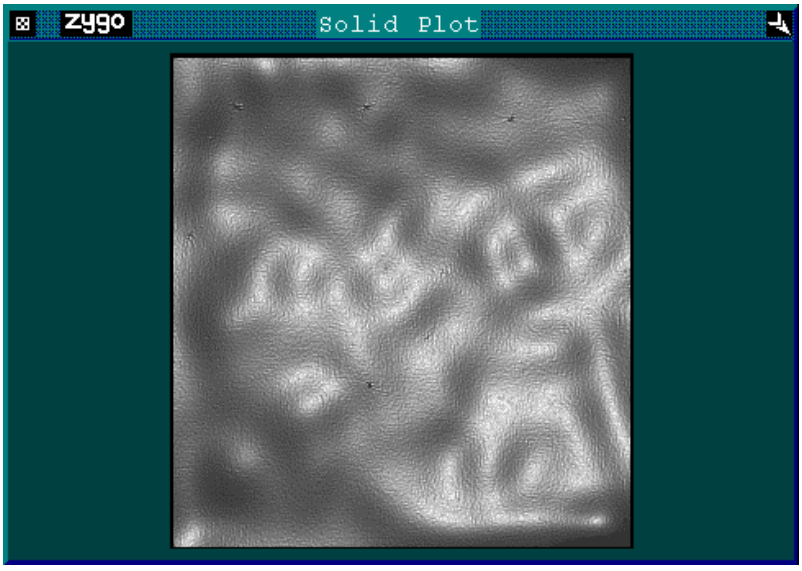

(d)

Figure II-10. Images obtained by optical interferometer from dry press sample; (a) green; (b) bisque fired, (c) processed, and (d) glazed samples. Images (a), (b), and (c) are filled plots in which the surface height is shown in different colors. Image (d) is a solid plot in which areas with different slopes are represented by different shades.

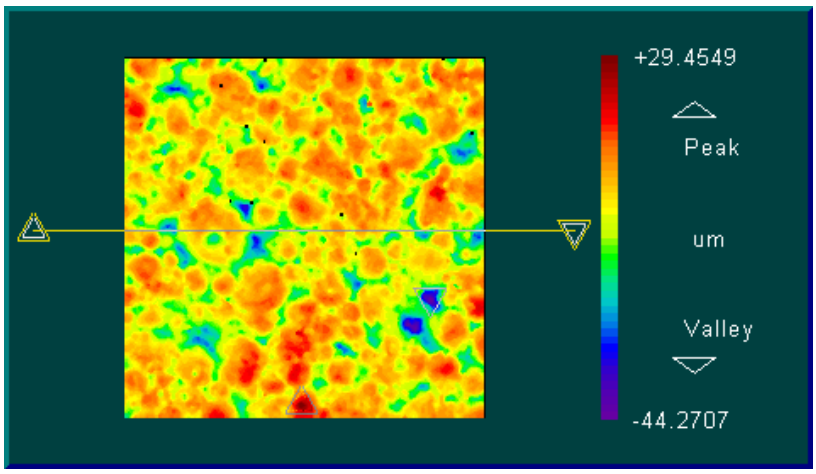

(a)

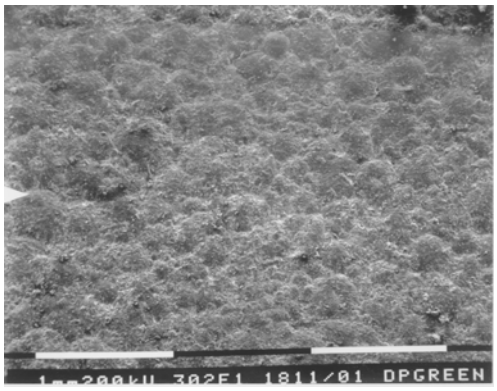

(b)

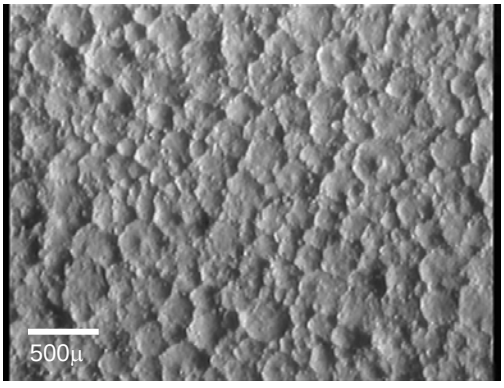

(c)

Figure II-11. Images of surface from a green dry press plate obtained by (a) Interferometer, (b) SEM, and (c) OM. All the images clearly show that spray dried granules retain their shapes after compaction.

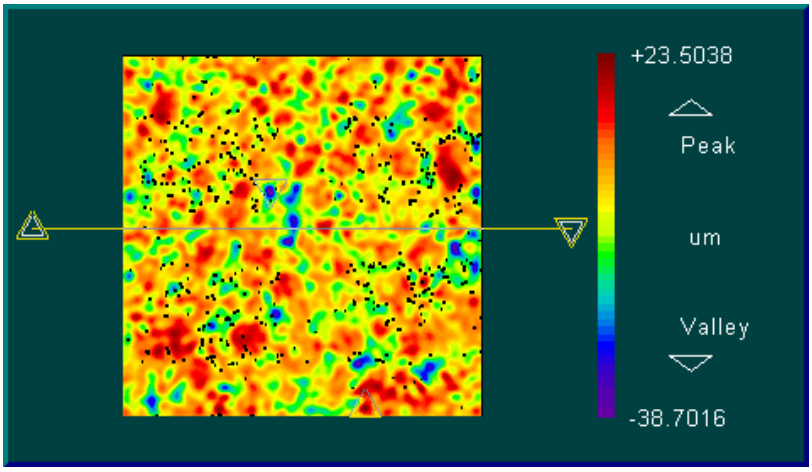

(a)

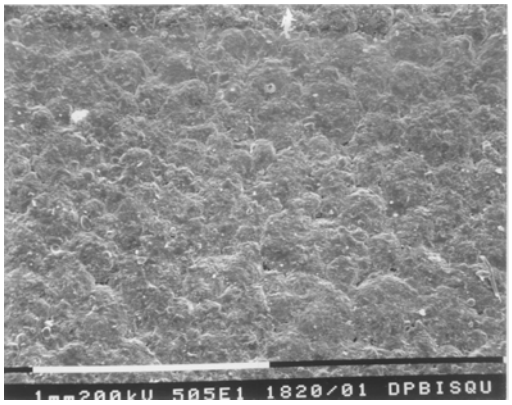

(b)

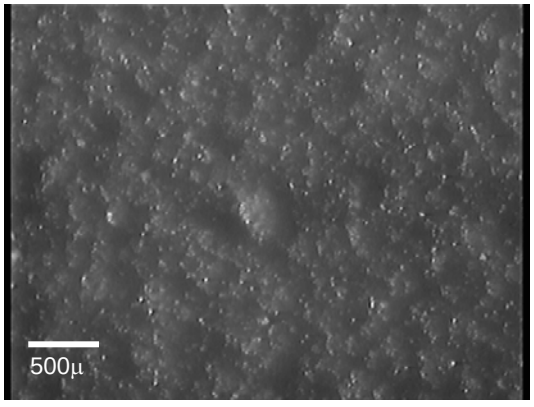

(c)

Figure II-12. Images of surface from a bisque fired dry press plate obtained by (a) Interferometer, (b) SEM, and (c) OM. After firing granule shapes are still shown on the surface of plate. Firing does not improve the surface roughness of plate.

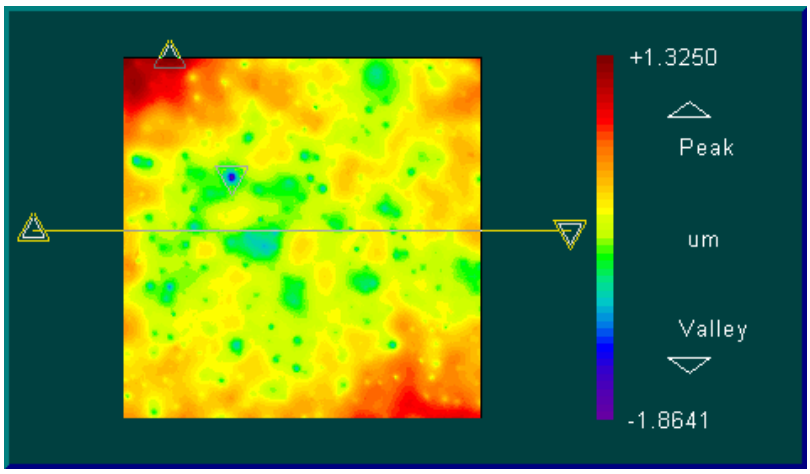

(a)

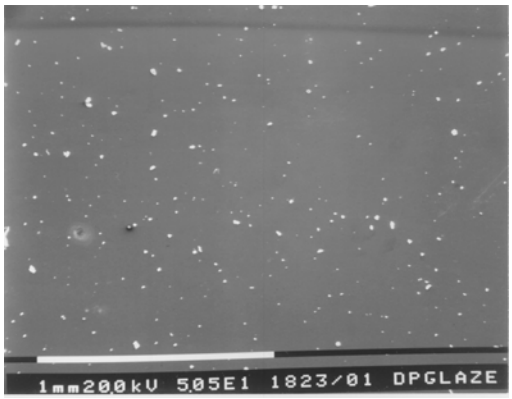

(b)

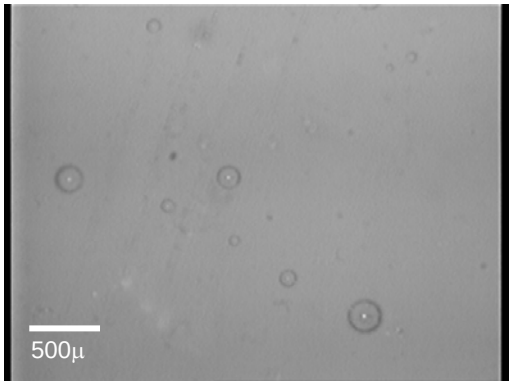

(c)

Figure II-13. Images of surface from a glazed dry press plate obtained by (a) Interferometer, (b) SEM, and (c) OM. Glazing covers rough surface, but allows visual evaluation of the underlying surface, which remains unacceptable to commercial customers.

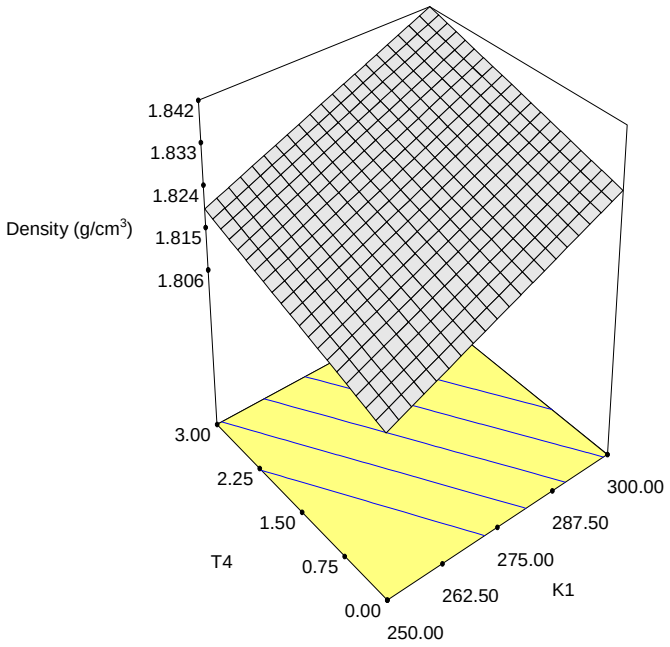

Figure II-14. Density dependence on isostatic pressure and dwell time at the pressure. All other variables are held at their average. Density increases linearly with an increase in applied pressure and dwell time at the pressure.

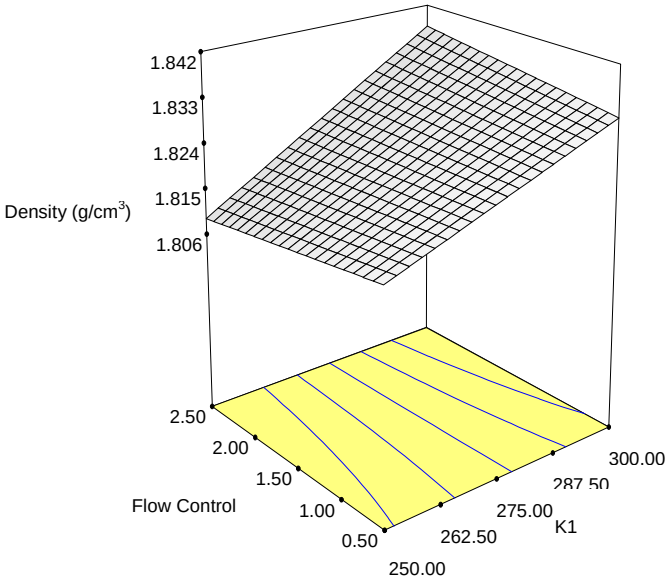

Figure II-15. Density dependence on isostatic pressure and flow rate. All other variables are held at their average. Density depends on the interaction between applied pressure and flow rate. Maximum density is obtained at the highest pressure and flow rate.

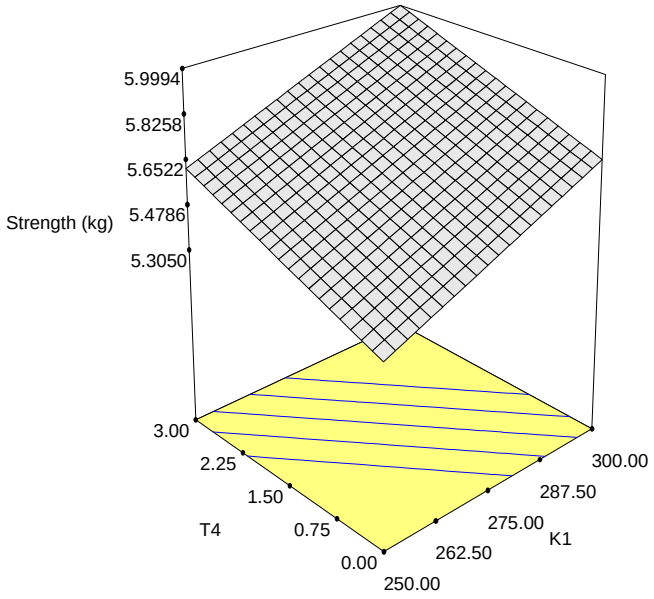

Figure II-16. Strength dependence on isostatic pressure and dwell time at the pressure. All other variables are held at their average. Strength increases linearly with an increase in applied pressure and dwell time at the pressure.

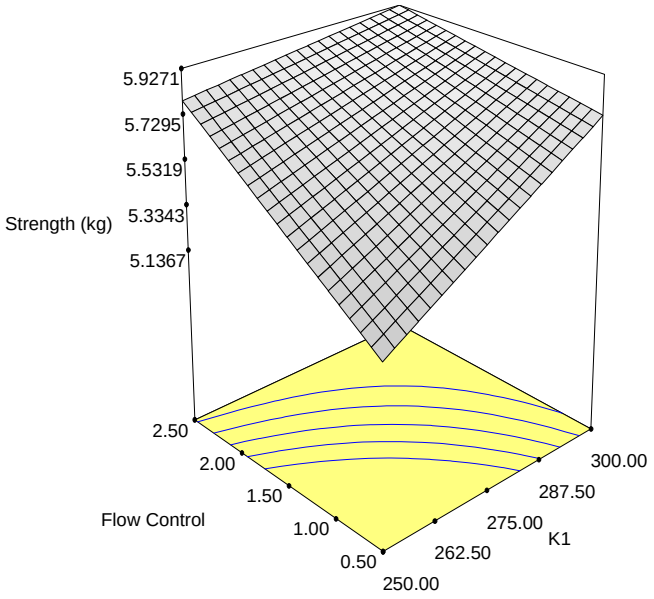

Figure II-17. Strength dependence on isostatic pressure and flow rate. All other variables are held at their average. Strength depends on the interaction between applied pressure and flow rate.

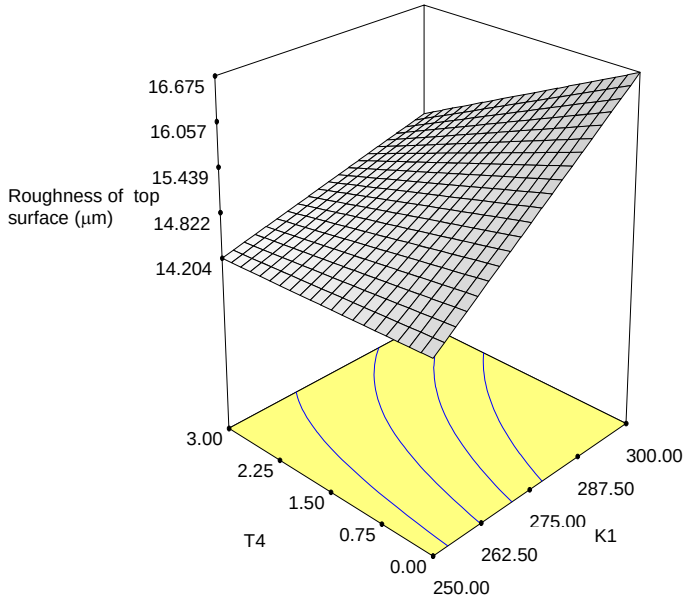

Figure II-18. Dependence of top surface roughness on isostatic pressure and dwell time at the pressure. All other variables are held at their average. Roughness depends on the interaction between applied pressure and dwell time.

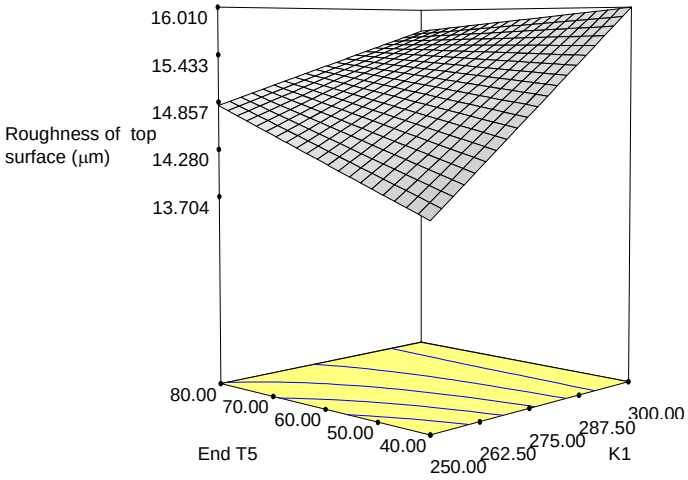

Figure II-19. Dependence of top surface roughness on isostatic pressure and End T5. All other variables are held at their average. There is an interaction between the applied pressure and T5. At low applied pressure level T5 has positive effect on the roughness. At high applied pressure level T5 has negative effect on the roughness.

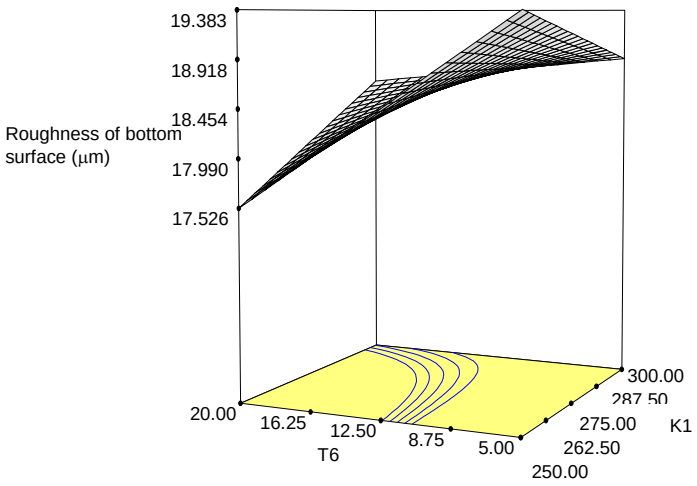

Figure II-20. Dependence of bottom surface roughness on isostatic pressure and T6. All other variables are held at their average. T6 has the most significant effect on the bottom surface roughness.

6. References

1. N. Ninos and W. M. Carty, "Improving Dry Pressing of Commercial Dinnerware," Proposal to NYS Energy Research and Development Authority, Alfred University, Alfred, NY, September, 1999.

2. H. Niffka, "Isostatic Dry Pressing of Flatware," *Am. Ceram. Soc. Bull.*, **59** [12] 1220 (1980).

3. A. P. S. Reymer, "Dry Pressing of Ceramic Powders," pp. 253-257 in Euro Ceramics, Vol. 1, *Processing of Ceramics*. Edited by G. de With, R. A. Terpstra, and R. Metselaar. Elsevier Applied Science, London, UK, 1989.

4. F. W. Dynys and J. W. Halloran, "Compaction of Aggregated Alumina Powder," *J. Am. Ceram. Soc.*, **66** [9] 655-59 (1983).

5. B. J. Briscoe and N. Ozkan, "Compaction Behavior of Agglomerated Alumina Powders," *Powder Technol.*, **90** [3] 195-203 (1997).

6. J. S. Reed, *Principles of Ceramic Processing*; pp. 418-449. John Wiley & Sons, New York, 1995.

7. H. Reh, "Economical Aspects of Dry Pressing," *Interceram*, **40** [4] 218-222 (1991).

8. J. Falcone, Jr., "New Forming Technologies for Ceramic Industry: Isostatic Dry Pressing of Flatware and Pressure Casting for Sanitaryware," *Ceram. Eng. Sci. Proc.*, **10** [1-2] 42-48 (1989).

9. K. Masters, "Applying Spray Drying to Ceramics," *Am. Ceram. Soc. Bull.*, **73** [1] 63-72 (1994).

10. J. S. Reed, "Spray Drying and Implications for Compactibility of Product Granules," *Ceram. Eng. Sci. Proc.*, **18** [2] 343-358 (1997).

11. J. W. Halloran, "Agglomerates and Agglomeration in Ceramic Processing," pp. 404-417 in *Ultrastructure Processing of Ceramics, Glasses and Composites*. Edited by L.L. Hench and D.R. Ulrich. Wiley-Interscience, New York, 1984.

12. J. W. Halloran, "Role of Powder Agglomerates in Ceramic Processing," pp. 67-75 in *Forming of Ceramics*. Edited by J. A. Mangels. American Ceramic Society, Columbus, OH, 1984.

13. E. Carlstrom, "Surface Chemistry in Dry Pressing," pp. 245-278 in *Surface and Colloid Chemistry in Advanced Ceramics Processing*. Edited by R. J. Pugh and L. Bergstrom. Marcel Dekker, New York, 1994.

14. S. J. Lukasiewicz, "Spray-Drying Ceramic Powders," *J. Am. Ceram. Soc.*, **72** [4] 617-24 (1989).

15. S. J. Lukasiewicz and J. S. Reed, "Character and Compaction Response of Spray-Dried Agglomerates," *Am. Ceram. Soc. Bull.*, **57** [9] 798-805 (1978).

16. J. M. Keller, J. D. French, B. Dinger, M. McDonough, B. Gold, C. Cloutier, L. Carinci, E. Van Horn, K. Ewsuk, and W. Blumenthal, "Industry, Government Team to Improve Ceramic Manufacturing," *Am. Ceram. Soc. Bull.*, **77** [10] 52-57 (1998).

17. S. Novak and J. Spino, "The Influence of Processing Additives on the Compaction Behavior of Spray Dried Al_2O_3," pp. 1113-1122 in *Ceramics Today-Tomorrow's Ceramics*. Edited by P. Vicenzini. Elsevier Science Publications, Amsterdam, Netherlands, 1991.

18. W. J. Walker, Jr., J. S. Reed, and S. K. Verma, "Influence of Granule Character on Strength and Weibull Modulus of Sintered Alumina," *J. Am. Ceram. Soc.*, **82** [1] 50-56 (1998).

19. A. Geigle, K. Hauswurz, and S. Mager, "Optimization of Spray-Dried Granulates for Isostatic Pressing of Tableware," *Interceram*, 42 [1] 16-19 (1993).

20. K. N. Kruglitsky, P. V. Kolotiy, and G. Z. Komsky, "Improvement of Spray Drying Efficiency by Controlling Structural and Mechanical Properties of Ceramic Slips," pp. 247-253 in *Ceramic Powders*. Edited by P. Vincenzini, Elsevier Science Publications, Amsterdam, Netherlands, 1983.

21. A. Tsetsekou, C. Agrafiotis, I. Leon, A. Milias, "Optimization of the Rheological Properties of Alumina Slurries for Ceramic Processing Applications," *J. Eur. Ceram. Soc.*, **21** [4] 493-506 (2001).

22. M. Naito, Y. Fukuda, N. Yoshikawa, H. Kamiya, and J. Tsubaki, "Optimization of Suspension Characteristics for Shaping Processes," *J. Eur. Ceram. Soc.*, **17** [2/3] 251-257 (1997).

23. W. J. Walker, Jr., J. S. Reed, and S. K. Verma, "Influence of Slurry Parameters on the Characteristics of Spray-Dried Granules," *J. Am. Ceram. Soc.*, **82** [7] 1711-19 (1999).

24. H. Takahashi, N. Shinohara, M Okumiya, K. Uematsu, T. JunIchiro, Y. Iwamoto, and H. Kamiya, "Influence of Slurry Flocculation on the Character and Compaction of Spay-Dried Silicon Nitride Granules," *J. Am. Ceram. Soc.*, **78** [4] 903-908 (1995).

25. K. J. Konsztowicz, G. Maksym, and H. W. King, "Spray Drying of Dense Aqueous Suspensions of Alumina," pp. 1103-1111 in *Ceramic Today-Tomorrow's Ceramics*. Edited by P. Vincenzini, Elsevier Science Publications, Amsterdam, Netherlands, 1991.

26. S. Baklouti, T. Chartier, and J. F. Baumard, "Mechanical Properties of Dry Pressed Ceramic Green Products: The Effect of the Binder," *J. Am. Ceram. Soc.*, **80** [8] 1992-1996 (1997).

27. T. Busch, D. Schweizer, and C. Sorg, "Spray Granulation of Alumina with Organic Binders," *CFI Ceram. Forum Int.*, **68** [10/11] 527-530 (1991).

28. J. S. Reed and R. B. Runk, "Dry Pressing," pp. 71-93 in *Ceramic Fabrication Processes*. Edited by F. F. Y. Wang. Academic Press, New York, 1976.

29. P.J. James, "Principles of Isostatic Pressing," pp. 1-28 in *Isostatic Pressing Technology*. Edited by P. J. James. Applied Science Publishers, Essex, UK, 1983.

30. P. Popper, *Isostatic Pressing*; pp. 23-32, Heyden & Son Ltd, London, UK, 1976.

31. D. Bortzmeyer, "Dry Pressing of Ceramic Powders," pp.102-146 in *Ceramic Processing*. Edited by R. A. Terpstra, P. P. A. C. Pex, and A. H. de Vries, Chapman & Hall, London, UK, 1995.

32. L. Mattson, "Surface Roughness and Microtopography," pp. 82-100 in *Surface Characterization: A User's Sourcebook*. Edited by D. Brune. Scandinavian Science Publisher, New York, NY, 1997.

33. P. Hariharan, *Basics of Interferometry*; Ch. 2 and 3. Academic Press, San Diego, CA, 1992.

34. I. P. Herman, *Optical Diagnostics for Thin Film Processing*; Ch. 10. Academic Press, San Diego, CA, 1996.

35. A. S. Holik, "Surface Characterization by Interference Microscopy by," pp. 991-1010 in *Analysis Instrumentation: Proceedings of The Annual ISA Analysis Instrumentation Symposium*. Elservier Publications, New York, NY, 1975.

36. J. C. Wyant, C. L. Koliopoulos, B. Bhushan, and D. Basila, "Development of a Three-Dimensional Noncontact Digital Optical Profiler," *J. Tribol.*, **108** [1] 1-8 (1986).

37. New View 5000 Operating Manual OMP-0423E, Zygo Corporation, Middlefield, CT, 1999.

38. Tencor P-10 Surface Profiler Reference, Tencor Instruments, Santa Clara, CA, 1996.

39. Tencor P-10 Surface Profiler Operations Manual, Tencor Instruments, Santa Clara, CA, 1996.

40. F. A. Stevie, “Surface Roughness,” pp. 698-710 in *Encyclopedia of Materials Characterization*. Edited by C. R. Brundel, C. A. Evans, Jr., and S. Wilson. Butterworth-Heinemann, Stoneham, MA, 1992.

41. A. F. von Recum, *Handbook of Biomaterials Evaluation : Scientific, Technical, and Clinical Testing of Implant Materials*; Chs. 8, 13. Taylor & Francis, Philadelphia, PA, 1999.

42. C. R. Perry, Evaluation of Dry Pressing Binders and Plasticizers for Dinnerware Production”, M.S. Thesis, Alfred University, Alfred, NY, 1999.

43. J. M. Bennett and L. Mattson, *Introduction to Surface Roughness and Scattering*; Ch. 2. Optical Society of America, Washington, D. C., 1999.

44. K. J. Moeggenborg, “Springback in Dry pressing: Time, Additive, and Processing Effects,” pp. 217-224 in Ceramic Transactions, Vol. 62, *Science, Technology, and Commercialization of Powder Synthesis and Shape Forming Processes*. Edited by J. J. Kingsley, C. H. Schilling, and J. H. Adair. American Ceramic Society, Westerville, OH, 1995.

7. Appendix

For ¼ fraction of a 2^{6-2} design used in this study sixteen treatment combinations are made out of six factors. Table II-XI shows plus and minus signs for the design. As shown in Table II-XII, ABCE, BCDE, and ADEF are called the generator of this particular fraction. The defining relation for the design is defined as;

$$I = ABCE = BCDF = ADEF$$

where, I is the identity. The defining relation for a fractional factorial is always the set of all columns that are equal to the identity column.

Table II-XI. Construction of the 2^{6-2} Resolution IV Design with the Generators.

	Basic Design					
Run	A	B	C	D	E=ABC	F=BCD
1	-	-	-	-	-	-
2	+	-	-	-	+	-
3	-	+	-	-	+	+
4	+	+	-	-	-	+
5	-	-	+	-	+	+
6	+	-	+	-	-	+
7	-	+	+	-	-	-
8	+	+	+	-	+	-
9	-	-	-	+	-	+
10	+	-	-	+	+	+
11	-	+	-	+	+	-
12	+	+	-	+	-	-
13	-	-	+	+	+	-
14	+	-	+	+	-	-
15	-	+	+	+	-	+
16	+	+	+	+	+	+

Six degrees of freedom generated by the treatment of combinations in the 2^{6-2} design are used to estimate the main effects. Referring to Table II-XII, the linear combinations of the observations are used to estimate the two-factor interactions. For examples,

$$l_{AB} = 1\text{-}2\text{-}3\text{+}4\text{+}5\text{-}6\text{-}7\text{+}8\text{+}9\text{-}10\text{-}11\text{+}12\text{+}13\text{-}14\text{-}15\text{+}16$$

$$l_{CE} = 1\text{-}2\text{-}3\text{+}4\text{+}5\text{-}6\text{-}7\text{+}8\text{+}9\text{-}10\text{-}11\text{+}12\text{+}13\text{-}14\text{-}15\text{+}16$$

It is shown that $l_{AB} = l_{CE}$. Therefore, it is impossible to differentiate between AB and CE. This tells that when AB is estimated, CE is also estimated. Two or more effects that have this property are called aliases. In this example AB and CE are aliases.

The alias structure for this design is easily determined by using the defining relation. The aliases for any column are obtained by multiplying the defining relation to the column. In this example, the alias of AB is

$$AB \cdot I = AB \cdot ABCE = A^2B^2CE$$

The square of any column is the identity I, therefore,

$$AB = CE$$

Table II-XII. Alias Relationships for 2^{6-2} Fractional Factorial Designs.

Design Generators	
E=ABC F=BCD	
Defining relation: I=ABCE=BCDF=ADEF	
Aliases	
A=BCE=DEF	AB=CE
B=ACE=CDF	AC=BE
C=ABE=BDF	AD=EF
D=BCF=AEF	AE=BC=DF
E=ABC=ADF	AF=DE
F=BCD=ADE	BD=CF
ABD=CDE=ACF=BEF	BF=CD
ACD=BDE=ABF=CEF	
2 blocks of 8: ABD=CDE=ACF=BEF	

III. POLYELECTROLYTE ADSORPTION AND SUSPENSION RHEOLOGY

1. Introduction

In the previous chapter press operation related variables encountered in the dry pressing process were studied. In this and next chapters granular feedstock related variables are examined. It is intended to specifically focus on the effect of polymeric additives on suspension property and spray dried granules.

To obtain granules with the desired properties the slurry for spray drying should be well dispersed and contain a high concentration of solids. This also reduces the problem of hollow granules. A slurry with a high solids content is desirable for technical reasons as well as to increase the energy efficiency in drying and the product yield. Dispersant is usually used to prepare a stable slurry of high solids content. In spray drying polymeric additives such as binders, plasticizers, and lubricants are also added into the dispersed slurry. These polymeric additives will be discussed in the next chapter.

Dispersion and flocculation of concentrated suspensions can be controlled through polymer adsorption and conformation. Polyelectrolytes are commonly used as dispersants of ceramic powders in aqueous media. The polyelectrolyte adsorbs at the solid-liquid interface and provides a repulsive force between the particles, which keeps the particles well dispersed. Polyelectrolyte adsorption is highly dependent on the electrostatic interactions between the polyelectrolyte and the surface.

The purpose of this study is to define the relationship between polymer adsorption, conformation, and suspension behavior. In this study the adsorption isotherm of polyacrylic acid (PAA) is measured at pH 6 and 9. Several different molecular weights of PAA are investigated. Also, adsorption kinetics of PAA are studied. The effect of solution chemistry and molecular weight on the adsorption behavior is verified. Viscosity of suspensions is measured with the increase of PAA concentration. The suspension properties are correlated with polymer adsorption and configuration changes.

2. Background Information

2.1 Surface Chemistry of Clay

The major constituent of kaolins and ball clays is kaolinite, which has a 1:1 sheet silicate composed of a $(Si_2O_5)^{-2}$ tetrahedral layer and an $(Al_2[OH]_4)^{+2}$ octahedral layer. The theoretical formula for kaolinite is $Al_2O_3 \cdot 2SiO_2 \cdot 2H_2O$.[1]

Surface charge develops on the kaolinite particles due to the crystal structure and contributes to the colloidal behavior of the particles. The basal surface charge arises from the isomorphic substitution in the lattice. Al^{3+} is commonly substituted for Si^{4+} in the tetrahedral sheet, so an overall negative charge develops in the substituted sheet unless the incomplete charge is balanced. Another way to develop a negative charge is substitution of Mg^{2+} or Fe^{2+} for Al^{3+} in the octahedral sheet.[2-6] The surface charge density created by isomorphic substitutions for two kaolinites, KGa-1 and KGa-2, described as "well crystallized" and "poorly crystallized" were reported as -6.3±0.1 and -13.6±0.5 $mmol_c/kg$, respectively.[4]

When a kaolinite particle is suspended in water, net surface charge develops through a series of acid-base reactions. The sign and magnitude of charge depend on pH of suspension. The mineralogy of kaolinite implies that tetrahedral sheet behaves similar to silica and octahedral sheet behaves similar to alumina. Silica has an isoelectric point (IEP) of 2.0-3.5, and alumina has an IEP of 8.5-10.4. At suspension pH levels above the IEP the particle is net negatively charged; below the IEP, the particle is net positively charged. Hence, between pH of ~3.5 and ~8.5 the silica-like surface is negatively charged and the alumina-like surface is positively charged.[2,4-7]

The crystal structure at the edges of a kaolinite particle is different from that of basal surface. At the edges the tetrahedral sheets and the octahedral sheets are disrupted, the primary bonds (Si-O-Si and Al-O-Al) are broken, and converted to silanol (Si-OH) and aluminol (Al-OH) groups. Charge develops from the protonation/deprotonation of surface hydroxyl groups at the edges and depends on the suspension pH level.[3,8]

The charge characteristics of kaolinite surfaces in aqueous medium can be indirectly studied by potentiometric titration. Potentiometric titration involves the measurement of the net adsorption of H^+ or OH^- at different pH and at different ionic

strength.[9-11] Schulthess and Sparks proposed a back-titration technique which takes account of dissolution reactions, that consume H^+ or OH^- during titration.[10-12]

During the titration ions are released from clay particles into solution. The amount of dissolved ions normally increases as the pH is adjusted away from the original pH. Thus, removal of H^+/OH^- during the titration is not only consumed through surface protonation. This will be a function of: (i) the protonation reaction at the surface, (ii) dissolution-precipitation reactions, and (iii) hydrolysis reactions of dissolved ions through the formation of metallic-hydroxo complexes. Therefore, the titration curve must be corrected for the dissolved ions to measure the amount and the sign of the variable charge (Q_v) in the clay. Consequently,

$$q = f(Q_v) + f(\text{dissolution-precipitation, hydrolysis}) \quad (1)$$

where, q is the net surface charge. It is assumed for this titration procedure that clay particles have very low anion exchange capacity. Accordingly, the protonation reactions involve only surface charged sites that are either neutral or negatively charged.[10-12]

2.2 Poly(acrylic Acid) (PAA)

PAA is prepared by direct polymerization of the appropriate monomer. Monomeric acrylic acid was first prepared by oxidation of acrolein in 1843 and its polymerization was observed in 1872. There are several industrially important methods for preparing acrylic acid. Remarkable progress on the catalytic oxidation of propene to acrylic acid via acrolein has led to almost complete replacement of these earlier processes. Polymerization by conventional free radical techniques is applicable and typical solution polymerization is carried out using water as the solvent. In a typical process a water-soluble initiator such as $K_2S_2O_8$ is added with an activator and a transfer agent. Sodium salt of PAA is prepared by neutralizing poly(acrylic acid) with sodium hydroxide.[13-17] The structure of PAA is shown in Figure III-1.

PAA is available in several different forms including pre-dissolved liquids, stabilized emulsions, and semi-solid gels depending on the application. The utility of PAA is directly related to their chemical structure, functionality, and molecular weight. The acid functional group is highly solvated by water, and is responsible for the solubility

of the polymer in aqueous solutions. The water solubility of these polymers has led to their use in mining, water treatment, dispersing agents for inorganic pigments, and thickeners for polymer latex used for textile finishes and paints. Also, the reactivity of acid groups allows simple chemical modifications, which change the polymer properties and augment the number of applications. The high polymerizability of the monomers allows the preparation of high molecular weight polymers, which are useful as flocculants. When the molecular weight is reduced to 2000-5000 g/mol, the polymers can be used as dispersants for clay slurries, pigments, or paper coating materials.[13,15,18]

PAA is soluble in water and in aqueous salt solutions. Small amounts of organic solvents dissolved in water are sometimes tolerated. The fully neutralized sodium salt has a glass transition temperature at about 250°C. This polymer is stable to moderate heat. PAA can form highly concentrated, aqueous solutions. Solution properties depend on polymer concentration, chemical capabilities, polymer crosslinking and modification, and shear. Solution viscosities increase rapidly with concentration. Above approximately 5% thixotropic solutions that gel with shear are formed. At concentrations approaching 50% stabilized gels are often formed. When dried, most water-soluble PAA form glossy, water resistant coatings and films.[13,16]

PAA is a polyelectrolyte, which is defined as a homopolymer where each monomer carries an ionizable group. PAA can be classified as a weak polyelectrolyte whose behavior in solution depends on pH. When a polyelectrolyte is dissolved in water, it acquires a certain amount of electrical charge. A strong electrostatic force is induced by the charges. The distance between elementary charges on the chain and the concentration of counter-ions in the solution determine the strength and the range of electrostatic. Since the internal repulsion is minimal for a straight line charge, the chain becomes more rigid with the charge development. The counter-ions are subjected to electrical field and to thermal motion and adopt a Boltzmann distribution. It results in a diffuse layer of countercharge around the charged body. The electrical field is screened by the counter-ions and decays rapidly with increasing distance. At low polyelectrolyte charge density the potential follows this charge density nearly linearly. As the charge density increases, the electric field becomes stronger. Thus, part of the counterions are

trapped within very short distances from the polyion and the potential at some distance becomes almost insensitive to the charge density of the polyion.[19]

The potentiometric titration is used to investigate changes of conformation undergone by polyelectrolyte in solution. Plots of pK_{app} vs. α provide the information of conformation changes. pK_{app} is apparent dissociation constant and α is the degree of dissociation of polyelectrolyte. The resulting curve shows two main steps corresponding to the titration of the helix and the coil respectively with a transitional region between them. pK_{app} is calculated as follows.

$$pK_{app} = pH + \log[(1-\alpha)/\alpha] \quad (2)$$

The value of intrinsic dissociation constant, pK_0, is obtained semiempirically extrapolating the curve to zero α.[20]

2.3 Polyelectrolyte Adsorption

The polymer, solvent, and surface play an interactive role on the amount and thickness of the polymer adsorbed.[21] The adsorption energy parameter, χ_S, and the solvency parameter, χ, govern the adsorption of uncharged polymers and the electrostatic interaction is the additional feature of polyelectrolytes. Three main factors, which decide the electrostatic interaction, include the surface charge density, σ_0, the polymer charge, q_m, and the ionic strength, c_s. The polymer charge can be expressed through the monomeric charge:

$$q_m = \tau\alpha e \quad (3)$$

where, α is the degree of dissociation of the polymer, τ takes values of ± 1 and determines the sign of q_m, and e is the elementary charge. The effect of pH may be accounted for in the values of σ_0 and α. Hence, the main parameters controlling the polyelectrolyte adsorption are σ_0, q_m, c_s, χ, and χ_S. c_s is the molar salt concentration.[22]

When the electrostatic force dominates, three situations can occur depending on the sign of charges on surface and polymer. Depletion occurs when σ_0 and q_m have the same sign, only weak adsorption is found on an uncharged surface, and charge compensation takes place when σ_0 and q_m have the opposite sign. The relevant feature of weak polyelectrolytes is that their charge is a function of the local pH. That is, the charge

near the surface is different from that in the bulk. As a result α depends on the distance from the surface. Dissociation of polymers adsorbed on a neutral surface is less than that in the bulk, whereas dissociation on an oppositely charged surface is higher than that in the bulk. The local α adjusts itself such as to effectively neutralize the surface charge.[22]

Linear flexible polymers can assume different conformations at the surface and exhibit varying degree of attachment to the surface.[23] At the solid-liquid interface the polymers lead to a conformation allowing maximum polymer-surface contact. The attachment of one segment increases the probability of neighboring segments being adsorbed and multiple bonding between the polymer and the surface occurs due to the many functional groups per molecule. The result is normally an interfacial conformation consisting of sequences of adsorbed segments (trains) alternating with three dimensional loops extending away from the surface and with the tails.[24]

Somasundaran *et al.* studied the confiormation of PAA adsorbed on alumina particles. As the solids loading in suspension increases, the polymer becomes stretched, suggesting the possibility of stronger interaction between particles with increase in solid loading. The adsorbed polymers become more dangled and/or have more loops or tails with increase in solids loading.[25] The stretching is less at the higher polymer concentration apparently due to crowding of the polymer chains on the particles at the large surface converge and resultant restricted expansion of the adsorbed coils.[26] PAA molecules stretch out with an increase in pH because of the ionization of carboxyl groups and the resultant electrostatic repulsion between charged groups.[27] PAA adsorbed in the stretched form on alumina at high pH could not become coiled because the conformation could not be altered by lowering the pH subsequently. In contrast, the polymer adsorbed in the coiled state at low pH did stretch out when the pH was increased.[24]

2.4 Suspension Rheology

The rheological properties of ceramic suspensions decide the ability of these materials to be processed. It is therefore important to understand analysis and control of the rheological properties of ceramic suspensions.[28,29]

There exist three kinds of forces acting on particles suspended in a medium. The nature and magnitude of forces in the system and the resulting microstructure are responsible for the rheological properties. Three forces include hydrodynamic forces, Brownian forces, and colloidal forces. Hydrodynamic or viscous forces arise from the relative motion of particles to the surrounding fluid, which affect the suspension viscosity via the viscosity of the continuous phase. The Brownian force is the ever-present thermal randomizing force. The force is strongly dependent on particle size, so that it has considerable influence on the particles below 1 μm. Colloidal forces come from the interactions between particles. They can be classified as attractive forces and repulsive forces. The net interaction between the particles is determined by the sum of forces, which are influenced by the nature of the solid particles, the properties of the suspending medium, and any chemical additives. Attractive forces are comprised of van der Waals, electrostatic attractive (oppositely charged surfaces), hydrophobic, bridging, and depletion forces. Repulsive forces are comprised of electrostatic (similarly charged surfaces), steric, hydration, and structural forces.[28-32] The rheological properties of concentrated suspensions are determined by the balance of these forces. The range of interaction is determined by the volume fraction and the size and shape distribution of the particles.[33]

The addition of polymers to a colloidal suspension can cause either flocculation or stabilization of the suspension depending on the amount added, the chemical nature, and the molecular weight of the polymer. If the polymer adsorbs and forms a layer on the surface, this can give rise to a repulsive force, so-called steric stabilization.[29] If the added polymer is polyelectrolyte, the repulsive force is induced by the charge of polymers as well as a physical barrier between the particles. The interaction between particles coated with polyelectrolyte layer is therefore electrosteric.[34]

The rheology is the study of the relation between the applied stress and the resulting deformation on a fluid or plastic system.[35] Shear stress and shear rate can be measured using rotational viscometers. The suspension is placed in the gap between plates and the shear rate is gradually increased by rotation; the torque on the other element is then measured, which allows one to calculate the stress. The most common

flow curve obtained with concentrated structured suspensions is shown in Figure III-2. This curve is characterized by three main parameters: The critical shear rate, $\dot{\gamma}_{cr}$, above which the curve becomes linear, the slope of this linear line, η_{pl}, and the extrapolated yield stress, τ_0. The flow may be analyzed using the Bingham model[36],

$$\tau = \tau_0 + \eta_{pl}\dot{\gamma} \quad (4)$$

It should be mentioned that the flow curve in Figure 2 represents that case where there is no time dependence of stress versus strain.

Concentrated suspensions with mutual attraction between the individual particles often exhibit a yield stress. The aggregation of particles forms flocs and in turn the interaction between flocs results in a continuous three dimensional network structure extending throughout the whole volume. These systems deform elastically with finite rigidity under the application of small stress. However, when the applied stress exceeds the yield value, the network collapses and continuous deformation occurs with the material flowing like a viscous fluid. The yield stress is then the minimum shear stress corresponding to the first indication of flow. The yield stress has been related to the strength of the coherent network structure.[37]

3. Experimental Procedure

3.1 Materials Characterization

3.1.1 Surface Chemistry of Clay

Huntingdon clay provided by United Clays (Brentwood, TN) was used in this investigation. Table III-I lists the chemical composition and physical properties of the clay. The reported chemical analysis of the powders revealed relatively high amount of TiO_2. Surface area measurement was obtained via Brunauer, Emmett, and Teller (BET) theory of nitrogen adsorption.

Table III-I. Chemical Composition and Physical Properties of Huntingdon Clay

	SiO_2	Al_2O_3	Fe_2O_3	TiO_2	CaO	MgO	Na_2O	K_2O	LOI	Surface Area (m^2/g)
Weight percent (%)	44.7	38.3	0.6	2.4	0.1	0.1	0.1	0.1	13.6	20
Normalized based on Al_2O_3	1.98	1.00	0.01	0.08	0.00	0.01	0.00	0.00	2.01	

Potentiometric titrations (ABU900, Radiometer, Cleveland, $OH^{)}$ were carried out for a suspension and a supernatant reference with automatic burette. For a suspension titration two grams of clay were suspended in 80 ml of electrolyte solution (0.01M KNO3) and stirred until a constant pH was obtained. The suspension was then titrated with 0.1M HNO_3 to pH 3 with two minutes equilibration period between each addition of titrant. The suspension was then allowed to equilibrate for one hour before back titrating with standardized 0.5M KOH at a titration rate of one ml/min to pH 10. For the reference titration the suspension was prepared and titrated to pH 3 as described above. The suspension was then centrifuged for 60 minutes at 5000 rpm and the supernatant was filtered. The supernatant solution was allowed to equilibrate 10 min with continuous stirring, then the solution was back titrated as described above. The surface charge due to hydroxyl consumption was calculated by subtracting the OH^- consumption of the reference from the sample back-titration at the same pH.

3.1.2 Potentiometric Study of PAA

Sodium salts of polyacrylic acids having different molecular weights were provided. The properties of these polymers are listed in Table III-II.

The potentiometric titrations were performed on polymer solutions and a blank solution. Before the titration pH probes used in this investigation were calibrated with standards of pH 4.0, 7.0, and 10.0 (Fisher Scientific, Pittsburgh, PA). Thus, some of the points measured were outside the range of calibration. In order to obtain pH titration curves for pH 2-10 solution was titrated with 1 M HCl to pH 2. One minute equilibration period was allowed between each addition of titrant. The suspension was then allowed to

equilibrate for one hour, and then back-titrated with standardized 2M NaOH (Fisher Scientific, Pittsburgh, PA). An identical titration was performed on a blank solution without polymers. The net uptake of hydroxyl ions as a function of pH was obtained by subtracting the blank titration curve from the sample curve.

Table III-II. Reported Properties of Tested PAAs

Dispersants	% Solid	M.W. (g/mol)	PDI*	Sources
Acumer 1010	44	2000	1.27-1.3	Rohm and Haas
Acumer 9400	42	3600	1.27-1.6	Rohm and Haas
Acusol 445N	45	4500	1.27-1.3	Rohm and Haas
Acusol 410N	40	10000	1.27-1.3	Rohm and Haas
Acumer 1510N	27	55000	1.27-1.3	Rohm and Haas
Darvan 811	43	3500-6000	1.5	R. T. Vanderbilt

* PDI : Polydispersity Index

3.2 Polymer Adsorption

Adsorption isotherms of PAA on clay particles were determined by the solution depletion method.[22] Huntingdon clay and PAAs of different molecular weights were used for this study. Suspensions at 15v/o were prepared by mixing clay in de-ionized water with increasing polymer concentration from 0 to 0.6 mg/m^2 based on clay surface area. The suspensions were adjusted to target pH values of 6 and 9 with tolerance of ±0.2. The suspensions were mixed in shaker bath for 24 hours. Suspensions were then centrifuged at 5000 rpm for 60 minutes, and the supernatant was removed without disturbing the sediment. The supernatants were adjusted to pH 10 using NaOH and then titrated with 0.25M HCl to pH 2. The amount of PAA in solution was determined by using calibration curves for PAA. All the calibration curves are shown in Figure III-3. The adsorbed amount was calculated as the difference between the added amount of polymer and the amount of polymer remaining in solution:

$$\Gamma^{ex} = \Delta C_p V / A_s \quad (5)$$

Adsorption kinetics of PAA on clay particles were studied by constructing adsorption isotherms at different adsorption times. Huntingdon clay and PAA with

molecular weight of 2000 g/mol were used for this study. Suspensions were prepared at two polymer concentration levels, 0.1 and 0.3 mg/m^2 and adjusted to pH 9. Suspensions were kept on a shaker table from 6 hours to 10 days. The adsorbed amount was determined as described above.

3.3 Suspension Characterization

3.3.1 Viscosity

Suspensions were prepared at 35 v/o solids loading by mixing the Huntingdon clay in distilled water. PAA was first dissolved in water and equilibrated for 10 minutes, and then clay was added slowly. Samples at different polymer concentrations from 0 to 1.0 mg/m^2 were prepared. The pH of the suspension was not adjusted. The pH of the suspension without PAA was 4.08 and the highest pH with the addition of PAA was 6.8.

Viscosity measurements were made using a strain-controlled rheometer (Advanced Rheometric Expansion System, Rheometric Scientific, Inc., Piscataway, NJ) and software (RSI Orchestrator Version V6.4.3, Rheometric Scientific, Inc., Piscataway, NJ). A steady state stress sweep test from high to low rates with 25 mm parallel plates was used for all viscosity measurements. Shear stress and strain rates were calculated via:[30]

$$\tau = M\left(\frac{2000G_c}{\pi R^3}\right) \tag{6}$$

and

$$\dot{\gamma} = \dot{\theta}\frac{R}{h} \text{ (maximum shear rate)}, \tag{7}$$

where M is the moment of inertia, G_c is the gravitational constant, R is the radius of the plates, $\dot{\theta}$ is the actual rate of angular displacement of the motor in radians, and h is the gap between the plates. The apparent viscosity η was then calculated:

$$\eta = \frac{3000MG_c h}{2\pi R^4 \dot{\theta}}\left[1 + \frac{d\ln 1000MG_c}{3d\ln\dot{\theta}}\right] \tag{8}$$

Assuming that

$$\frac{d \ln 1000 MG_c}{d \ln \dot{\theta}} \approx 1, \tag{9}$$

and

$$\eta = \frac{2000 \mathrm{MG_c h}}{\pi \mathrm{R}^4 \dot{\theta}} \tag{10}$$

3.3.2 Zeta Potential Measurement

The ζ-potentials were obtained through electroacoustic means (ESA-8000 AcoustoSizer, Matec Applied Sciences, Hopkinton, MA) on 5 v/o suspensions. All pH adjustments were made using the automatic titration system accompanying the AcoustoSizer.

The instrument makes an assumption of spherical particles for zeta-potential calculations. It could be argued that the measurement techniques are not valid for these suspensions due to the plate-like shape of kaolinite particles. A theory has been developed for spheroid geometries, i.e. disc and rods, and demonstrated that spherical results with radius (r) are similar to a spheroid with an effective radius of (r).[38] Kaolinite particles have oppositely charged basal plane surfaces, and it is proposed that kaolinite particles should exhibit a tumbling motion in an alternating electric field, thus approximating a spheroid particle morphology. If the proposal that a kaolinite particle exhibits a spheroid morphology is invalid, the applicability of the zeta potential results obtained from acoustophoretic mobility measurements may be limited. However, measurements have been found to be self-consistent with the relative magnitudes being similar for similar colloidal species. The zeta potential trends should be a reasonable illustration of behavior.[39]

4. Experimental Results and Discussions

4.1 Clay Surface Charge

The acid-base potentiometric titration results for Huntingdon clay are shown in Figure III-4. Protonation/deprotonation on alumina-like surface and at edges and ion exchange at the silica-like surface are primarily involved in the charge variations over the pH range 4 to 10. At pH<7.5 the charge variation can be assigned to the protonation at the edges and alumina like surface and ion exchange at silica like surface. At pH>7.5 the rising part of the curve is assigned to the negative ionization of aluminol groups.[10,11]

4.2 Ionization of PAA

The degree of ionization of PAA is calculated from the net uptake of hydroxyl ions and is shown as a function of pH in Figure III-5. It is known that the potentiometric titration curve of the PAA is essentially independent of molecular weight because the dissociation is determined by short range electrostatic interactions.[40] All the titration curves for PAA show similar trends and there is a slight increase in ionization with decreasing molecular weight in the intermediate degree of dissociation (α). PAA starts to ionize around pH 3 and is fully ionized at pH 10. The most visible consequence of ionization is the solubility in water.[41] The polymer charge becomes strong enough to overcome the chain hydrophobicity at high pH, thereby making hydrophobic acids water soluble. Unlike low molecular weight acids the charged groups on polyacids are correlated because they are linked together along the chain. Therefore, as charge density on the chain varies, the chain conformation is affected and, in turn, influences the dissociation of other groups.

Using the data in Figure III-5 the apparent dissociation constant, pK_{app}, is calculated and plotted in Figure III-6 as a function of α. A pK_0 value can be obtained by extrapolating the linear portion of the plot at low α to the y-axis. The estimated pK_0 values are summarized in Table III-III. All the values are close to the reported pK_0 value of carboxylic acid group, 4.6.

Table III-III. The Estimated pK_0 Values of PAAs.

Polymers	Acumer 1010	Acumer 9400	Acusol 445N	Acusol 410N	Acumer 1510N	Darvan 811
M.W. (g/mol)	2000	3600	4500	10000	55000	3500-6000
pK_0	4.6	4.5	4.6	4.8	4.7	4.4

An important characteristic of polyelectrolytes is their structural transition as charge density increases along the flexible chain; polyelectrolyte molecules undergo expansion from a coiled to a stretched conformation. The polyelectrolyte chains are coiled due to van der Waals attractive forces and hydrogen bonding between segments, and the cooperative transition occurs due to electrostatic repulsion between neighboring ionized sites.[42] Mathieson and McLaren identified the transition of PAA in titration data.[20] They distinguished four regions in the titration curves, similar to Wada's study on the helix-coil transition of polyglutamic acid. The four regions were associated with conformational changes in PAA. As shown in Figure III-6, the first short region shows a drop off and is probably due to some instability in the solution, such as aggregation preceding precipitation. The second region (B) corresponds to the ionization of the coiled state. The third region (C) represents the transition region that is associated with coil expansion. The fourth region (D) represents ionization of the stretched state.

4.3 Adsorption Isotherm

The adsorption isotherm of PAA on Huntingdon clay was determined from suspension without added salt. Figure III-7 shows one of the adsorption isotherms obtained from this study. The adsorption isotherm fits a Langmuir type if it is plotted alternately with equilibrium concentration as the x-axis.[43] The adsorption isotherm of PAA deviates from the 100% adsorption line and reaches a plateau around polymer concentration of 0.3 mg/m^2. The adsorption density at the plateau is 0.13 mg/m^2.

Polyelectrolyte adsorption is highly dependent on the electrostatic interactions between the polyelectrolyte and the surface. The pH determines the degree of dissociation and the conformations of PAA in solution as well as the sign and density of

charges on the kaolinite particle surface. At pH 6 about 50 % of functional groups on PAA are dissociated and PAA is negatively charged. The PAA forms coil compact in solution. At pH 6 the alumina-like surface of kaolinite will be positively charged and there are also a few positive sites present on the edges. Polymer adsorption occurs due to the electrostatic interactions between them. Figure III-8 shows that the adsorption of the negatively charged polymer decreases the zeta potential. This confirms previous work that electrostatic forces are mainly responsible for the adsorption of PAA on clay.[44]

The gray line on Figure III-7 indicates 100 % adsorption of polymer. The adsorption isotherm slightly diverges from the 100 % adsorption line. The slope of the isotherm curve in this region depends on the binding energy between the polymer and the particle surface as well as the type of bonding.[21,45]

The rounded portion of the isotherm curve is explained by the polydispersity of polymer. When polymer concentration is low, all polymer chains can adsorb on the surface. As the polymer concentration increases, adsorption saturation is reached and the adsorption becomes preferential. This means that longer molecules displace smaller molecules on the surface. Therefore, the increase in adsorption with polymer concentration is not primarily due to the polymer concentration, but associated with the increase of the average molecular weight of the adsorbing fraction. A few studies have shown that the adsorption isotherm curve becomes more "rounded" with the mixture of polymer fractions whereas they have a very sharp high affinity type for monodisperse polymer.[22,46]

4.4 Adsorption Kinetics of PAA (m.w. = 2000)

The adsorption kinetics of PAA onto Huntingdon clay was determined at two polymer concentrations, 0.1 and 0.3 mg/m^2. These two polymer additions correspond to the maximum amount of polymer adsorbed and the amount of polymer necessary to achieve the plateau region, respectively. The pH of all the suspensions was kept at 9.0 ± 0.2. Mixing time of suspensions was from six hours to ten days since there is a relatively large uncertainty for short mixing times due to the time needed for centrifugation.

Figure III-9 shows the change in adsorption with time. The adsorbed amount at polymer concentration of 0.1 mg/m^2 increases rapidly over 24 hours and reaches a plateau region. For polymer concentration at 0.3 mg/m^2 polymer adsorption seems to increase over the entire test period. The adsorbed amount at polymer concentration 0.3 mg/m^2 is slightly lower than that for polymer concentration at 0.1 mg/m^2.

The dependence of adsorption on time at different polymer concentrations may be affected by the displacement of initially adsorbed small polymer molecules by higher molecular weight ones. For polymer concentration of 0.1 mg/m^2 most polyelectrolyte molecules adsorb on the surfaces and the number of longer molecules left in solution will be small. Accordingly, the displacement of small molecules on the surface with longer ones will be minimal. However, in the case of polymer concentration 0.3 mg/m^2, there will be a relatively large number of longer molecules in solution. Therefore, an exchange process will occur with time.

It is noteworthy to explain the kinetic aspect of polyelectrolyte adsorption to understand the exchanging process in polyelectrolyte systems. Theoretical calculations predict the preferential adsorption of the high molecular weight fraction of polydisperse uncharged homopolymers, and the results are confirmed by several experiments.[47-50] However, a difference is shown from the experimental results with polyelectrolyte. A. de Laat and G. van den Heuvel summarized experimental results and proposed the mechanism of displacement in polyelectrolyte systems.[51] The difference is that the electrostatic barriers formed on particles by the adsorption of charged polyelectrolytes hinder the displacement of small molecules by longer ones. When no electrostatic interaction is involved, an exchange process is caused by the diffusion and concentration of the chains in various lengths in solution. For polyelectrolytes the total charge of the PAA covered surface of the particles and the total charge on the chain in the solution determine the height of the electrostatic barriers. The charge on the chain is directly related to chain length and solution pH. Assuming preferential adsorption of the longest chains in thermodynamic equilibrium, an exchange process will begin directly after initial adsorption occurs. However, the diffusion of polyelectrolytes towards the surface is effected by the electrostatic barrier; the longer the chains the less chance they have of

reaching the surface. Polymers above a certain chain length will have too high of an electrostatic barrier and displacement of lower molecular weight will not occur. In a study of PAA adsorption on $BaTiO_3$ the limiting molecular weight is reported around 48000 g/mol. Also, the addition of salt facilitates the exchanging process by screening the charges. As the salt concentration increases, more short chains are displaced by longer ones. Therefore, in the system studied here an exchange process occurs and the process is accelerated with the dissolution of cations from clay.

4.5 The Effect of Suspension pH and Molecular Weight of PAA on Adsorption

The adsorption isotherms of PAA of different molecular weights were determined at pH 6 and 9. The mixing time was 24 hours for all suspensions.

Figures III-10 and III-11 show the adsorption behavior of PAA at pH 6 and 9. The adsorption plateau for tested PAAs ranges from 0.03 to 0.08 mg/m^2 at pH 9, and from 0.1 to 0.16 mg/m^2 at pH 6. The dependence of adsorbed amount on the molecular weight of PAA is not shown.

As pH increases, the net positive surface charge on alumina-like surface decreases while PAA is fully dissociated and negatively charged. Therefore, adsorption of PAA decreases. As reported earlier, at pH 6 the adsorbed polymer chains exhibit a coiled conformation. As the pH increases, the adsorbed PAA stretches out.[25] The stretching is less at the higher polymer concentration apparently due to crowding of the polymer chains on the particles at the higher surface coverage and resultant restricted expansion of the adsorbed coils.

The adsorption behavior of PAA on silica-like surface may be assumed from the PAA adsorption study on silica. Small amounts of PAA adsorb on silica in the acidic condition. However, PAA is completely desorbed from the surface with increasing negative surface charge and increasing dissociation.[52] Therefore, in the suspensions tested here the adsorption of PAA on silica-like surface will be negligible.

The adsorbed amount was lower than expected at both pH 6 and 9. A kaolinite particle is composed of a silica-like and an alumina-like surfaces with edges of a mixture of alumina and silica sites. The behavior of each surface in water is similar to silica and

alumina, respectively. Polymers were presumed to primarily adsorb on the edge of the clay particles. However, Carty proposed that polymer adsorption occurs on a basal surface rather than the edge based on the relative adsorption limits and SEM analysis.[7] PAA also has a weak affinity for silica surfaces. Therefore, polymers will adsorb on the alumina-like surface as well as the edge of the clay platelet. Assuming the adsorption on one basal plane and the platelet edge, when normalized for the specific surface area of the powder, the adsorption limit for clay is expected to be 59% of the polymer adsorbed on an alumina surface. This value is based upon an aspect ratio of 0.095 (2L:h) for the clay platelet. PMAA has very similar chemical structure and adsorption behavior to PAA. The adsorbed PMAA amount on alumina particles was ~0.35 mg/m^2 at pH 9 and ~0.7 mg/m^2 at pH 6.[53] Therefore, expected adsorption on clay particles is 0.21 mg/m^2 at pH 9 and 0.41 mg/m^2 at pH 6. However, the experimental value was much lower than the expected values. The discrepancy was greater at pH 9.

Table III-IV. Maximum Adsorbed Amount of PAAs at Different pH of Suspensions.

	M.W. (g/mol)	pH 6 (mg/m^2)	pH 9 (mg/m^2)
Acumer 1010	2000	0.13	0.05
Acumer 9400	3600	0.13	0.05
Acusol 445N	4500	0.10	0.03
Acusol 410N	10000	0.12	0.03
Acumer 1510N	55000	0.16	0.05
Darvan 811	3500-6000	0.14	0.08

It is proposed that the discrepancy is caused by the interference of organic matter in the clay. The loss on ignition (LOI) of Huntingdon clay is reported as 13.6 %. Figure III-12 shows the TGA analysis of Huntingdon clay. Based on the chemical formula of kaolinite, LOI is believed to be mostly from physically and chemically adsorbed water. However, a small amount of organic material still exists in the clay. It is known that humic substances constitute 70 – 80 % of the organic matter in most mineral soils.[54] Accordingly, the organic matter in Huntingdon clay is proposed to be the humic

substances. Humic substances are structurally complex macromolecules. The mass distribution of humic substances can range from thousands to tens of thousands, and even higher. They have a yellow to black appearance, and are acidic and generally heterogeneous. The structure of humic substances is not well defined. Humic substances are classified into three classes based on operational definitions; fulvic acid (FA), humin, and humic acid (HA). Only HA and FA are considered here; the simplified structures of these two substances are shown in Figure III-13. The HA and FA are differentiated by their solubility at different pH. HA are soluble at pH>2 while FA are soluble in water under all pH conditions. HA has higher molecular weight than FA. It is known that HA and FA can bind metal ions from dissolved rocks and minerals and can interact with other soil components such as clay particles.

HA and FA are a mixture of heterogeneous polyelectrolytes. The adsorption of HA and FA on clay particles is known to occur by electrostatic and specific interactions. Schulthess and Huang showed that HA and FA strongly adsorbed on kaolinite from pH 2 to 10. They determined that adsorption occurred mostly on the alumina-like surface of kaolinite by comparing with the adsorption on silica and alumina.[55] Jones and Bryan also reported that the adsorption of HA decreases with increase in pH.[56] From these it can be concluded that PAA should compete with pre-absorbed HA and FA molecules for adsorption. This potentially explains the low adsorption values for PAA. At pH 9 there will be a very limited extent of adsorption sites on kaolinite particles. Therefore, the competition between PAA and HA and FA for adsorption will be strong. This explains the higher discrepancy at pH 9. In addition, carboxyl groups on dissolved HA and FA interact with OH^- during titration of supernatant, which results in the false amount of unadsorbed PAA. This leads to low adsorption amount of PAA.

An observation was made during the sample preparation that a dark brown supernatant was obtained from suspensions of pH 9, and a light brown supernatant was separated from high polymer concentration suspensions at pH 6. This suggests that desorption of HA and FA at high pH results in the dark brown color supernatant. At pH 6 most HA and FA are believed to adsorb on the kaolinite surface. However, at the high polymer concentration the displacement of small HA and FA on particle surface with

longer PAA molecules occurs and gives light brown color supernatant. Some residue was observed at the bottom of solution after titration was performed down to pH 2 for both supernatants obtained from suspensions at pH 6 and 9. This is believed to be the precipitation of HA at acidic conditions. Schulthess and Huang showed that the precipitation starts around pH 3.

The adsorption isotherms of each PAA at pH 9 and 6 were plotted in Figures III-14 - III-19. At both pH values the polymer adsorption follows the same slope at low polymer concentrations, and the adsorption curve at pH 6 goes further and reaches the plateau. The same slope may suggest the same adsorption affinity at both pHs.[57] The long rounded portion at pH 6 may be related to the preferential adsorption. Vermeer and Koopal noted that the molecular weight dependence in the preferential adsorption increases with decreasing pH.[58]

At both pH values the adsorbed amount does not essentially depend on the molecular weight. Blaakkmeer *et al.* developed adsorption model of weak polyacids at a charged surface in a low ionic strength medium. They expected a weak dependence on chain length at slightly higher pH values near pK_0 value and no dependence at high pH values.[59]

4.6 Suspension Rheology

The steady shear properties of Huntingdon clay with polyacrylic acid addition were determined. PAAs of different molecular weight were added into the suspension up to 1.0 mg/m^2. The pH of each suspension was measured, but not adjusted for these experiments.

Figures from III-20 to III-25 show the dependence of the viscosity on the shear rate with the addition of PAA. All the suspensions show shear thinning behavior in which viscosity decreases with shear rate. The viscosity of suspension without PAA decreases linearly with shear rate. Firth and Hunter explained this phenomenon as a result of the increasing liquid volume released by breaking the agglomerates.[60,61] At pH 4.08, which is the pH of Huntingdon clay suspension without PAA, clay particles exhibit different charges on each surface. Clay particles flocculate and form agglomerates in

suspension. The liquid within the agglomerates is relatively immobile since it flows with the agglomerates. The agglomerates break down during shearing, i.e. the large agglomerate breaks into smaller agglomerates, and the liquid kept inside is released. This results in a decrease of the effective solids loading and a decrease in viscosity. However, other researchers explained that the shear thinning region is associated with the formation of a shear induced layer structure or ordered liquid like string structure.[28,30] With the increase of shear rate the imposed velocity gradient induces an orientation of the particle structure. The orientation enables particles to move past each other more freely than at low shear rates.

The decrease in viscosity and degree of shear thinning with the addition of PAA implies a decrease in the degree of flocculation. The charged PAA adsorbs on the oppositely charged surface sites of clay particles and exhibits short-range repulsion. Both steric and electrostatic forces may contribute to the overall repulsion. The charge density and the conformation of PAA are altered by adjusting the solution conditions.[28] Under acidic conditions, where all the tested suspensions were prepared, ionization of PAA is relatively small and PAA forms a compact coil.[62]

Around 0.2 mg/m^2 PAA concentration most suspensions reach the minimum viscosity. Figure III-26 shows that the zeta potential reaches the plateau region around 0.2 – 0.3 mg/m^2 PAA addition. The adsorption isotherm at pH 6 also indicates that plateau is reached around this polymer concentration. This suggests that electrostatic repulsion by adsorbed polyelectrolyte is high enough to overcome attractive forces. In addition, the adsorbed polymer layer on the surface is strong and sufficiently thick with high surface coverage, thus, steric repulsion occurs.

With further addition of PAA the viscosity of suspensions increases, this reflects a transition from stabilization to flocculation. For long chain polymers bridging is most likely to happen. When non-adsorbing polymers exist in the suspension, depletion flocculation could arise as the particles approach and the polymers are excluded from the gap due to an osmotic pressure gradient between the particles.[28] Other possibilities could be due to an increase in ionic strength, which may weaken the electrostatic repulsion, and/or the increase in the medium viscosity due to the increase of the free polymer. At

higher dispersant levels the dispersants themselves contribute enough ions to the suspension to achieve the critical coagulation concentration.[63]

In the case of PAA with m.w.=55000 g/mol there is a slight difference in the shear thinning behavior. The degree of shear thinning is less than other polymers tested at the polymer concentration of 0.2 mg/m^2, this seems to be related to the high molecular weight.

The apparent viscosity was obtained by extrapolating to the shear rate at 1.0 s^{-1}. Figure III-27 shows the apparent viscosity of suspensions with the addition of PAA. All the suspensions with PAAs show the minimum viscosity at 0.2 mg/m^2. The minimum viscosity was plotted versus molecular weight in Figure III-28. The lowest viscosity was obtained at molecular weight of 10000 g/mol. This suggests an optimum chain length of PAA for effective dispersion. The increase in viscosity at higher polymer concentrations is dependent on the molecular weight of the polymers. PAA of the highest molecular weight (m.w. = 55000 g/mol) shows the lowest dispersability.

Guo suggested that the evaluation of suspension stability by merely the measurement of apparent viscosity at a fixed shear rate can be misleading in some cases.[57] When the viscosity was plotted versus shear rate, a few cases showed that level of viscosities for two suspensions was reversed depending on the shear rate where the measurement was made. Therefore, flow curves were plotted as shear stress versus shear strain and the linear portion was extrapolated to the axis to measure shear yield stress. Measured shear yield stresses are listed in Table III-V and flow curves at two polymer concentrations are shown in Figures III-29 - III-30.

The degree of shear yield stress reduction is dependent on the PAA molecular weight and concentration. Shear yield stress decreases with increasing additive concentration. At a given low polymer concentration 0.05 mg/m^2 the shear yield stress tends to decrease with decreasing molecular weight. The theory of polyelectrolyte adsorption predicts a conformation of loops and tails for low charge or neutral polymers. Accordingly, adsorbed PAA would provide a thick barrier at low pH. However, the surface should be covered effectively. At low polymer concentrations the low molecular weight PAA can cover the surface more effectively than is high molecular weight. At a

given concentration the number of molecules is higher for lower molecular weight polymers than higher molecular weight polymers.

Table III-V. Log Shear Yield Stress of Suspensions.

Polymer concentration (mg/m^2)	Acumer 1010 (Log [Pa])	Acumer 9400	Acusol 445n	Acumer 410n	Acumer 1510n	Darvan 811
M.W. (g/mol)	2000	3600	4500	10000	55000	3500-6000
0.0	$4.46x10^{2}$	$4.46x10^{2}$	$4.46x10^{2}$	$4.46x10^{2}$	$4.46x10^{2}$	$4.46x10^{2}$
0.05	$2.03x10^{2}$	$1.77x10^{2}$	$1.88x10^{2}$	$2.01x10^{2}$	$2.89x10^{2}$	$2.19x10^{2}$
0.1	$5.63x10^{0}$	$8.22x10^{-1}$	$1.29x10^{0}$	$1.01x10^{0}$	$9.84x10^{1}$	$1.86x10^{0}$
0.15	$1.02x10^{-1}$	$5.04x10^{-2}$	$6.62x10^{-2}$	**$1.10x10^{-2}$**	$6.48x10^{0}$	$2.36x10^{-1}$
0.2	**$1.00x10^{-2}$**	**$4.72x10^{-2}$**	**$6.36x10^{-2}$**	$3.94x10^{-2}$	**$1.28x10^{0}$**	**$5.79x10^{-2}$**
0.3	$1.20x10^{-1}$	$2.46x10^{-1}$	$1.48x10^{-1}$	$1.98x10^{-1}$	$2.08x10^{0}$	$2.82x10^{-1}$
0.4	$2.90x10^{-1}$	$3.92x10^{-1}$	$4.91x10^{-1}$	$1.14x10^{0}$	$2.35x10^{0}$	$5.81x10^{-1}$
0.5	$6.64x10^{-1}$	$9.53x10^{-1}$	$1.15x10^{0}$	$1.94x10^{0}$	$3.32x10^{0}$	$5.57x10^{-1}$
0.6	$9.06x10^{-1}$	$1.53x10^{0}$	$1.66x10^{0}$	$2.56x10^{0}$	$4.12x10^{0}$	$9.40x10^{-1}$
0.7	$1.20x10^{0}$	$1.99x10^{0}$	$2.15x10^{0}$	$3.10x10^{0}$	$4.57x10^{0}$	$1.32x10^{0}$
0.8	$1.39x10^{0}$	$2.32x10^{0}$	$2.68x10^{0}$	$3.61x10^{0}$	$5.24x10^{0}$	$1.71x10^{0}$
0.9	$1.60x10^{0}$	$2.79x10^{0}$	$3.11x10^{0}$	$4.06x10^{0}$	$5.77x10^{0}$	$2.19x10^{0}$
1.0	$1.80x10^{0}$	$3.20x10^{0}$	$3.39x10^{0}$	$4.15x10^{0}$	$6.49x10^{0}$	$2.37x10^{0}$

The shear yield stress of suspensions is plotted versus polymer concentration in Figure III-31 and strong similarity with Figure III-27 is found. It was earlier suggested that it could be misled in analyzing viscosity data by obtaining apparent viscosity. However, no crucial difference is shown in using either apparent viscosity or shear yield stress as the rheological property of suspensions.

5. Conclusions

This study confirms the relationship between polymer adsorption and suspension rheology. The adsorption of PAA on clay particles decreases with increase in pH. The surface charge of the clay particle and the polymer conformation change due to polymer charge explain the adsorption behaviors of PAA on clay particles. However, it is shown

that organic matter in clay interferes the adsorption of PAA and results in lower adsorption amount. It is suggested that the HA and FA in clay compete with PAA for adsorption and dissolved HA and FA are counted as PAA in supernatant during titration. The PAA adsorption amount is not influenced by the molecular weight of PAA. A kinetic study of PAA adsorption reveals that the polymer adsorption is influenced by the displacement of initially adsorbed PAA.

PAA adsorption on clay particles decreases the viscosity of suspensions. Clay suspensions show the minimum viscosity at a certain amount of PAA addition, which suggests that electrostatic force and sufficient coverage of particles with PAA are necessary for stable suspensions. Also, there is an optimum chain length of PAA for effective dispersion. It is shown that either shear yield stress or apparent viscosity can be used in analyzing the rheological property of suspensions.

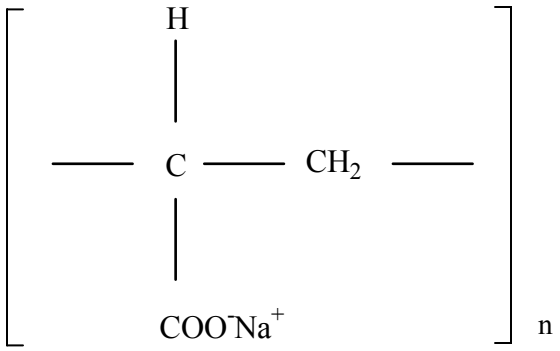

Figure III-1. Schematic illustration of the sodium salt of Poly(acrylic acid) structure. Carboxylic acid group dissociates depending on the solution pH, resulting in the change in conformation of the polymer.

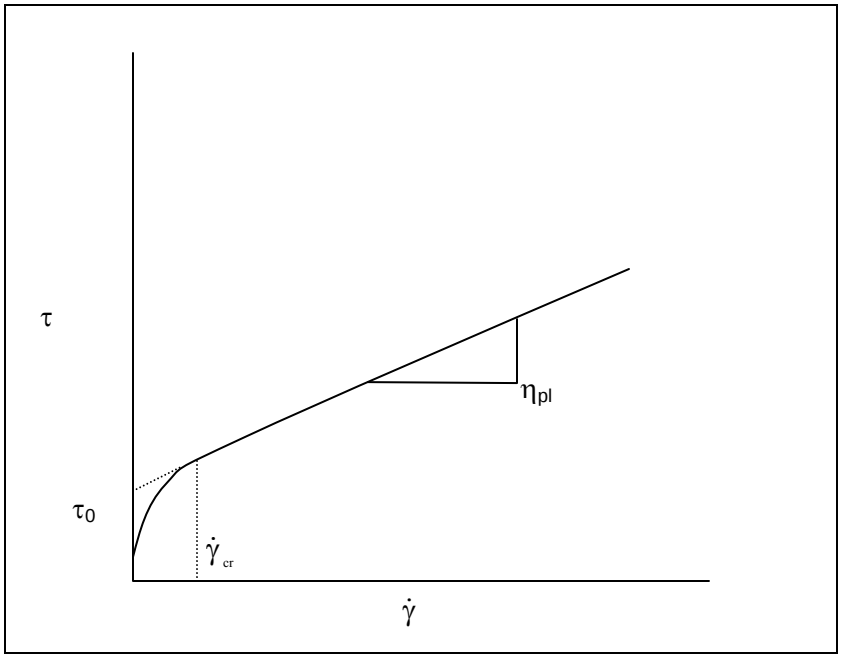

Figure III-2. Flow curve for a pseudoplastic system. τ is shear stress and $\dot{\gamma}$ is shear rate. Above the critical shear rate ($\dot{\gamma}_{cr}$) the curve becomes linear. The extrapolation to the Y-axis is yield stress (τ_0).

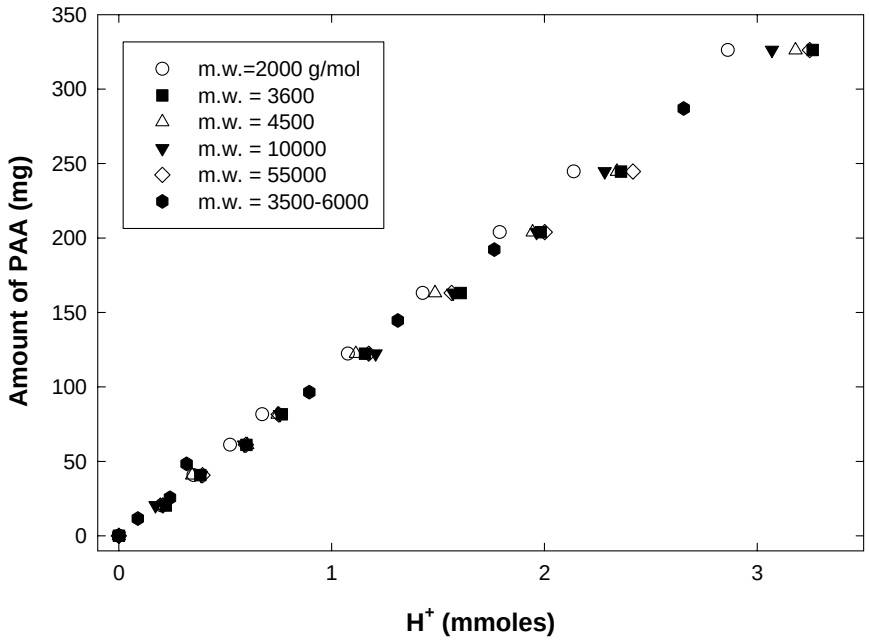

Figure III-3. Calibration curves for the tested PAAs to determine the adsorption isotherm. The relationship between the amount of polymer solution and the concentration of H^+ necessary to completely titrate the PAA was calculated so that the concentration of PAA in an unknown solution could be determined.

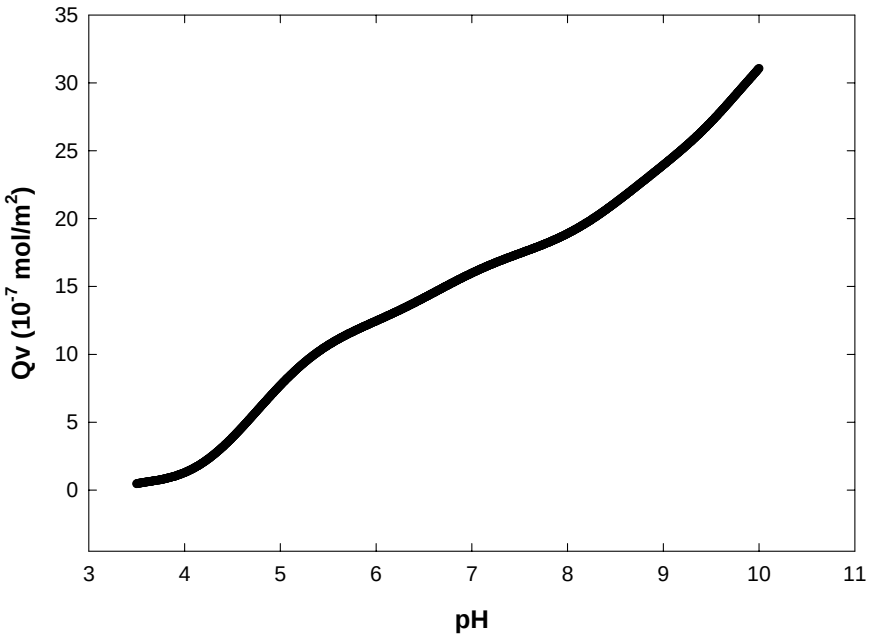

Figure III-4. Surface charge of Huntingdon clay with respect to pH. Protonation/deprotonation on alumina-like surface and at edges and ion exchange at the silica-like surface are primarily involved in the charge variations.

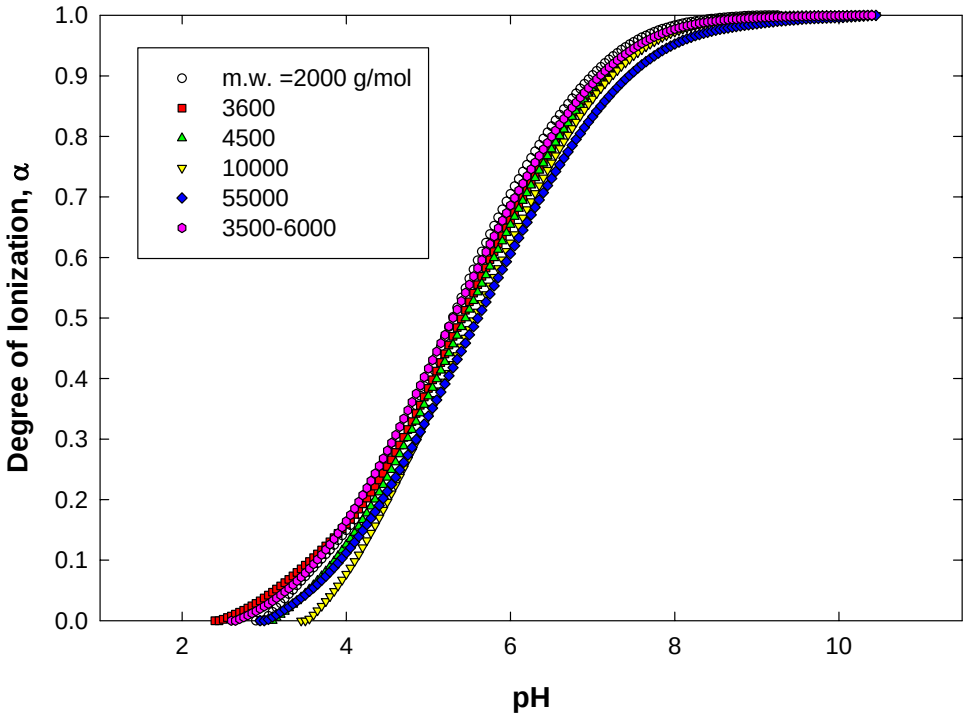

Figure III-5. Degree of ionization (α) of PAAs with pH. Degree of ionization of PAA is essentially independent of molecular weight.

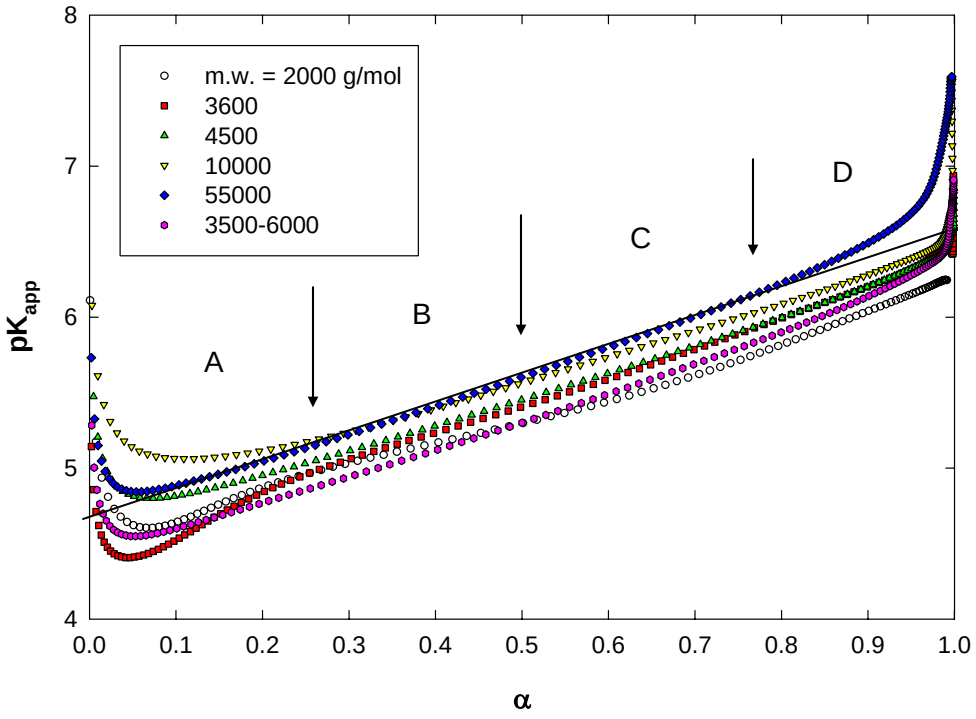

Figure III-6. Apparent dissociation constant (pK_{app}) vs. degree of ionization (α). pK_0 value is obtained by extrapolating the linear portion of the plot to the Y-axis. The four regions denoted as A, B, C, and D are associated with conformational changes in PAA.

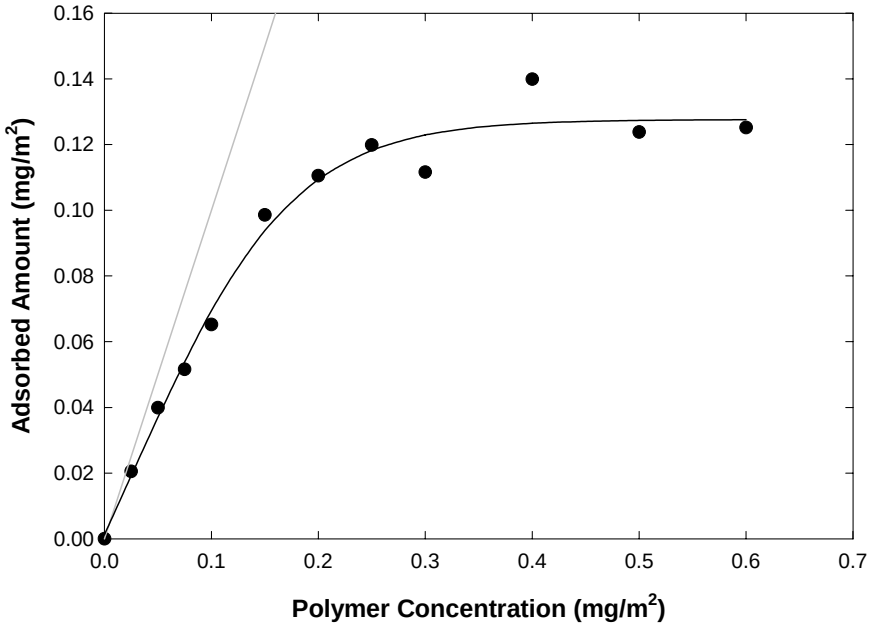

Figure III-7. Adsorption isotherm of PAA (m.w. = 2000 g/mol) on Huntingdon clay at pH 6. The adsorption isotherm of PAA deviates from the 100% adsorption line and reaches a plateau around polymer concentration of 0.3 mg/m^2.

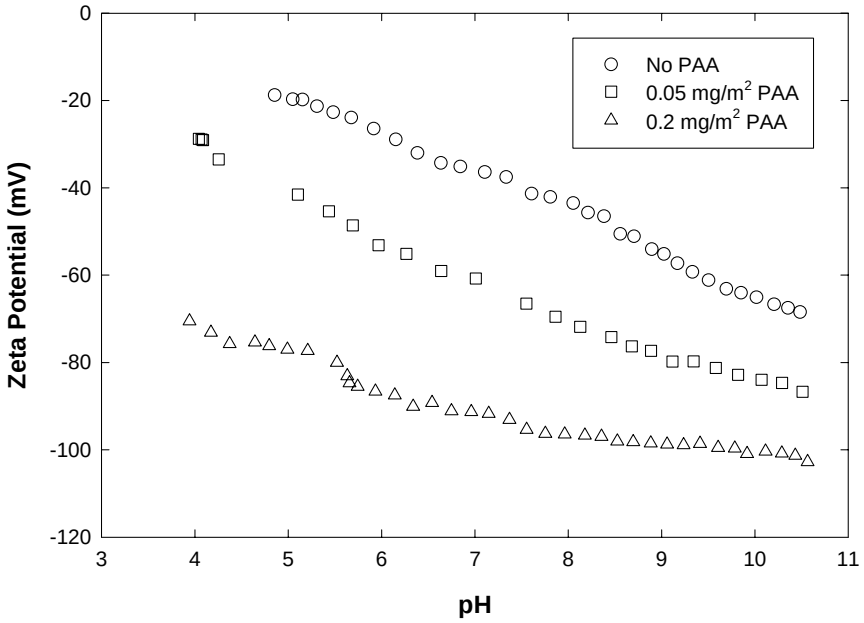

Figure III-8. Zeta potential of Huntingdon clay with the change in pH. The adsorption of the negatively charged PAA decreases the zeta potential, resulting in a more dispersed system at high pH.

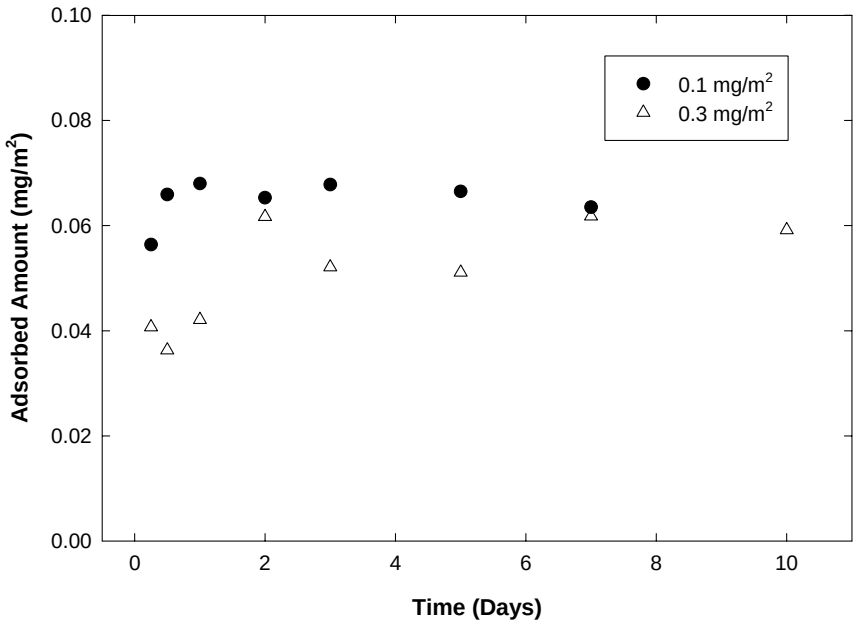

Figure III-9. Kinetics of PAA adsorption on Huntingdon clay. The adsorbed amount at low polymer concentration increases rapidly and reaches a plateau region.

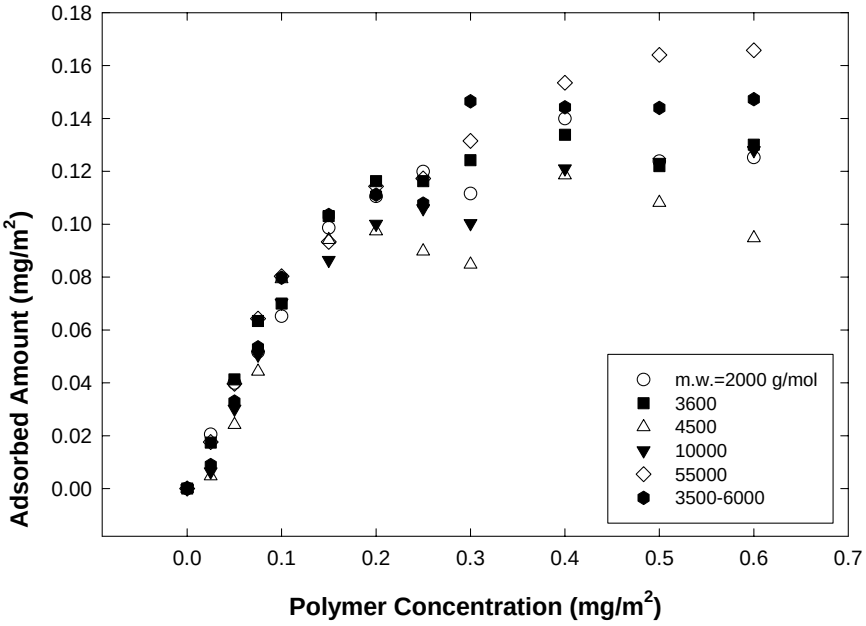

Figure III-10. Adsorption isotherm of various PAAs on Huntingdon clay at pH 6. Little effect of polymer molecular weight is seen on the adsorption plateau value.

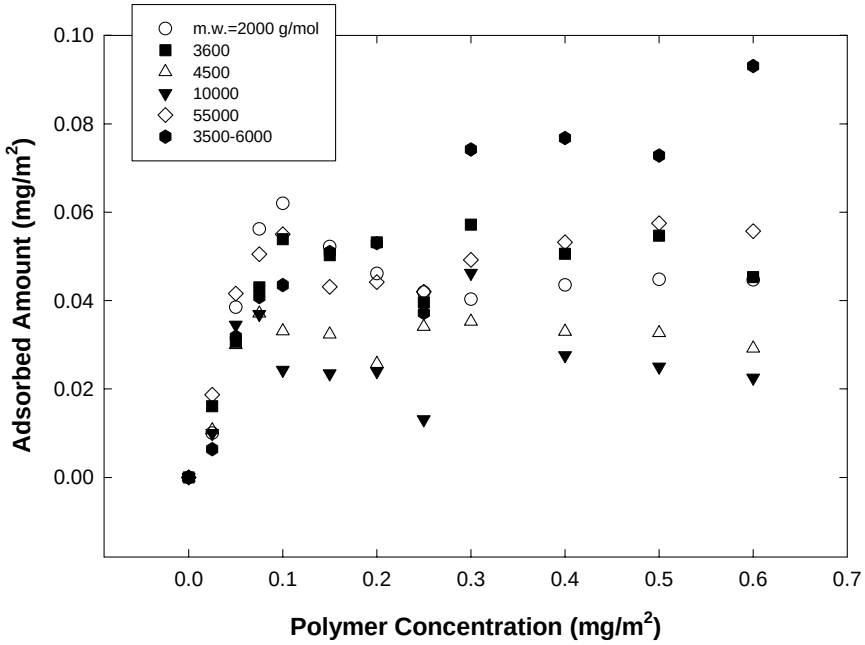

Figure III-11. Adsorption isotherm of various PAAs on Huntingdon clay at pH 9. Scatter is seen in the data due to the presence of HA and FA in the solution.

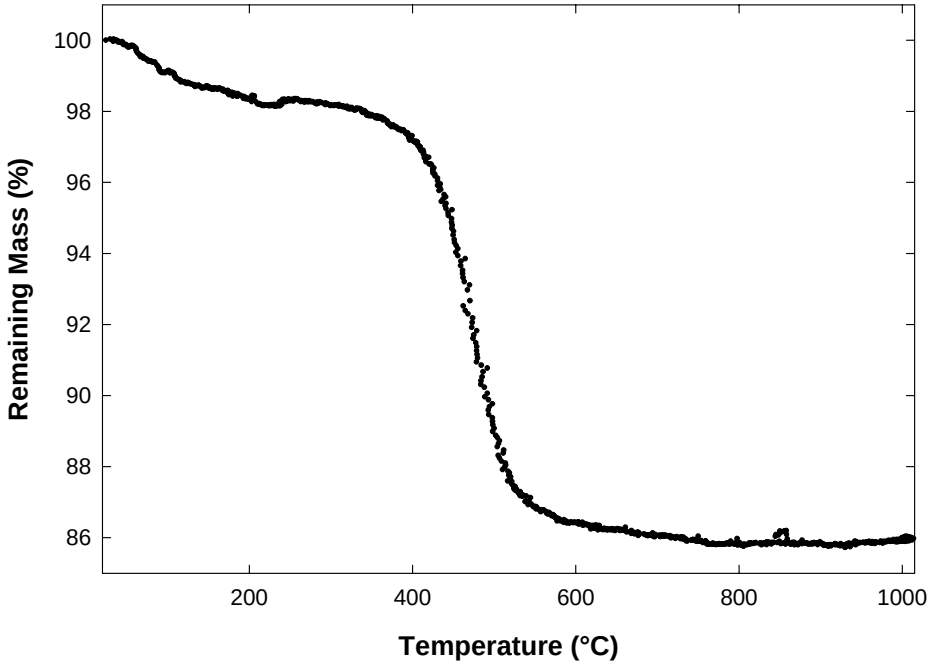

Figure III-12. Thermogravimetric analysis of Huntingdon clay. Physically adsorbed water is removed below 150°C. Organic materials and chemically bonded water are removed below 600°C.

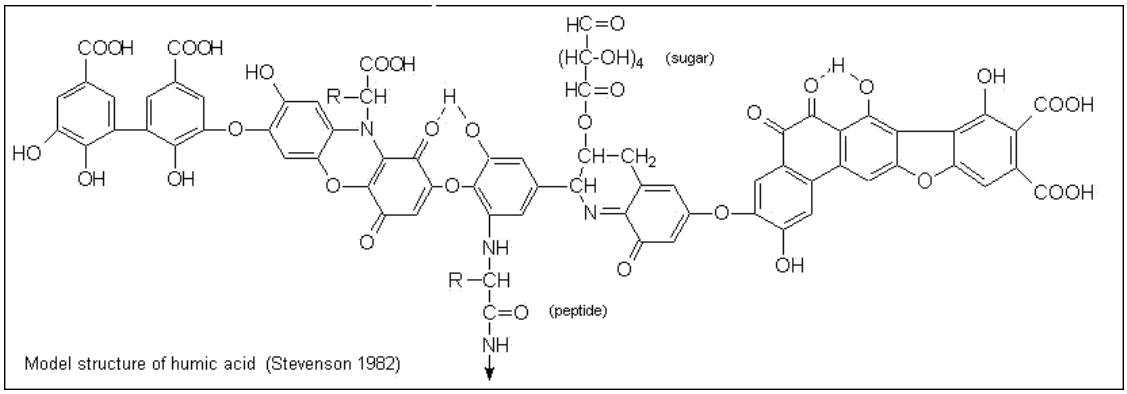

(a)

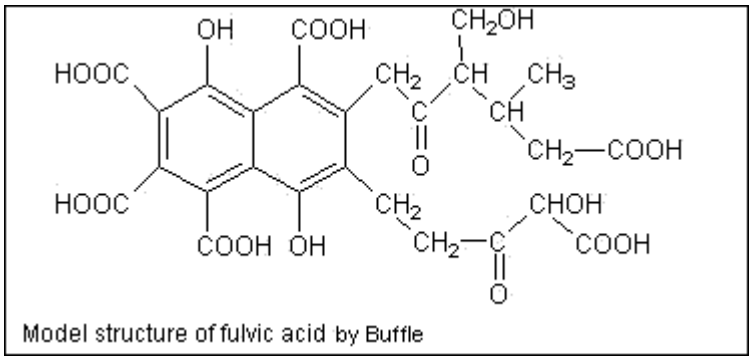

(b)

Figure III-13. Schematic illustration of (a) HA and (b) FA structures.[64,65] Both HA and FA have pH active functional groups that interfere with the titration method used to determine the concentration of PAA adsorbed on the clay surface.

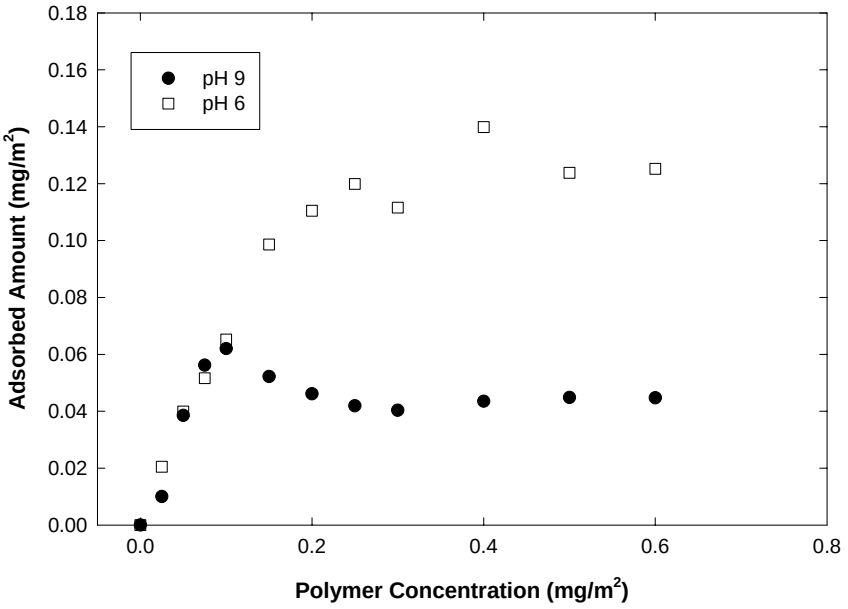

Figure III-14. Adsorption isotherm of PAA (m.w. = 2000 g/mol) on Huntingdon clay at pH 6 and 9. At both pH values the adsorption follows the same slope at low polymer concentrations and at pH 6 the adsorption curve goes further and reaches the plateau due to the difference in conformation of the polymer.

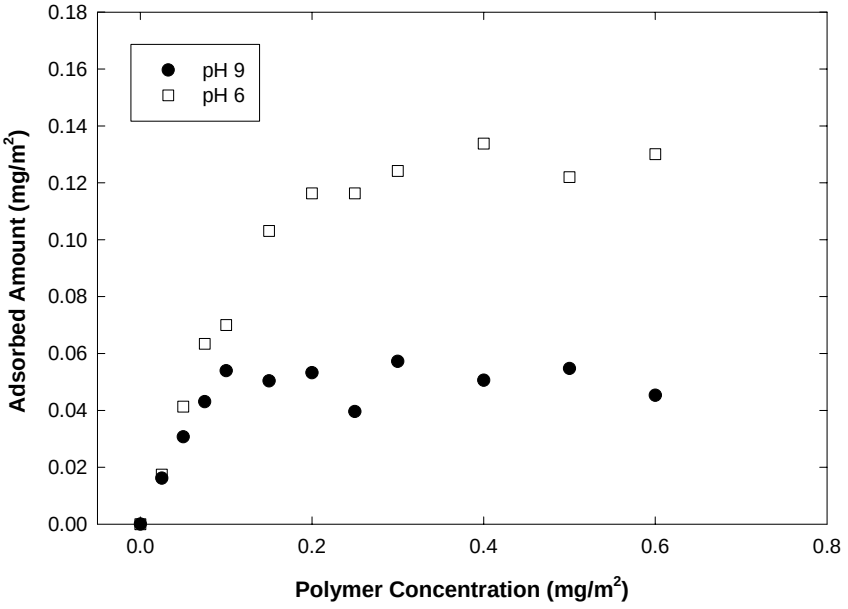

Figure III-15. Adsorption isotherm of PAA (m.w. = 3600 g/mol) on Huntingdon clay at pH 6 and 9. The adsorption reaches a plateau at 0.13 mg/m^2 at pH 6 and 0.05 mg/m^2 at pH 9.

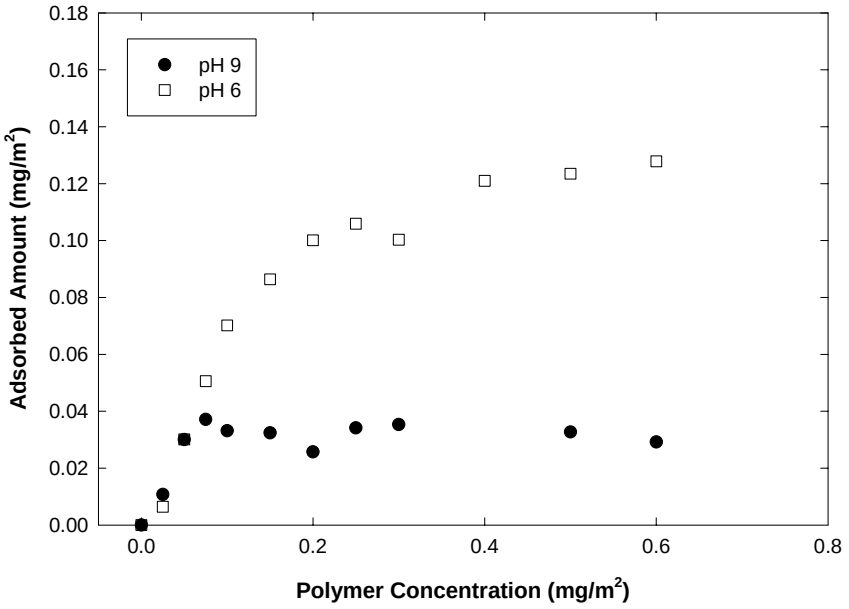

Figure III-16. Adsorption isotherm of PAA (m.w. = 4500 g/mol) on Huntingdon clay at pH 6 and 9. The adsorption reaches a plateau at 0.10 mg/m^2 at pH 6 and 0.03 mg/m^2 at pH 9.

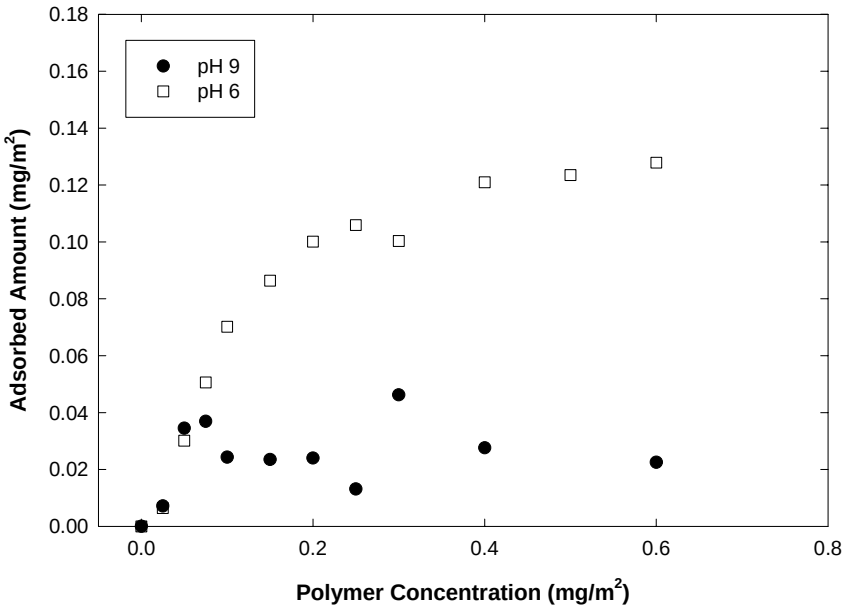

Figure III-17. Adsorption isotherm of PAA (m.w. = 10000 g/mol) on Huntingdon clay at pH 6 and 9. The adsorption reaches a plateau at 0.12 mg/m^2 at pH 6 and 0.03 mg/m^2 at pH 9.

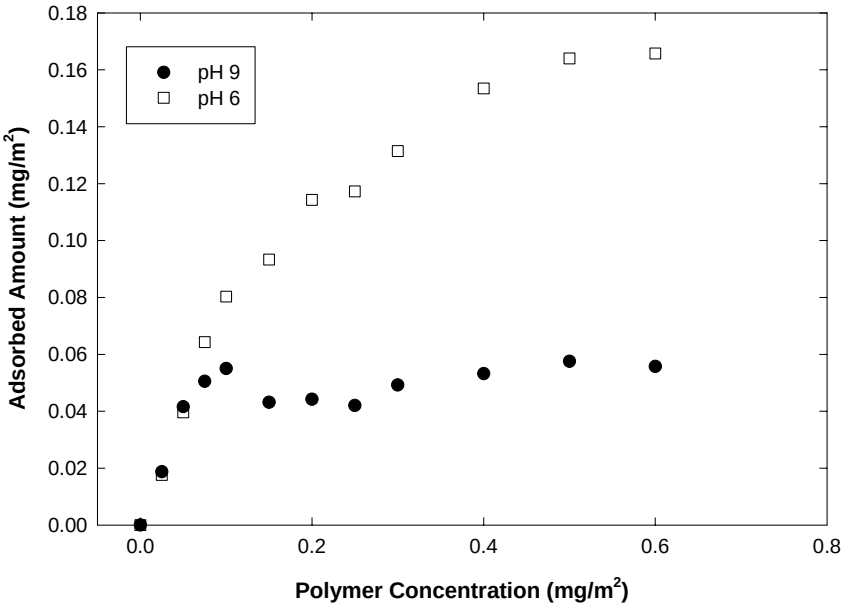

Figure III-18. Adsorption isotherm of PAA (m.w. = 55000 g/mol) on Huntingdon clay at pH 6 and 9. The adsorption reaches a plateau at 0.16 mg/m^2 at pH 6 and 0.05 mg/m^2 at pH 9.

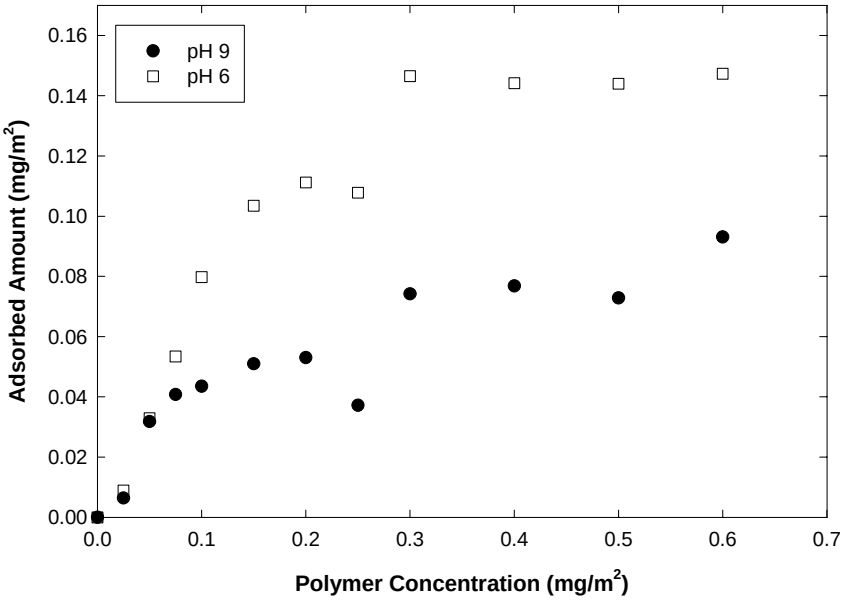

Figure III-19. Adsorption isotherm of PAA (m.w. = 3500-6000 g/mol) on Huntingdon clay at pH 6 and 9. The adsorption reaches a plateau at 0.14 mg/m^2 at pH 6 and 0.08 mg/m^2 at pH 9.

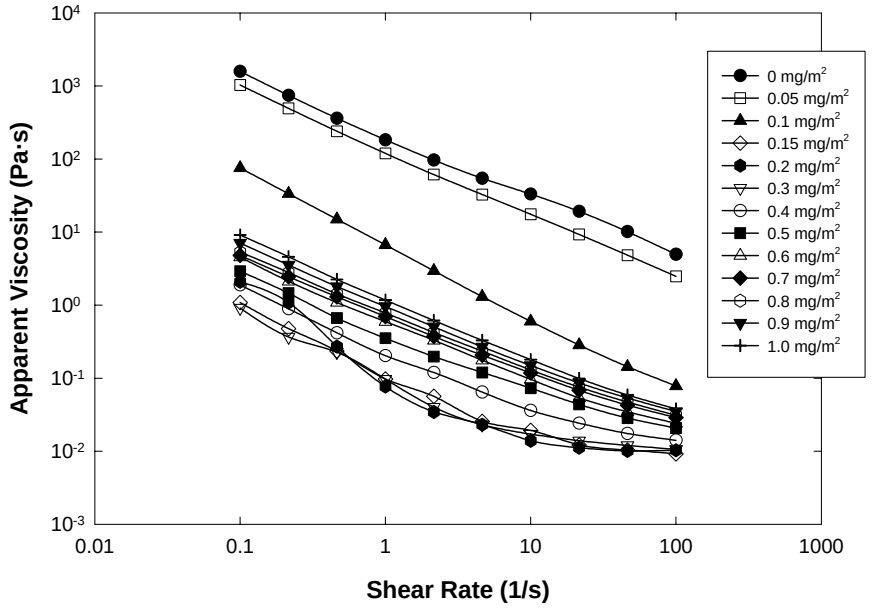

Figure III-20. Apparent viscosity versus shear rate of Huntingdon clay with the addition of PAA (m.w. = 2000 g/mol). Viscosity decreases with shear rate for all polymer concentrations tested.

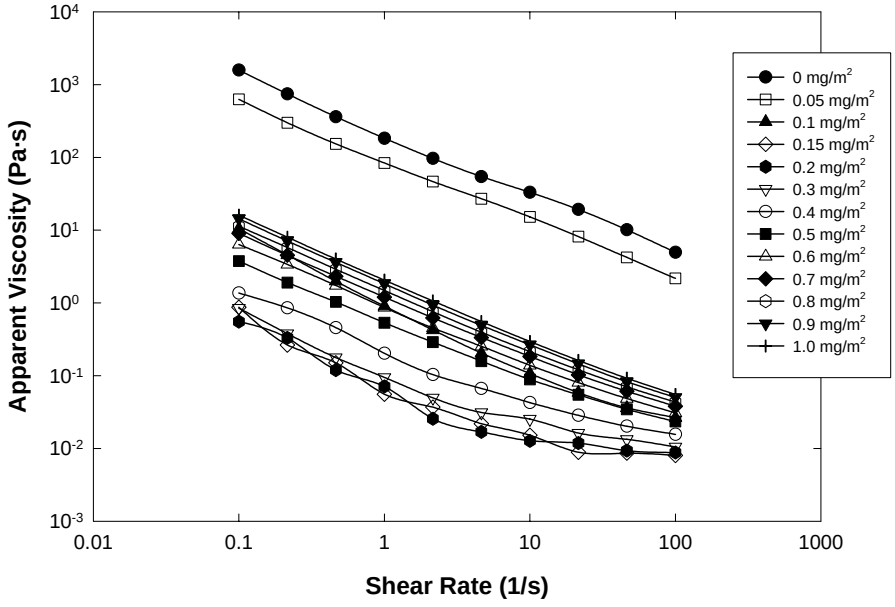

Figure III-21. Apparent viscosity versus shear rate of Huntingdon clay with the addition of PAA (m.w. =3600 g/mol). Shear rate thinning behavior is seen for all polymer concentrations tested.

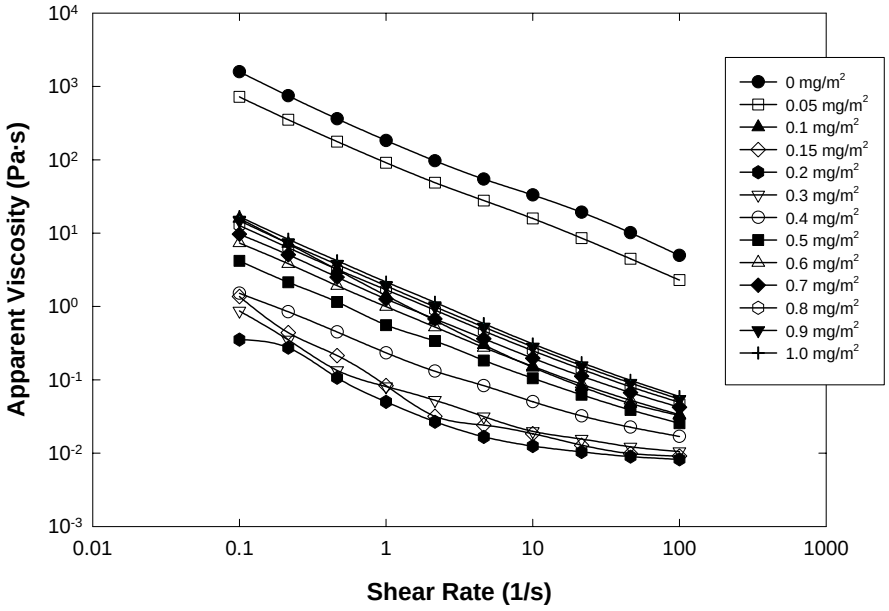

Figure III-22. Apparent viscosity versus shear rate of Huntingdon clay with the addition of PAA (m.w. = 4500 g/mol). Shear rate thinning behavior is seen for all polymer concentrations tested.

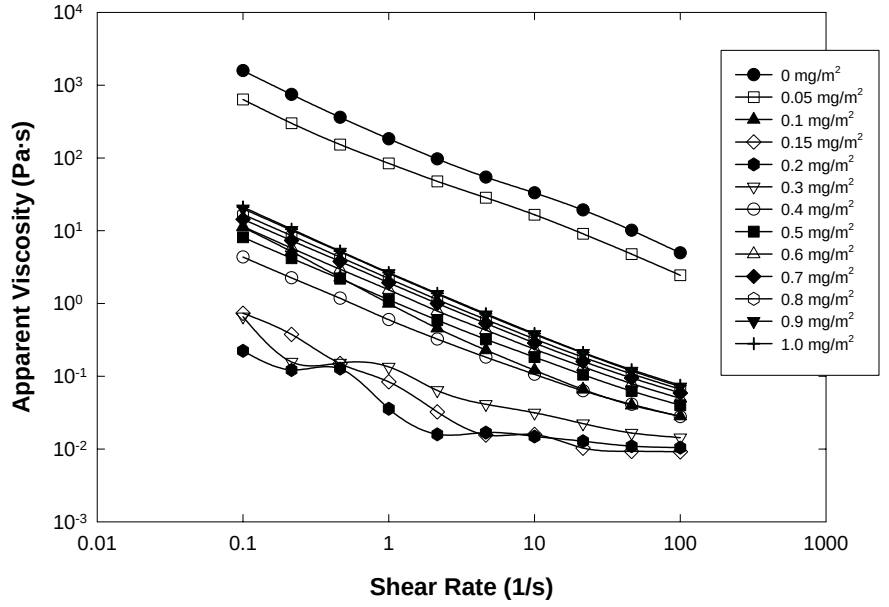

Figure III-23. Apparent viscosity versus shear rate of Huntingdon clay with the addition of PAA (m.w. = 10000 g/mol). Shear rate thinning behavior is seen for all polymer concentrations tested.

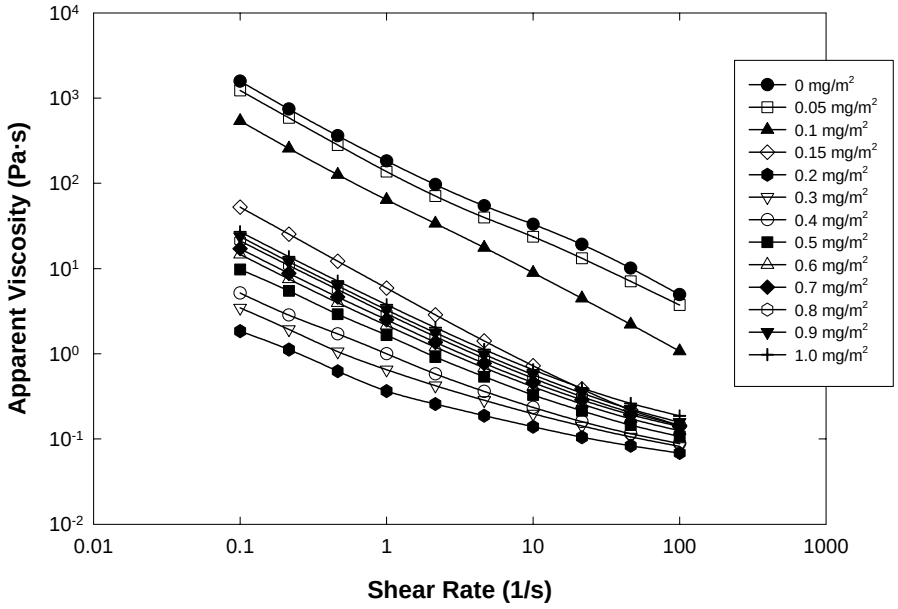

Figure III-24. Apparent viscosity versus shear rate of Huntingdon clay with the addition of PAA (m.w. = 55000 g/mol). Shear rate thinning behavior is seen for all polymer concentrations tested.

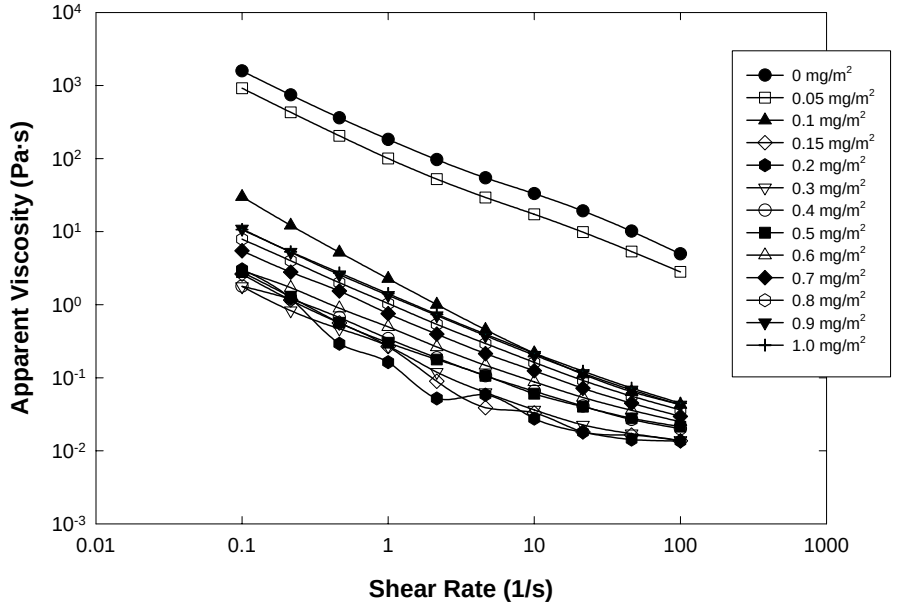

Figure III-25. Apparent viscosity versus shear rate of Huntingdon clay with the addition of PAA (m.w. = 3500-6000 g/mol). Shear rate thinning behavior is seen for all polymer concentrations tested.

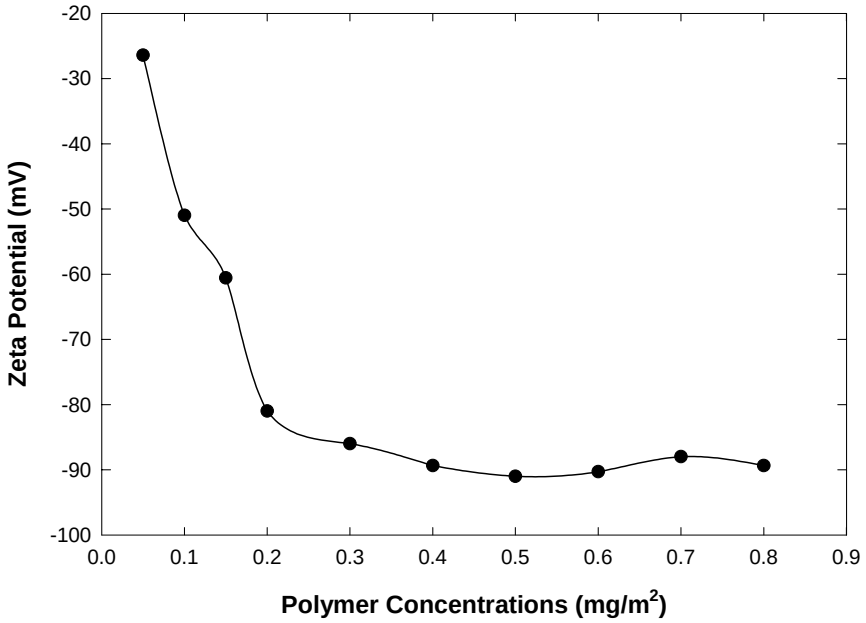

Figure III-26. Zeta potential of Huntingdon clay with the addition of PAA. Zeta potential reaches the plateau region around 0.3 mg/m^2 PAA addition.

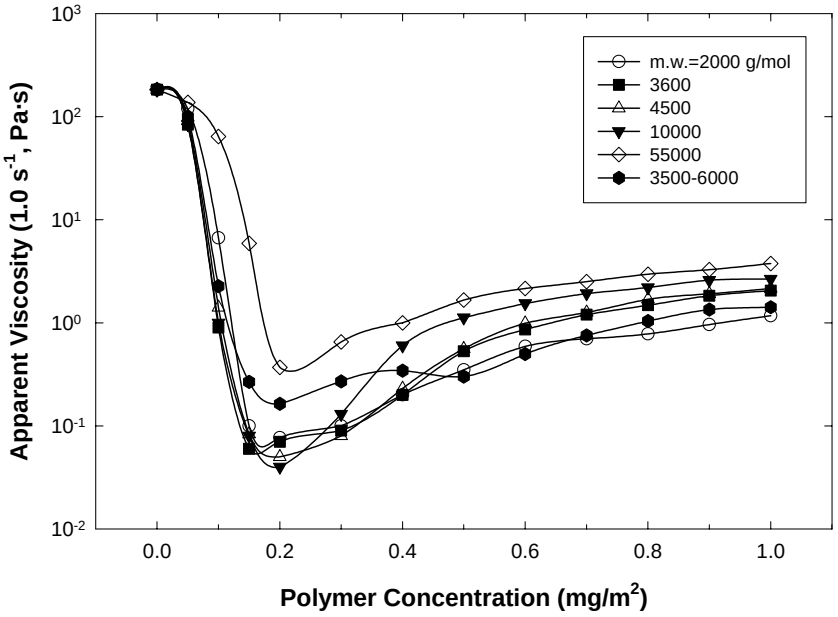

Figure III-27. Apparent viscosity change with the addition of PAAs. All the suspensions show the minimum viscosity approximately at 0.2 mg/m^2 PAA addition. pH was not adjusted in these suspensions.

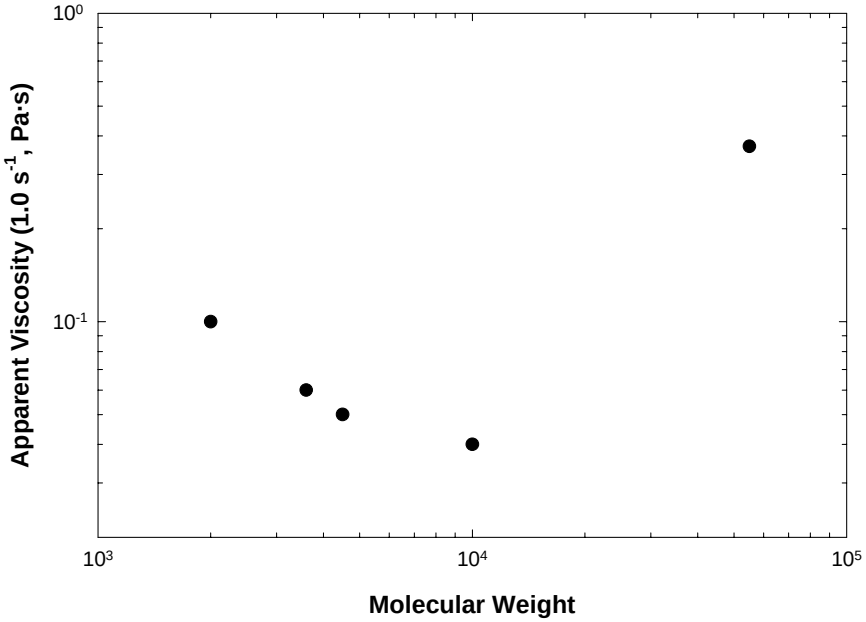

Figure III-28. Apparent viscosity versus molecular weight of PAAs. The lowest viscosity is obtained at molecular weight of 10000 g/mol.

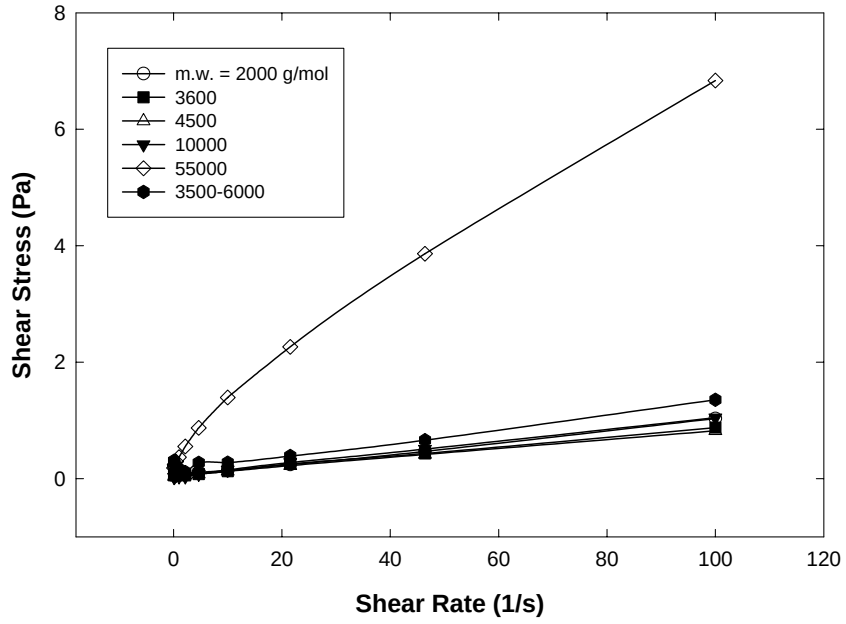

Figure III-29. Shear stress versus shear rate with PAA addition of 0.2 mg/m^2. The linear portion of the curve is extrapolated to the Y-axis to measure shear yield stress.

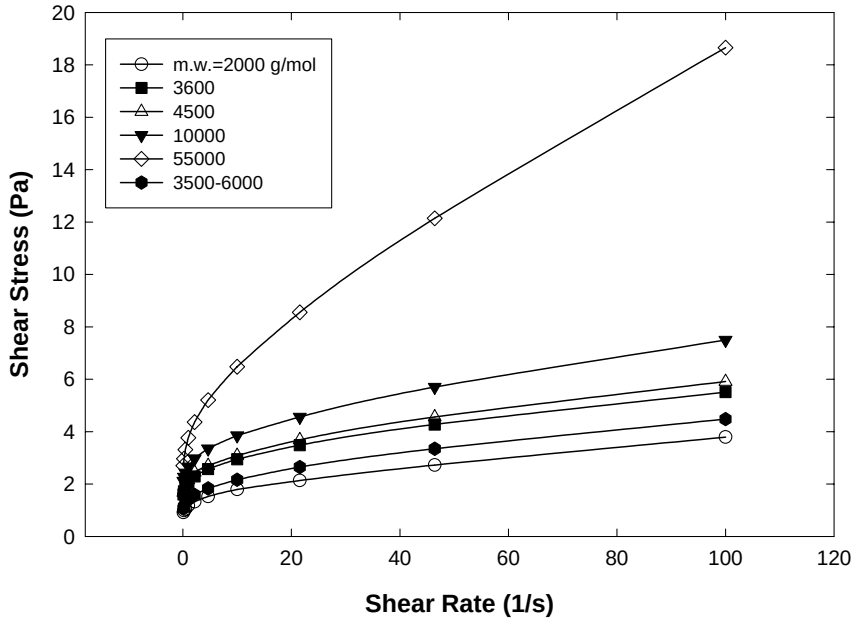

Figure III-30. Shear stress versus shear rate with PAA addition of 1.0 mg/m^2.

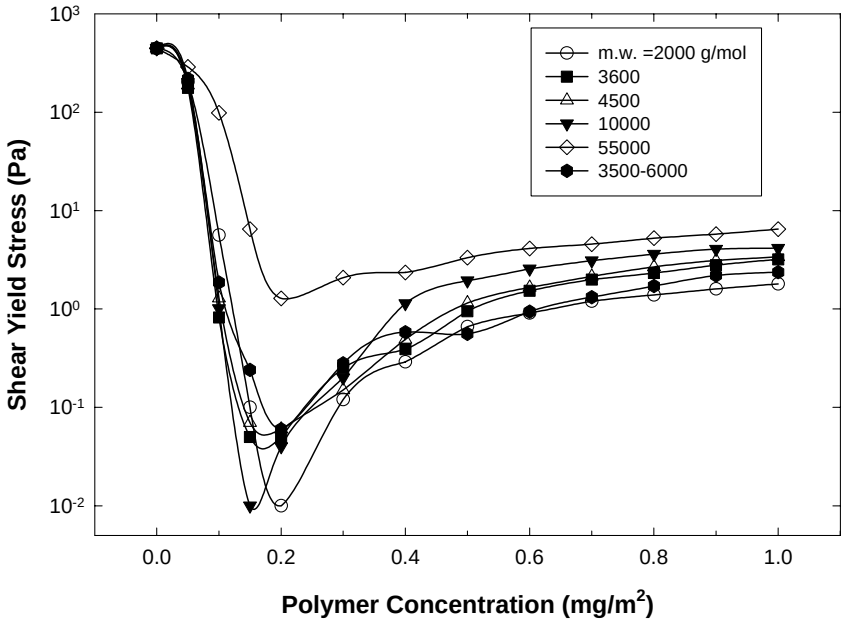

Figure III-31. Shear yield stress of suspensions with the addition of PAA. A similar trend is found in the result as seen in Figure III-27 (apparent viscosity at 1.0 s^{-1} versus polymer concentration).

6. References

1. B. Velde, *Introduction to Clay Minerals*; pp. 60. Kluwer Academic Publishers, Norwell, MA, 1992.

2. G. Sposito, *The Surface Chemistry of Soils*; pp. 12-18, 35-42, 78-81. Oxford University Press, New York, 1984.

3. D. M. Moore and R. C. Reynolds, Jr., *X-ray Diffraction and the Identification and Analysis of Clay Minerals*; pp. 102-201. Oxford University Press, New York, 1989.

4. B. K. Schroth and G. Sposito, "Surface Charge Properties of Kaolinite," *Clays Clay Miner.*, **45** [1] 85-91 (1997).

5. G. Uehara and G. P. Gillman, "Charge Characteristics of Soils with Variable and Permanent Charge Minerals: I. Theory," *Soil Sci. Soc. Am. J.*, **44** [2] 250-252 (1980).

6. M. D. A. Bolland, A. M. Posner, and J. P. Quirk, "pH-Independent and pH-Dependent Surface Charges on Kaolinite," *Clays Clay Miner*, **28** [6] 412-418 (1980).

7. W. M. Carty, "The Colloidal Nature of Kaolinite," *Am. Ceram. Soc. Bull.*, **78** [8] 72-76 (1999).

8. N. Guven, "Molecular Aspects of Clay/Water Interactions," pp. 2-80 in *Clay-Water Interface and Its Rheological Implications*. Edited by N. Guven and R. M. Pollastro. The Clay Minerals Society, Boulder, CO, 1992.

9. E. Marcano-Martinez and M. B. Mcbride, "Comparison of the Titration and Ion Adsorption Methods for Surface Charge Measurement in Oxisols," *Soil Sci. Soc. Am. J.*, **53** [4] 1040-1045 (1989).

10. M. Duquette and W. Hendershot, "Soil Surface Charge Evaluation by Back Titration: I. Theory and Method Development," *Soil Sci. Soc. Am. J.*, **57** [5] 1222-1228 (1993).

11. M. Duquette and W. Hendershot, "Soil Surface Charge Evaluation by Back Titration: II. Application," *Soil Sci. Soc. Am. J.*, **57** [5] 1228-1234 (1993).

12. C. P. Schulthess and D. L. Sparks, "Back Titration Technique for Proton Isotherm Modeling of Oxide Surfaces," *Soil Sci. Soc. Am. J.*, **50** [6] 1406-1411 (1986).

13. D. Saxman, *Water Soluble Polymers*; pp. 170-175. Business Communications Company, Norwalk, CT, 1991.

14. Chemical Safety Information, "Acrylic Acid," (1996) International Programme on Chemical Safety. Accessed on: September, 2002. Available at <http://www.inchem.org/documents/ehc/ehc/ehc191.htm>

15. F. L. Buchholz, "Polyacrylamides and Poly(Acrylic Acids)," pp. 143-158 in *Ullmann's Encyclopedia of Industrial Chemistry*, Vol. A21. Edited by F. T. Campbell, R. Pfefferkorn, and J. F. Rounsaville. VCH Publishers, Weinheim, Germany, 1985.

16. M. L. Miller, "Acrylic Acid Polymers," pp. 197-225 in *Encyclopedia of Polymer Science and Technology: Plastics, Resins, Rubbers, Fibers*, Vol. 1. Edited by H. F. Mark, N. G. Gaylord, and N. M. Bikales. Interscience Publishers, New York, 1964.

17. H. G. Elias, *Macromolecules*; pp. 919-920. VCH Publishers, Weinheim, Germany, 1997.

18. K. J. Saunders, *Organic Polymer Chemistry*: *An Introduction to the Organic Chemistry of Adhesives, Fibres, Paints, Plastics, and Rubbers*; pp. 130-134. Chapman & Hall, London, UK, 1988.

19. F. W. Billmeyer, Jr., *Textbook of Polymer Science*; pp. 389-390. Wiley, New York, 1984.

20. A. R. Mathieson and J. V. McLaren, "Potentiometric Study of the Conformational Transition in Poly(acrylic acid)," *J. Polym. Sci.: Part : Gen. Pap.*, **3,** 2555-2565 (1965).

21. J. Cesarano III, "Polyelectrolyte Adsorption in α-Alumina and Aqueous Suspension Behavior"; M.S. Thesis. University of Washington, Seattle, WA, 1986.

22. G. J. Fleer, M. A. Cohen Stuart, J. M. H. M. Scheutjens, T. Cosgrove, and B. Vincent, *Polymers at Interfaces*; pp. 17-24, 339-371. Chapman & Hall, London, UK, 1998.

23. D. H. Napper, *Polymeric Stabilization of Colloidal Dispersions*; Ch. 4. Academic Press, London, UK, 1983.

24. F. TH. Hesselink, "On the Theory of Polyelectrolyte Adsorption," *J. Colloid Interface Sci.*, 60 [3] 448-466 (1997).

25. Z. Pan, A. Campbell, and P. Somasundaran, "Polyacrylic Acid Adsorption and Conformation in Concentrated Alumina Suspensions," *Colloids Surf., A*, **191** [1-2] 71-78 (2001).

26. K. F. Tjipangandjara and P. Somasundaran, "Effects of Changes in Adsorbed Polyacrylic Acid Conformation on Alumina Flocculation," *Colloids Surf.*, **55,** 245-255 (1991).

27. P. Somasundaran, X. Yu, and S. Kridhnakumar, "Role of Conformation and Orientation of Surfactants and Polymers in Controlling Flocculation and Dispersion

of Aqueous and Non-Aqueous Suspensions," *Colloids and Surf., A*, **133** [1-2] 125-133 (1998).

28. Z. Zhou, P. J. Scales, and D. V. Boger, "Chemical and Physical Control of the Rheology of Concentrated Metal Oxide Suspensions," *Chem. Eng. Sci.*, **56** [9] 2901-2920 (2001).

29. L. Bergstrom, "Rheology of Concentrated Suspension," pp. 193-244 in *Surface and Colloid Chemistry in Advanced Ceramic Processing*. Edited by R. J. Pugh and L. Bergstrom. Marcel Dekker, New York, 1994.

30. H. A. Barnes, J. F. Hutton, and K. Walters, *An Introduction to Rheology*; Chs. 2, 7. Elsevier Science Publications, Amsterdam, Netherlands, 1989.

31. W. B. Russel, "Concentrated Colloidal Dispersions," *MRS Bull.*, **XVI** [8] 27-31 (1991).

32. W. B. Russel, "Review of the Role of Colloidal Forces in the Rheology of Suspensions," *J. Rheol.*, **24** [3] 287-317 (1980).

33. Th. F. Tadros, "Correlation of Viscoelastic Properties of Stable and Flocculated Suspensions with their Interparticle Interactions," *Adv. Colloid Interface Sci.*, **68** [1-3] 97-200 (1996).

34. J. Lyklema, G. J. Fleer, and J. M. H. M. Scheutjens, "Contribution of Adsorbed Polymers to the Stability of Colloidal Systems," *Kolloidn. Zh.*, **49** [2] 211-216 (1987).

35. R. J. Hunter, *Introduction to Modern Colloid Science*; pp. 97-130. Oxford University Press, Oxford, UK 1993.

36. J.W. Goodwin and R. W. Hughes, *Rheology for Chemists An Introduction*; pp. 215. The Royal Society of Chemistry, Cambridge, UK, 2000.

37. N. Q. Dzuy and D. V. Boger, "Yield Stress Measurement for Concentrated Suspensions," *J. Rheol.*, **27** [4] 321-349 (1983).

38. M. T. Brumbach, "Surface Charge, Rheology, and Variability of Kaolinitic Clays"; M.S. Thesis. Alfred University, Alfred, NY, 2002.

39. D. Myers, *Surfaces, Interfaces, and Colloids: Principles and Applications*; pp. 79-95. John Wiley & Sons, New York, 1999.

40. S. Kawaguchi, T. Takahashi, H. Tajima, Y. Hirose, and K. Ito, "Preparation, Characterization, and Dissociation Properties of Poly(acrylic acid) and Poly(methacrylic acid) with Narrow Molecular Weight Distribution," *Polym. J. (Tokyo, Jpn.)*, **28** [9] 735-741 (1996).

41. I. Borukhov, D. Andelman, R. Borrega, M. Cloitre, L. Leibler, and H. Orland, "Polyelectrolyte Titration: Theory and Experiment," *J. Phys. Chem. B*, **104** [47] 11027–11034 (2000).

42. M. Sakurai, T. Imai, F. Yamashita, K. Nakamura, and T. Komatsu, "Temperature Dependence of Viscosities ad Potentiometric Titration Behavior of Aqueous Poly(acrylic acid) and Poly(methacrylic acid) Solutions," *Polym. J.*, **25** [12] 1247-1255 (1993).

43. L-C Guo, Y. Zhang, N. Uchida, and K. Uematsu, "Influence of Temperature on Stability of Aqueous Alumina Slurry Containing Polyelectrolyte Dispersant," *J. Eur. Ceram. Soc.*, **17** [2-3] 345-350 (1997).

44. P. Somasundaran and S. Krishnakumar, "Adsorption of Surfactants and Polymers at the Solid-Liquid Interface," *Colloids Surf., A*, **123-124,** 491-513 (1997).

45. J. E. Gebhardt and D. W. Fuerstenau, "Adsorption of Polyacrylic Acid at Oxide/Water Interface," *Colloids Surf.*, **7** [3] 221-231 (1983).

46. L. K. Koopal, "The Effect of Polymer Polydispersity on the Adsorption Isotherm," *J. Colloid Interface Sci.*, **83** [1] 116-129 (1981).

47. B. Vincent, "The Effect of Adsorbed Polymers on Dispersion Stability," *Adv. Colloid Interface Sci.*, **4** [2-3] 193-277 (1974).

48. R. E. Felter and L. N. Ray, "Polymer Adsorption Studies at the Solid-Liquid Interface Using Gel Permeation Chromatography I. Molecular Weight Distribution Along the Adsorption Isotherm," *J. Colloid Interface Sci.*, **32** [2] 349-360 (1970).

49. C. V. Linden and R. Van Leemput, "Adsorption Studies of Polystyrene on Silica II. Polydisperse Adsorbate," *J. Colloid Interface Sci.*, **67** [1] 63-69 (1978).

50. J. M. H. M. Scheutjens and G. J. Fleer, "Statistical Theory of the Adsorption of Interacting Chain Molecules I. Partition Function, Segment Density Distribution, and Adsorption Isotherms," *J. Phys. Chem.*, **83** [2] 1619-1635 (1979).

51. A. W. M. de Laat and G. L. T. van den Heuval, "Molecular Weight Fractionation in the Adsorption of Polyacrylic Acid Salts onto $BaTiO_3$," *Colloids and Surf., A*, **98** [1-2] 53-59 (1995).

52. G. R. Jopplen, "Characterization of Adsorbed Polymers at the Charged Silica-Aqueous Electrolyte Interface," *J. Phys. Chem.*, **82** [20] 2210-2215 (1978).

53. J. Cesarano III, I. A. Aksay, and A. Bleir, "Stability of Aqueous α-Al2O3 Suspensions with Poly(methacrylic acid) Polyelectrolyte," *J. Am. Ceram. Soc.*, **71** [4] 250-255 (1998).

54. T. B. S. Christopher, “Humic Substances,” (1996) Universiti Putra Malaysia. Accessed on: September 2002. Available at <http://agri.upm.edu.my/jst/resources/as/om_humicsubs.html>

55. C. P. Schulthess and C. P. Huang, “Humic and Fulvic Acid Adsorption by Silicon and Aluminum Oxide Surfaces on Clay Minerals,” *Soil Sci. Soc. Am. J.*, **55** [1] 34-42 (1991).

56. M. N. Jones and N. D. Bryan, “Colloidal Properties of Humic Substances,” *Adv. Colloids Interface Sci.*, **78** [1] 1-48 (1998).

57. L. Guo, Y. Zhang, N. Uchida, and K. Uematsu, “Adsorption Effects on the Rheological Properties of Aqueous Alumina Suspensions with Polyelectrolyte,” *J. Am. Ceram. Soc.*, **81** [3] 549-556 (1998).

58. A. W. P. Vermeer and L. K. Koopal, “Adsorption of Humic Acids to Mineral Particles. 2. Polydispersity Effects with Polyelectrolyte Adsorption,” *Langmuir*, **14** [15] 4210-4216 (1998).

59. J. Blaakkmeer, M. R. Bohmer, M. A. Cohen Stuart, and G. J. Fleer, “Adsorption of Weak Polyelectrolytes on Highly Charged Surfaces. Poly(acrylic acid) on Polystyrene latex with Strong Cationic Groups,” *Macromolecules*, **23** [8] 2301-2309 (1990).

60. B. A. Firth and R. J. Hunter, “Flow Properties of Coagulated Colloidal Suspensions I. Energy Dissipation in the Flow Units,” *J. Colloid Interface Sci.*, **57** [3] 248-256 (1976).

61. B. A. Firth and R. J. Hunter, “Flow Properties of Coagulated Colloidal Suspensions III. The Elastic Flow Model,” *J. Colloid Interface Sci.*, **57** [2] 266-275 (1976).

62. Y. K. Leong, P. J. Scales, T. W. Healy, and D. V. Boger, “Interparticle forces Arising from Adsorbed Polyelectrolytes in Colloidal Suspensions,” *Colloids and Surf., A*, **95** [1] 43-52 (1995).

63. B. R. Sundlof, “Aqueous Processing of Alumina and Phase Behavior of Polymeric Additives”; Ph.D. Thesis. Alfred University, Alfred, NY, 1999.

64. F. J. Stevenson, *Humus Chemistry. Genesis, Composition, Reactions*; John Wiley and Sons, New York, 1982.

65. J. A. E. Buffle, "Les substances humiques et leurs interactions avec les ions mineraux", Conference Proceedings de la Commission d'Hydrologie Appliquee de A.G.H.T.M., 3-10 (1977).

IV. PVA MIGRATION VIA POLYMERIC INTERACTION

1. Introduction

Poly(vinyl alcohol) [PVA] is one of the most commonly used organic binders in dry pressing. In the spray drying process of a ceramic suspension containing a water-soluble binder such as PVA, the binder moves to the surface of a droplet and segregates with the vaporization of water. The segregation of PVA to the surface of granules is believed to make granules harder (case-hardening), which results in voids inside compacts and in a rough pressed surface.

Several studies explain the PVA migration behavior during spray drying process from the physical aspects of capillary force and diffusion. In those studies the interaction of PVA with other polymeric additives was not considered or assumed as negligible.[1-4] However, the polymeric interactions can not be ignored because in a sense the functional groups and configurations of polymers can lead to reaction or cross-liking between polymers depending on solution chemistry. Also, the adsorption of polyelectrolyte used as dispersant changes the surface property and behavior of particles, thus, the PVA migration should be considered in the presence of other polymers. In addition, the situation during the drying process can be compared to the case where relative polymer concentration increases, which can considerably change the polymeric interactions. The way polymeric interactions occur can be either beneficial or problematic depending on the desired performance of the final product. PVA migration in granules negatively influences the properties of granules and pressed compacts.

It is hypothesized that the primary cause of case-hardening is polymeric binder migration to the granule surface during the drying process due to incompatibility between the polymeric additives used for dispersion and those added to provide green strength to the pressed part. Therefore, it is assumed that distribution of PVA can be controlled by adjusting the compatibility of the polymers. In this study the effect of polymer compatibility on binder migration is demonstrated to verify the hypothesis. Phase behaviors of polymer mixtures are predicted from Flory-Huggins calculations and the polymeric interactions are studied using a light scattering technique and an optical

microscopy. The PVA binder within spray-dried granules is stained and the migration behavior is correlated to the phase behavior and polymeric interaction.

2. Background Information

2.1 Polymers

2.1.1 Polyacrylates (PMAA)

Polymethacrylic acid (PMAA) is one of the most common anionic polyelectrolytes. PMAA is the closest chemical analog of PAA, but has different properties from PAA. The properties of PAA are reviewed in Chapter III.

PMAA and PAA are ionized in water and act as dispersants in the ceramic industry. The degree of ionization (α) for PMAA and PAA increases as the solution pH increases. However, PMAA shows quite a different dissociation behavior as shown in Figure IV-1. PMAA chains resist expansion before a critical charge density. PMAA chains exist as hypercoils at a low degree of ionization, $\alpha < 20\%$, due to the attractive interactions such as hydrogen bonding between carboxyl or carboxylate groups, and van der Waals or hydrophobic interactions between methyl groups. Within these hypercoils most of methyl groups are in the interior due to hydrophobic interactions, providing non-polar cores for the solubilization of hydrophobic molecules. The conformation transition of PMAA from the compact to the expanded form, brought about by repulsive Coulombic interactions of the ionized carboxyl groups, is assumed to be highly cooperative. The dissociation of one acid group is correlated in a complex way to the position and number of other charged groups on the chain. That is, when the amount of charge on the chain varies, the chain conformation is affected and ,in turn, influences the dissociation of other groups. At a high degree of ionization and low ionic strength PMAA of low molecular weights, <10000 g/mol, are generally believed to possess planar zigzag structures. The most visible consequence of ionization of the functional group is the solubility in water.[5-7]

The intrinsic viscosity dependence of PMAA on the degree of dissociation is shown in Figure IV-2. The intrinsic viscosity of PAA increases monotonously with

increasing neutralization due to the increase in electrostatic repulsion between charges on the polymer chains. However, for PMAA in the low degree of dissociation region the polymer coil expands only little up to a critical degree of ionization. The anomalous viscosity behavior can be considered as one of the evidences of the compact to extended coil transition of PMAA.[5,7]

The adsorption study of PMAA on alumina particles by Cesarano shows that adsorbed amount increases with decreasing pH as shown in Figure IV-3. As pH decreases, the net positive charge of Al_2O_3 and the number of available adsorption sites increase while the number of negative sites on the PMAA decreases. Therefore, with decreasing pH the PMAA molecules are more tightly coiled and adsorb as more compact units, allowing more PMAA to be adsorbed before a complete monolayer has been formed.[8]

The suspension viscosity is strongly related to the polymer adsorption. It is reported that until the adsorption plateau level was reached, the systems were flocculated and had relatively high viscosities and thick sedimentation layers after centrifugation. After the plateau level was reached and the particle was completely covered, the viscosity decreased greatly and a stable suspension was resulted.[8,9]

2.1.2 Sodium silicate

Sodium silicate is a compound containing sodium orthosilicate (Na_4SiO_4), sodium metasilicate (Na_2SiO_3), sodium disilicate ($Na_2Si_2O_5$), and sodium tetrasilicate ($Na_2Si_4O_9$). Sodium silicate is typically produced by fusing sand and sodium carbonate in various proportions. Sodium silicate is a transparent glassy or crystalline solid, and is water-soluble.[10] The major advantages of sodium silicates are the relatively low price, the abundance of raw materials for their production, and the purely inorganic character of the products resulting in higher temperature applications.[11] Sodium silicate is commonly known as water glass. The greatest single use of sodium silicates is as a raw material for making silica gel.

It is known that soluble silicates polymerize in solution. The solution pH and concentration and the SiO_2/Na_2O ratio determine the rate and degree of polymerization.

The monomeric orthosilicate ions that are present in very dilute or very alkaline solutions polymerize as the concentration increases or the pH drops, and most solutions of practical importance appear to contain an equilibrium mixture of species.[12] Generally, it can be stated that at higher SiO_2 concentration and higher SiO_2/Na_2O ratios larger polysilicate ions will prevail. The silicate anions seem to form predominantly rings or cage-like structures. Q^4 units were definitely detected only in highly concentrated alkaline silicate solutions. Q^n denotes a silicon atom connected to n other silicon atoms via bridging oxygen atoms. The reaction rates for structural rearrangement in solution seem to slow down with increasing size of the anions.[11]

Marinangeli *et al.* investigated the equilibrium species in an aqueous sodium silicate solution over a wide range of pH. The investigation was carried out using a concentrated sodium silicate solution. Above pH 13.6 SiO_3^{2-} is the principal ion present, and between pH 13.6 and 10.9 the main ion present is disilicate, $Si_2O_5^{2-}$. Below pH 10.9 the presence of polysilicate ions of undefined structure and polysilicic or silicic acids has been proposed. Below a pH of 9.0, the silica exists mainly as $Si(OH)_4$.[13,14]

Nauman *et al.* determined the molecular weight of silicate in a dilute solution using a light scattering technique. They found that no aggregation occurs in relatively dilute sodium metasilicate solutions, even up to a very high concentration. From turbidity measurements on dilute solutions having concentrations up to 0.1 g/cc molecular weights for the species present have been crudely determined as 325 g/mol for 3.32/1 (=SiO_2/Na_2O) and 400 g/mol for 3.75/1. With time an increase is seen in the turbidity of a dilute solution and the solution pH increases. The turbidity increases more rapidly the more dilute the solution.[15]

Glasser *et al.* studied the structure change of silicate with time and pH in a dilute solution (1.0 mol/dm^3), where SiO_2/Na_2O = 3.41:1. There is no significant change in the silicate structure with time in a dilute solution. They determined the average degree of polymerization as 5.5 for the number average molecular weight (11.4 for the weight average molecular weight) after two days. The presence of both orthosilicate and disilicate (or dimer) in solution diminishes steadily with falling pH, but the other species all show a slight increase in concentration before finally falling off as the pH decreases.

Below pH 9 the only detectable low molecular weight species were orthosilicate and visible gelling of the solution was noticed by pH 7.5.[12]

The adsorption of sodium silicate on ceramic particles is rarely found in literature due to the difficulty in determining the adsorption isotherm. Phair *et al.* determined the adsorption isotherms of sodium silicate on zirconia by equilibration of the anion in a suspension of zirconia in the presence of an inert electrolyte medium. The adsorption isotherm for monomeric and polymeric silicates is shown in Figure IV-4. It is shown that monomeric silicate at concentrations below $3x10^{-3}$ M is adsorbed according to a Langmuir isotherm. Also, the adsorption isotherm of polysilicate seems to follow the Langmuir isotherm at lower concentrations, where the polysilicate would exist as smaller oligomeric species.[16]

2.1.3 Sodium Lignosulfonate

Lignosulfonate (LS) is a water-soluble, non-linear polyelectrolyte, which has considerably different properties from conventional polyelectrolytes. The structure and shape of the LS molecules are not clearly known. It is assumed that a solvent-swollen microgel has the sulfonate groups on the surface of a hydrophobic hydrocarbon core. Depending on ionic strength, the LS molecule expands and contracts like a typical polyelectrolyte. LS molecules behave like relatively rigid, colloidal or sub-colloidal spheres or ellipsoids with a low axial ratio. Sulfonic and hydroxyl groups spread out from the surface of relatively short chains. The usual molecular weight ranges from 1000 to 50000 g/mol. LS shows Newtonian flow in solution at concentrations of 35% or more. Salt addition to a concentrated LS solution increases the viscosity and changes the Newtonian behavior to pseudoplastic.[17,18]

Bell *et al.* studied the adsorption of LS on kaolin particles. As shown in Figure IV-5, the maximum amount of LS adsorbed decreases with an increase in the molar mass, while the mass of adsorbed LS rises slightly. The isotherms display features typical of adsorption in a monomolecular layer. It is known that the adsorption amount decreases with an increase in pH.[19] The capability of LS to serve as an effective dispersant is related to its ability to adsorb on particle surface. The principal adsorption mechanism is

hydrogen bonding between the hydroxyl, phenol, and carboxyl groups on LS and the particle surface. Methylation of the available hydroxyl groups eliminates the adsorption ability. The adsorption of LS on kaolin was found be practically irreversible with respect to dilution, except for very low molecular weight fractions. However, desorption occurs with an increase in pH.[17,20]

Generally, LS in the molecular weight range of 5000 – 40000 g/mol acts as a dispersant while higher molecular weight LS shows flocculating properties by causing inter-particle bridging. The molecular weight may be the most important factor effecting the dispersant properties, while sulphur and methoxyl content is less important. Higher molecular weight also gives a broader minimum viscosity region. The mechanism by which LS increases dispersion stability is somewhat ambiguous. Electrosteric stabilization is mainly discussed as the mechanism.[17]

2.1.4 Poly(vinyl) Alcohol

PVA is commonly used as a binder in many ceramic applications. It may also act as a dispersant or a viscosity modifier. PVA is typically synthesized from vinyl acetate in a two stage process. At the first stage vinyl acetate is dissolved in methanol and polymerized to the desired molecular weight in solution. In the second stage, acetate groups are converted to alcohol groups using a caustic catalyst (NaOH), and the methanol is converted to methyl acetate. The degree of hydrolysis is controlled at this stage. Some of the sodium hydroxide catalyst remains in the final product as sodium acetate, referred to as the ash content.[21]

The structure of PVA is shown in Figure IV-6. PVA is in reality a copolymer of vinyl alcohol and vinyl acetate. The ratio of vinyl alcohol to vinyl acetate strongly influences the properties of PVA. PVA is predominantly an amorphous polymer. However, there are some crystallites that result from the segments of polymer chains lining up and interacting with each other through hydrogen bonding between polymer chains. The degree of crystallinity of the polymer varies with hydrolysis level. Partially hydrolyzed grade of PVA (87-89 % hydrolyzed) is approximately 25% crystalline whereas the fully and super hydrolyzed grades of PVA (98-99 % hydrolyzed) are

approximately 50% crystalline. In the partially hydrolyzed PVA randomly placed acetyl groups along the polymer chains reduce crystallinity.[21,22]

The dissolution of PVA in water is mainly due to hydrogen bonding between the OH groups of the polymer and water molecules. Although water at room temperature is not a poor solvent for PVA (water is a moderate solvent for PVA), the PVA exhibits a high Huggins viscosity coefficient, indicating a low viscosity polymer solution. The low viscosity is attributed to association of PVA molecules. The PVA molecules are not completely dissolved at room temperature due to the crystallites, even at high dilution. PVA particles often form a soft transparent microgel. They are not easily visible in the dissolution vessel, and they are not easily filtered out. PVA does not achieve ultimate performance as a binder if it is not completely solubilized. The microgel particles consist of para-crystalline and amorphous domains. These domains are prone to grow with aging of the polymer solution, which results in an increase in the apparent viscosity of a PVA solution. Amorphous domains consist of unorganized macromolecules, which are bound to each other and to the para-crystalline domains by weak hydrogen bonds. Despite their high molecular weight, the contribution of para-crystalline domains to viscosity is negligible. They are resistant to dilution. The main contribution to viscosity comes from the molecules participating in the amorphous domains, which are solubilized by dilution.[23]

Heating the PVA solution to 80-100 °C destroys hydrogen bonds with an increase of the role of intramolecular and intermolecular hydrophobic interactions. Therefore, it is generally expected that there is a decrease in the size of macromolecular coils and the intrinsic viscosity to a level corresponding to the unperturbed state at theta conditions. However, the association between hydrophobic parts of the chains can override the decrease in the association between hydrophilic groups. Heating in the above temperature range may not destroy the para-crystalline regions in the microgel completely. On the contrary, it may increase their size and amount as a consequence of recrystallization at elevated temperature. These changes hardly affect the viscosity of solutions unless heating is sustained for long periods of time.[23]

When the PVA solution is dried at elevated temperatures, the solubility of PVA varies significantly. Heat treatment causes the crystallinity of fully hydrolyzed PVA to increase, reducing the solubility in water. In practice, fully hydrolyzed PVA does not lose solubility if the heat treatment temperature is kept below 100°C. Partly hydrolyzed PVA (87-89% hydrolyzed) maintains nearly the same water solubility unless subjected to the relatively severe treatment of 180°C for 1 hour. It has been suggested that the marked decrease in solubility observed with more severe heat treatment is due to an increase in the rigid junction points formed in the amorphous regions of the polymer. Solubility, therefore, depends on the degree of crystallinity and on the structure of the amorphous regions. The nature of these regions is likely to depend on the randomness of residual acetate groups, and on branching of the polymer chain.[22]

Many inorganic salts are able to precipitate PVA from aqueous solutions. Most compounds are only effective in this respect with fully hydrolyzed grades. The coagulation power of these anions is in the order: $SO_4^{2-} > CO_3^{2-} > PO_4^{3-}$. The coagulation powers of Cl^- and NO^{3-} are very weak. With cations, coagulation is in the rough order: $K^+ > Na^+ > NH^{4+}$. This is in approximate agreement with ionization potentials. Strong bases and acids have a weak coagulation power. In practice, sulfates are used as coagulants.[22]

In aqueous oxide solutions containing PVA, the acetate groups (hydrophobic groups) adsorb on an oxide particle. The hydrophilic polar side groups, –OH, prefer to extend into the aqueous solution, and are able to hydrogen bond with hydroxyl groups on the particle surface.[24,25] The amount of a copolymer adsorbed depends on its primary structure. Random copolymers are often not very different from homopolymers; the adsorbed amount and structure are intermediate between those of the corresponding homopolymers. The solvency also plays an important role. In selective solvents polymer micelles can form, which implies that the concentration of free molecules is nearly as important over a large concentration range. In the non-selective case this does not occur.[26]

2.2 Thermodynamics of Polymer Solutions

The Flory-Huggins theory has been used to explain the thermodynamic properties of mixed polymer solutions. Prigogine and Flory extended this theory by introducing the free volume effect, but for many practical purposes the Flory-Huggins theory is still preferred due to the insufficient experimental data required to determine the necessary parameters for Prigogine-Flory theory. The Flory-Huggins theory uses statistical means to calculate the contributions of enthalpy and entropy of mixing to the Gibbs free energy. In lattice theory solutions are considered to be three-dimensional lattices and each lattice site is occupied by either a segment of the polymer molecule or a solvent molecule. Thus, for a polymer solution, sets of contiguous lattice sites are required for accommodation of polymer molecules. The free energy of mixing for a ternary system consisting of two polymers and a solvent is given by,

$$\Delta G = \frac{RTV}{V_s}\left[\varphi_s \ln\varphi_s + \frac{\varphi_1}{r_1}\ln\varphi_1 + \frac{\varphi_2}{r_2}\ln\varphi_2 + \chi_{12}\varphi_1\varphi_2 + \chi_{1s}\varphi_1\varphi_s + \chi_{2s}\varphi_2\varphi_s\right] \qquad (1)$$

where R is the gas constant, T is temperature, V is the total volume of the mixture, V_s is the molar volume of a solvent, φ_i is the volume fraction of ith component, r is the number of segments of polymer, and χ_{ij} is the Flory-Huggins interaction parameter. Subscripts 1 and 2 denote polymers 1 and 2, and s denotes the solvent. According to the second law of thermodynamics, mixing occurs spontaneously for a system if the Gibbs free energy of mixing is negative.[27,28]

Two main thermodynamic effects contribute to Gibbs free energy; the entropy and enthalpy of mixing. The combinatorial entropy of mixing is related to the combination numbers which polymer molecules can be assigned on the lattice sites. The positive entropy change results in a negative contribution to the Gibbs free energy, which is favorable for mixing. The positive entropy change of a polymer solution is reduced with increasing polymer molecular weight and phase separation of the polymer solution becomes easier. The molecules of the two polymeric components usually interact through the dispersion forces, in which the interaction between different components is relatively weak compared to that between the same components. The dispersion force

interaction or random dipole-induced dipole interaction always increases the Gibbs free energy, which is unfavorable for mixing. A negative contribution to the Gibbs free energy occurs by a specific interaction such as hydrogen bonding or a weak charge transfer complex between the polymers, but this is rarely observed. This interaction can lead to mixing of the polymers. For either dispersion forces or specific interactions, the main effect is on the Flory-Huggins interaction parameter, reflecting the enthalpy of mixing.[29,30]

A polymer becomes soluble mainly due to an increase in entropy in the presence of a solvent. Normally, there is an attractive interaction between the polymer segments. However, the entropy of mixing terms are strong enough to ensure complete miscibility between solvent and polymer as long as the interaction parameters χ_{12} and χ_{13} are smaller than 0.5. As the molecular weight of the polymer increases, the contribution of the entropy of mixing to the Gibbs free energy becomes negligible. When two different soluble polymers are mixed, the entropy of mixing depends only on the overall solvent volume fraction. The free energy of mixing is largely influenced by the terms involving the interaction parameters on the right side of Equation 1. Therefore, relatively small changes in these parameters can result in either a homogeneous system or phase separation.[31,32]

When there is sufficient solvent to dissolve polymers in a ternary system, homogeneous mixing can be obtained. However, phase separation occurs when the concentration of total polymer is increased above a critical value. For symmetrical systems in good solvents, phase separation must be driven by the polymer-polymer interaction. An effective repulsion between the polymers leads to a segregative phase separation, whereas an effective attraction between them induces an associative phase separation. In general, however, the phase behavior of a ternary system cannot be solely determined by polymer-polymer interactions. The polymer-solvent interactions are also important for the phase behavior. An associative phase separation is influenced by the solvency of the polymers because the formation of a concentrated phase is facilitated in poor or marginal solvents. The polymer-solvent interactions are also known to be important for polymer segregation. Thus, calculations on the Flory-Huggins level have

shown that a segregative phase separation may be driven by differences in polymer-solvent interactions alone, even if the two polymeric components mix ideally. Similar phase diagram may be found even when the polymer-solvent interactions are unequal. Phase separation in ternary systems is strongly promoted by any asymmetry in the polymer-solvent interactions (i.e. $\chi_{12} \neq \chi_{13}$). Furthermore, the polymer incompatibility in solution may be influenced more by the polymer-solvent interaction asymmetry than by the interaction between the polymers. There is a possibility of polymer incompatibility in solution due to the slight difference in the polymer-solvent interactions even when $\chi_{23}=0$.[30,33-35]

The Flory-Huggins interaction parameter characterizes a variety of polymer-solvent and polymer-polymer interactions. For the polymer-solvent interactions,

$$\chi_{s1} = \frac{V_s(\delta_s - \delta_1)^2}{RT} + \beta \tag{2}$$

where δ is the solubility parameter for each polymer and β is 0.34.

For the interaction of the two polymers,

$$\chi_{12} = \frac{V_1(\delta_1 - \delta_2)^2}{RT} \tag{3}$$

Then, one finds,

$$\chi_{12} = \frac{RT(\chi_{s1} - \chi_{s2})^2}{\upsilon(\delta_1 + \delta_2 - 2\delta_s)^2} \tag{4}$$

where υ is the molar volume of the segments in the solvent molecules.

χ is inversely proportional to T and is a function of composition.[27] χ increases greatly with polymer concentration, particularly in the case where a poor solvent is used. In some cases with good solvents, χ seems to be independent of composition. In a few cases, mostly with highly exothermic systems, χ decreases with concentration. χ also depends on the molecular weight of the polymer. χ may depend on the molar mass of the

polymer even for concentrated solutions.[36] If the value of χ is below 0.5, the polymer should be soluble if it is amorphous and linear. When χ is equal to 0.5, the Flory theta conditions exist. If the polymer is crystalline, it must be heated nearly to its melting temperature so that the total free energy of melting plus dissolving is negative.[37]

Solubility parameters can be calculated by several different methods from knowledge of the chemical structure of the polymer. One of the methods is calculating from energy of vaporization.

$$\delta = \left(\frac{\Delta E_v}{V_m} \right)^{1/2} \tag{5}$$

where E_v is the energy of vaporization and V_m is molar volume.[36]

Scott and Tompa applied the Flory-Huggins theory to polymer compatibility for symmetrical systems, where $\chi_{1s}=\chi_{2s}$. They theoretically studied the spinodal curve and the critical solution point of a ternary system. Zeman and Patterson calculated spinodals, which separate the regions of metastable and unstable states, for asymmetrical cases. The equation for the spinodals is given by;

$$\begin{aligned} &r_s\phi_s + r_1\phi_1 + r_2\phi_2 - 2r_s r_1(\chi_s + \chi_1)\phi_s\phi_1 + r_s r_2(\chi_s + \chi_2)\phi_s\phi_2 \\ &+ r_1 r_2(\chi_1 + \chi_2)\phi_1\phi_2 + 4r_s r_1 r_2(\chi_s\chi_1 + \chi_s\chi_2 + \chi_1\chi_2)\phi_s\phi_1\phi_2 = 0 \end{aligned} \tag{6}$$

where r_i's are the numbers of segments in the component molecules, ϕ_i's are the volume fractions of the component molecules, and χ_i's are the interaction parameters; for example, $2\chi_1 = \chi_{12}+\chi_{13}-\chi_{23}$.[33,38-40]

Flory-Huggins theory is not expected to give quantitatively precise predictions of the phase behavior of any ternary system. Even if problems associated with the lattice model are neglected, the mean field approximation inherent in the Flory-Huggins expressions introduces serious errors in the predicted phase boundaries. These errors are due to an overestimation of the number of contacts between monomers. The overestimation becomes worse with the dilution of the system and with the increase in degree of polymerization of the polymers. The implications are that predictions based on

Flory-Huggins calculations are generally quantitatively incorrect, even for simple mixtures of nonpolar molecules.

For the application of the theory to aqueous polymer mixtures, there are additional problems. These problems come from two main sources. First, in the original derivation of the theory, a solvent molecule was assumed to occupy the same volume as a monomer unit of the polymer. However, there is a difference in size between a polymer segment and a solvent molecule. This makes the determination of the entropy of mixing more involved, but the main result is qualitatively the same. Secondly, water is a structural solvent with a complicated behavior. In an aqueous system, the interpretation of the interaction parameter, χ, has to be modified. The solvation of a monomer unit involves many water molecules, and it is associated with changes in the internal degrees of freedom of these water molecules. Primarily, this implies that χ has the character of a free energy even though it is purely enthalpic in the conventional Flory-Huggins theory and through comparison with experimental results χ is found to be strongly temperature dependent. Secondly, the fact that many solvent molecules are involved with the interaction of one monomer unit implies that at low solvent contents conditions change in a more complex manner than accounted for in the Flory-Huggins theory based only on pair nearest neighbor interactions.[32,35] Despite the above serious limitations, the Flory-Huggins theory is quite useful for obtaining physical insight into the various factors that govern polymer phase behavior in aqueous media.

2.3 PVA Binder Migration during Spray Drying

The PVA binder migration during spray drying process results in a higher concentration of binder on the granule surface and a lower concentration in the interior. This leads to a granule having a strong surface layer that resists fracture and deformation during compaction. Therefore, granule structures and large pores are formed in the green body and these defects survive through sintering.

The foremost reason for binder migration is the presence of non-adsorbing binder in a suspension, especially in the presence of dispersants. When a polymer competes with another chemically different polymer for surface sites, the condition with the lowest

free energy should be satisfied. This is achieved when the more readily adsorbed polymer covers the surface. Hence, for a binary polymer mixture only one component adsorbs unless the difference in adsorption energy per monomer unit is negligible. If the less readily adsorbing species is adsorbed first, exchange should eventually occur although this may depend on kinetic factors.[41] The adsorption study of PVA and PAA in alumina suspensions shows that adsorption of PVA is noted only in the absence of PAA. However, no PVA can adsorb on the powder surfaces in the presence of PAA with the concentration over 1.0 mg/m^2. In the presence of PVA there is no effect on the adsorption of PAA on an alumina surface. When PVA is adsorbed on the alumina surface, the PVA is fully replaced by PAA in a short period of time after PAA addition.[42] Therefore, most PVA added into the suspension exists as free polymer in solution.

Zhang *et al.* studied the PVA binder migration behavior during spray drying of a flocculated slurry. They considered the solvent evaporation and the solute diffusion as two major mass transport processes. During the spray drying process, water-soluble organic binders such as PVA tend to follow moisture flow. In the stage of constant-rate drying, PVA in a solution moves to the surface along with the solvent, and the PVA concentration at the surface region is increased. PVA simultaneously diffuses toward the inside of the drop due to the concentration gradient of PVA caused by migration according to Fick's law. In other words, binder segregation occurs as the overall result of migration toward the surface and diffusion in the opposite direction. The binder migration results in a non-uniform distribution of PVA within the spray-dried granules.[1-3] However, in their study the calculated binder migration region was much thinner compared to that directly observed in spray dried granules, which suggests more severe binder migration during spray drying process. The calculation was performed assuming that the initial distribution of PVA was homogeneous in the slurry and flows to the surface of droplets during evaporation. The thick migration region that was experimentally observed suggests that this assumption might not be true or that there is another factor causing PVA migration.

Deegan *et al.* systematically studied the drying behavior of droplets on a substrate.[43,44] Although their experiments were confined on a substrate, the theory

developed in this experiment can be still applied to drying of droplets. They examined a variety of solutes in different carrier fluids and concluded that solute migration is caused by an outward flow of carrier fluid within the drop that is driven by the loss of solvent during evaporation and geometrical constraint that the drop maintains an equilibrium droplet shape with a fixed boundary. An outward flow in a drying drop of liquid is produced when the contact line is pinned so that liquid removed by evaporation from the edge of the drop must be replenished by a flow of liquid from the interior. This flow is capable of transferring 100% of the solute to the contact line and thus accounts for the strong perimeter concentration of many solutes. Furthermore, their theory relies only on a generic property of the substrate-solvent interaction, the presence of surface roughness or chemical heterogeneities that produce contact line pinning, and therefore it accounts for the ubiquitous occurrence of ring-like stains.

They observed that ring-like deposits were formed whenever the surface was partially wet by the fluid irrespective of the chemical composition of the substrate for both aqueous and non-aqueous solvents. The ring-like deposits were found with solutes ranging in size from the molecular to the colloidal and with solute volume fractions ranging from 10^{-6} to 10^{-1}. Likewise, environmental conditions such as temperature, humidity, and pressure could be extensively varied without affecting the ring-like deposits. Their study confirms that non-adsorbing solute migrates to the surface region during drying by capillary forces where it is deposited during evaporation.

Lukasiewicz illustrated binder migration as the liquid flow in tube. The liquid flow rate is a direct function of surface tension, contact angle, and passageway radius. Also, it is an inverse function of the viscosity of the migrating liquid. The passageway radius, controlled by the particle size of the powder, the surface tension, and contact angle do not vary greatly in a given manufacturing process. It is the liquid viscosity within a spray drying run and between runs that will tend to vary. It should be emphasized that it is the viscosity of the migrating liquid that is rate controlling, not the viscosity of the slurry. Low viscosity grade binders, which are beneficial for achieving a high solid content slurry, may increase the amount of binder migration that occurs. The viscosity grade of the binder used in formulating the slurry should be selected to

minimize binder migration while still allowing maximum solid content.[45] It is noted that viscosity of a solution is a function of temperature. Therefore, the viscosity change during spray drying process should be considered during the binder selection.

Comeforo compared the migration behavior of several different binders.[46] The migration characteristics of an organic binder can be drastically effected by changes in the solubility of the binder and the viscosity and gelation properties of the binder-water mixture. If the solubility of the binder can be reduced or prohibited without effecting its binding properties, migration of the binder will be reduced or prohibited. The degree of migration is approximately proportional to the viscosity of the binder-water mixture. Gelation should alter the migration characteristics of a binder since it increases the resistance to flow. The solubility, viscosity, and gelation properties are dependent, to a certain extent, on two main variables; namely temperature and pH. The migration behavior can be greatly altered by changes in the drying temperature. Changes in pH may result in changes in solubility, viscosity, and gelation.

2.4 PVA Staining

It has been known that PVA gives a characteristic blue color when stained with iodine in an aqueous solution. The blue color reaction of PVA with iodine was first observed by Hermann and Haehnel, who synthesized PVA.[47,48] Aggregate and helix models were presented to explain the complexation of PVA with iodine by Tebelev[49] and Zwick[47] respectively in 1965 and have been supported by many different groups. However, the mechanism of the color reaction is still not clear.

The aggregate model was proposed by Tebelev *et al.* to explain the blue color reaction of PVA of different properties with iodine. They suggested that one of the necessary conditions for the formation of a blue complex is the aggregation of PVA molecules, creating favorable conditions for the penetration of iodine into supra-molecular structure or into interstices between them. PVA aggregation is formed due to the intermolecular hydrogen bonds.[48,49]

Zwick proposed the mechanism of the PVA-iodine reaction based on the assumption of helix formation in individual polymer segments and the development of a

helix cluster structure. A PVA molecule in a dilute solution is induced to form helix at a number of isolated sites along the polymer chain when coming into contact with iodine and iodide ions. However, these helices are not long and stable enough to host extensive linear polyiodide chains on their own. Stability is obtained by grouping into a cluster of helices. A slow process of recrystallization starts as several helices have joined a crude imperfect cluster. During this slow recrystallization stage, PVA channels in the interior of the helices become long and regular enough that they are able to link up a polyiodide chain, and thus display its blue color.[47]

Verification of these models is outside the scope of this review. It is noted that many studies on the PVA-iodine interaction show the same trend of results even though both models explain the results based on different assumptions. The PVA-iodine complexation showed a dependence on the concentrations of PVA, boric acid, and iodine solutions.[47,49-52]

There is a linear dependence of color intensity with PVA concentration when sufficient iodine is present.[53] The final color intensity and, even more so, the rate of color development are known to be temperature sensitive.[47]

In Zwick's model boric acid has a stabilizing effect on the helix by the occasional linking of two OH groups belonging to successive turns of the helix, which have become close neighbors in the helical configuration of the PVA chain. In the presence of boric acid, PVA and iodine are complexed at a much lower reactant level.[54] Also, as more boric acid is added, the amount of iodine complexed by PVA increases. Nearly four times the iodine binds to PVA at high boric acid levels compared to system prepared in the absence of boric acid.[47]

3. Experimental Procedure

3.1 Preliminary PVA Staining Study

The analytical possibility for the detection of PVA embedded in ceramic particles was examined using the color reaction of iodine, boric acid, and PVA.[55] Polymeric

additives investigated included sodium salts of poly(acrylic acid) [PAA-Na] and poly(methacrylic acid) [PMAA-Na], poly(ethylene glycol) [PEG], and PVA.

Spray dried granules were produced with alumina (A-16 S.G., Alcoa, Pittsburgh, PA) and the polymeric additives. A 2.0 liter alumina suspension at 30 v/o solids was mixed with each polymer for an hour. After eleven hours the suspension was spray dried to form a granulated feed material. Table IV-I lists the compositions of the polymer test batches. A mixed flow type spray drier (BE 985, Bowen Engineering, North Branch, NJ) with a two fluid nozzle was used. Spray drying conditions were the same for all batches made in this study. Inlet and outlet air temperatures were 250°C and 120°C, respectively. Nozzle atomization air pressure was 7 psi and the suspension volumetric flow rate was 1 ml/sec. The prepared granules were stored in a plastic bag for future use.

Two grams of granule were pressed into a pellet using a cylindrical metal die at 150 MPa for one minute. The pellet was immersed in liquid N_2 and fractured. 0.52 mol boric acid (United States Borax Inc., Valencia, CA) solution was sprayed on to the fracture surface and then 0.02 N Iodine solution (Fisher Scientific, Pittsburgh, PA) was sprayed. The fracture surface was observed visually and using optical microscopy (Polyvar Met, Reichert-Jung, Wien, Austria) to locate PVA within granules.

Table IV-I. Polymer Composition of Test Batches for Preliminary PVA Staining Study.

PVA	PVA 1w/o	
PVA-PEG	PVA 1w/o	PEG 1w/o
PMAA-PEG	PMAA 0.4 mg/m^2	PEG 1w/o
PAA-PEG	PAA 0.4 mg/m^2	PEG 1w/o

3.2. Polymers and Flory-Huggins Calculations

All the polymers used in this study and the reported properties are summarized in Table IV-II. The effect of polymer compatibility on the binder migration was investigated by using four different dispersants to produce spray-dried granules with a PVA binder. Polymeric additives involved in the manufacture of hotel china were chosen

for this study. This included sodium salts of poly(acrylic acid) [PAA-Na] and poly(methacrylic acid) [PMAA-Na], sodium silicate [SS], and sodium lignosulfonate [LS] as dispersants, and poly(vinyl alcohol) [PVA] as the binder. Reported information of the polymers is listed in Table IV-II and the structure of monomers is shown in Figure IV-6.

Table IV-II. Reported Properties of Polymers.

	Polymethacrylic acid*	Polyacrylic acid*	Sodium silicate	Sodium lignosulfonate	Polyvinyl alcohol
Commercial name	Darvan 7	Darvan 811	Sodium silicate solution	A 373	Airvol 205
Abbreviation	PMAA	PAA	SS	LS	PVA
Reported m.w.	10-16000	3500-6000	NA**	38500	31-50000
Polydispersity	1.9	1.5	NA	10	2.03
Source	R. T. Vanderbilt	R. T. Vanderbilt	Fisher Scientific	Lignotech	Airproducts

*PMAA and PAA have sodium salts.
**NA: Not Available

The phase behavior of each dispersant with PVA in aqueous solution was calculated using Equation 6 from the Flory-Huggins theory. The sum of all the component fractions is one. Therefore, another equation can be simply made.

$$\phi_s + \phi_1 + \phi_2 = 1 \quad (7)$$

Equation 6 becomes a quadratic equation for any of the components with the two possible roots being two spinodal points if one component fraction is substituted with other components based on Equation 7. Spinodal curves, which separate stable and meta-stable regions from an unstable region, were obtained from the calculation.

3.3 Polymer Mixture Preparation and Turbidity Characterization

For the polymer compatibility study each dispersant was mixed with PVA from 0:10 to 10:0 dispersant:PVA ratios at 21 w/o of total polymer concentration. The pH of all the solutions was adjusted to 9.5 ± 0.2. Range of polymer solutions from 5 to 21 w/o

total polymer concentrations was prepared for the PAA-PVA and PMAA-PVA systems. The pH of the solutions was again adjusted to 9.5 ± 0.2.

The prepared polymer solutions were tested using a turbidimeter (Model 2100AN Laboratory Turbidimeter, Hach, Loveland, CO) to measure the extent of light scattering. The turbidimeter measures the amount of light scattered from a focused tungsten light source by a solution. The intensity of the scattered light compared to that of the standard is presented in Nephelometric turbidity units (NTUs). The light source for the turbidimeter is Tungsten filament lamp.

Optical observations were made on the polymer solutions from the turbidity study using a phase contrast light microscope (Polyvar Met, Reichert-Jung, Wien, Austria). Polymer solution samples were dried on glass slides at 50 °C and observed under a microscope using transmitted light. Images were captured using a digital camera and software (ImagePro, Media Cybernetics, Silver Spring, MD).

Dilute polymer mixtures in deionized water (105 ml) were prepared to study the morphology of droplets after drying. The polymer compositions are summarized in Table IV-III. The polymer mixtures were adjusted to pH 9.5 and stirred for 24 hours. The drops of mixtures on glass slides were dried at room temperature and 100 °C and observed under optical microscopy using transmitted light.

Table IV-III. Polymer Composition in Dilute Polymer Mixtures.

		PVA
PMAA-PVA	PMAA 0.64g	1.79 g
PAA-PVA	PAA 0.64g	1.79 g
SS-PVA	SS 0.64g	1.79 g
LS-PVA	LS 0.96g	1.79 g

3.4 Suspension Preparation and Spray Drying

All the suspensions made for this study are summarized in the Table IV-IV. Suspensions were prepared at 30 v/o alumina (A-16 S.G. Alcoa, Pittsburgh, PA). Dispersant was added first into deionized water, alumina was added, and the suspension

was mixed for one hour (Stirrer RZR50, Caframo, Ontario, Canada). Binder was added to the suspension and mixed for two hours followed by a gentle agitation on a shaker (Orbit Shaker Bath, Lab Line Instruments, Melrose, Park, IL) for 22 hours. Suspension pH was not adjusted for the polymer compatibility study.

The spray dryer used for the granulating of all suspensions was a laboratory-scale mixed flow spray dryer (BE985, Bowen Engineering, North Branch, NJ). The slurry was pumped in from the bottom through a nozzle atomizer while hot air was forced in at the top. The inlet temperature, i.e. the temperature of the air entering the chamber, was kept between 250 – 275°C. The outlet temperature was dependent on the inlet temperature and the suspension pump rate. The pump used was a peristaltic pump (7553-20, Cole-Parmer Instruments Co., Chicago, IL) with a Cole-Palmer Masterflex controller to adjust the flow rate. The pump was kept at a constant rate such that the outlet temperature held at 110°C. Prior to the suspension being pumped, deionized water was pumped through at the pump rate of 1 ml/sec. The air pressure into the nozzle was set at 25 psi. When the spray drying cycle was completed, the collected powder was sealed in a bag.

Table IV-IV. Polymer Composition of Suspensions Made for the Polymer Compatibility Study

Dispersants	Binder
PMAA 0.4 mg/m^2	PVA 1 w/o
PAA 0.4 mg/m^2	PVA 1 w/o
Sodium silicate 0.4 mg/m^2	PVA 1 w/o
Lignosulfonate 0.6 mg/m^2	PVA 1 w/o

3.5 PVA Binder Migration Characterizations

Spray dried granules were classified by sieving (Fisher Scientific, Pittsburgh, PA). Granules of 180-212 μm were pressed to make pellets for PVA staining study and pellets made from granules of 45-53 μm were tested with a photospectrometer.

The extent of binder migration was analyzed by staining the PVA in granules as described earlier. Two grams of granulate were pressed using cylindrical metal die at

150 MPa for one minute. The pellets were immersed in liquid nitrogen for 1 minute and fractured. Boric acid (0.52 M) solution was sprayed on to the fracture surface and followed by iodine (0.02 N) solutions. The stained surface was observed using optical microscopy under reflected light.

4. Experimental Results and Discussions

4.1 Preliminary PVA Staining Study

The images obtained from fracture surface of pellets treated with boric acid and iodine solutions are shown in Figure IV-7. It is clearly shown that blue color in a pellet is unique to the reaction with PVA. The majority of the blue color reaction is shown around the surface of spray-dried granules, which indicates the migration of PVA binder during spray drying. Uniform blue color over some granules is due to coloring of PVA on granule surface, i.e. inter-granule failure. SEM examination confirms that the crack propagates between one third of the granules. There is no indication of a reaction with PAA or PMAA. PEG seems to react with the solutions in PVA-PEG sample due to brown coloring in the pellet. However, no interactions are shown in PMAA-PEG and PAA-PEG pellets. Therefore, it is concluded that the brown coloring is still related to PVA in samples.

The PVA adsorption on alumina particles is small. The amount of adsorbed PVA increases more or less linearly with the PVA concentrations. Compared to fully hydrolyzed PVA, partially hydrolyzed PVA molecules tend to achieve a flatter conformation with a greater number of train segments when adsorbed. The number of loops and tails increases with a decrease in the concentration of acetate groups allowing the polymer chains to extend into the solution.[56] The plateau value for PVA adsorption is 0.17 mg/m^2.[24] Thus, most of the PVA added into the suspension exists as free polymer and contributes to the migration.

Figure IV-8 shows that mixing of PVA and water is a spontaneous process, but at low polymer concentrations the PVA solution can be easily separated into two phases. Figure IV-9 represents a temperature-composition diagram since 1/K is proportional to

the absolute temperature. K is defined as $2BV_1/RT$, where B is a constant, V_1 is a molar volume of component, R is gas constant, and T is the absolute temperature. However, due to the lack of information the exact relationship between K and T could not be calculated. The calculation shows an asymmetrical phase composition relationship. As shown in the Figure IV-9, the solvent is readily soluble in the polymer even at large values of K (low temperature), but the polymer will dissolve perceptibly in the solvent only very near the critical point, and then only to a small extent.[57]

It is well known that PVA can form physical gels in water by lowering temperature. Water is a marginal solvent for PVA at room temperature, but PVA is known to behave as if it were in a poor solvent due to association between PVA molecules. Acetate groups on PVA keep the polymer chains from approaching too closely or orient properly to crystallize. Acetate groups decrease the association of PVA. The formation of a gel is a time dependent diffusion process. With time the molecules will be more associated. It is generally agreed that gelation results from network formation. A widely accepted view considers tie points in the network to be polymer crystallites. Pines *et al.* applied the concept of spinodal decomposition to the gelation process and explained the origin of network structure in terms of the connectivity of a polymer rich phase.[58] Komatsu *et al.* studied sol-gel transition in aqueous solutions of PVA. They showed that the liquid-liquid phase separation by the spinodal decomposition does not always induce gelation. Furthermore, spinodal decomposition is not a necessary condition for gelation. The development of the interconnected structure in the polymer-rich phase is the origin of gelation. The polymer rich phase is immobilized by gelation. It suppresses further coarsening of the interconnected structure developed by spinodal decomposition. Gelation starts by hydrogen bonding followed by crystallization of the polymer chains.[59]

Figure IV-10 shows the dried droplet of PVA solution on glass slide. PVA solution was mixed with deionized-water for 24 hours and a droplet of the solution was dried at 100 °C for 10 minutes. The image shows a homogeneously dried transparent PVA film on a slide. According to the temperature-composition diagram developed by Komatsu, the PVA solution will be in a sol state before drying and additionally

association of PVA molecules at room temperature will be destroyed with the elevation of temperature. The homogeneously distributed PVA molecules in solution result in a PVA gel without phase separation during drying, which is supported by the transparent PVA film.[60]

Based on the adsorption behavior of PVA on alumina particles and the behavior of PVA in solution during drying described above, the behavior of PVA in an alumina suspension during spray drying process is deduced. PVA will dissolve homogeneously in an alumina suspension at room temperature. Application of heat during spray drying will somewhat break down associated PVA molecules and induce more homogeneous mixing. During drying a connected structure of solid particles will be formed with the loss of solvent. PVA molecules migrate to the surface through the channels of the structure. The migration of PVA imparts a polymer rich phase at the surface of droplets. This will induce the network structure of the PVA molecules and results in the gelation of PVA molecules. Even though the temperature of sprayed droplets is much higher than the reported spinodal decomposition temperature, network formation of PVA molecules might occur due to the migration of PVA, which is similar to that of phase separation. The crystallization of PVA is also expected as water is progressively removed during evaporation. The kinetics of crystallization varies with the rate of evaporation of water.

In the study of PVA staining in aqueous solution, the blue color reaction is a tedious process. However, in this study the blue color reaction shows up immediately in all the samples after treatment with boric acid and iodine solutions. The heat treatment of PVA increases the density, which results in the increase in crystallinity.[22] In addition, PVA migration during drying may help to form clusters on the surface of granules. This may explain the fast color development.

4.2 Polymer Compatibility Study

4.2.1 Phase Behavior of Polymer Solutions

Flory-Huggins theory describes mixing of polymer solutions based on the second law of thermodynamics. If the Gibbs free energy of mixing is negative, spontaneous mixing occurs. The Gibbs free energy of mixing consists of an enthalpy term and an

entropy term. When the free volume effect is ignored, two main thermodynamic effects contribute to the enthalpy and entropy of mixing. These contributions are the intermolecular interaction arising from the different forces surrounding the molecules and the combinatorial entropy of mixing. The intermolecular interaction can be controlled by the chemical nature of polymers such as structure and functional groups and environments such as polymer concentration, pH, and ionic strength of solutions.

Spinodals of ternary polymer systems were calculated as described in Section 3.2 due to the difficulty in calculating binodals. This provides a qualitatively similar phase diagram to those seen for the binodals, which separate the stable from metastable and unstable regions. Interaction parameters of polymer-solvent and polymer-polymer used in the calculation were obtained using solubility parameters and summarized in Table IV-V. The calculated solubility parameter of water was low compared to the measured value, but the calculated value was used for the following calculations. Krause suggested that for values of polymer solubility parameters used in polymer-polymer compatibility calculations most accurate predictions are made when calculated rather than experimental values of solubility parameter are used for the predictions.[61] It is noted that due to the lack of information in structure of sodium lignosulfonate the obtained values probably deviate from the real values.

Table IV-V. Calculated Solubility and Interaction Parameters of the Tested Polymers.

	Solubility ($cal^{1/2}cm^{-3/2}$)	χ
PMAA	12.56	0.52
PAA	14.07	0.37
SS	16.13	0.38
LS	14.01	0.37
PVA	15.4	0.34
Water	15.00	

One of the main tasks of the investigation in the field of thermodynamics of mixing is to find the conditions of mixing and ranges of mutual solubility of different

polymers depending on their chemical nature and molecular weight. As shown in Figure IV-11, PMAA-PVA-Water system shows phase separation in most of mixture ratios and the phase separation occurs at the lowest polymer concentration. PAA and PVA are homogeneously mixed in PVA rich region. As the polymer concentration increases above 50 %, phase separation starts to occur. Sodium silicate is completely mixed with PVA in all ratios and concentration levels. Lignosulfonate-PVA shows similar phase behavior with the mixture of PAA and PVA.

PMAA-PVA shows quite different mixing behavior from PAA-PVA even though there is a similarity in structure. This difference comes from the differences in polymer-solvent interaction parameter, χ, and polymer chain length. χ is a dimensionless quantity which characterizes the interaction energy per solvent molecule divided by kT (the energy of a thermal vibration acting in favor of the mixing process). The quantity χ represents merely the difference in energy of a solvent molecule immersed in the pure polymer compared with one surrounded by molecules of its own kind, i.e., in the pure solvent. In this study χ was calculated from the solubility parameter. It is the first requirement of mutual solubility that the solubility parameter of the polymer and that of the solvent do not differ too much, which leads to smaller χ value. This concept can be applied to the polymer-polymer mixture as well. PMAA shows a relatively large difference in solubility with water and PVA, which results in a large χ value. This results in the poor mixing behavior of PMAA with PVA in water compared to PAA. Also, PMAA used in this study has a longer chain length than PAA. The chain length of polymer is directly related to the entropy of mixing in Flory-Huggins theory. As the chain length increases, the contribution of entropy to free energy of mixing decreases, which results in low negative or positive free energy of mixing. The longer chain length is another reason that PMAA has poor mixing behavior with PVA.

Sodium silicate is known to change the degree of polymerization depending on solution pH. In this calculation the degree of polymerization was assumed to be four based on the study by Nauman.[15] Due to the low molecular weight and solubility parameter of sodium silicate close to water and PVA, it results in a completely homogeneous mixtures at all compositions.

It is very hard to determine the molecular weight of lignosulfonate due to the complexity of the polymer structure. The reported relative molecular weight of lignosulfonate is 77000 g/mol and the actual molecular weight is assumed to be half this value, 38500, as reported by the provider. The lignosulfonate shows a slightly larger phase separation area with PVA than PAA does. This is mainly caused by the large chain length of the polymer.

All the polymer combinations tested in this study have a polyelectrolyte. The dissociation of counterions on polyelectrolytes has a profound effect on the phase behavior since it gives a very large contribution to the entropy of mixing. In a sense, the polyelectrolyte solution can be considered as an intermediate between a monomer and a polymer solution. The dissociation of counterions enhances the solubility of a polyelectrolyte and the miscibility with other polymers. When phase separation occurs at all, it may be expected that the separating phases differ widely in their overall polymer concentration with the phase enriched in the uncharged polymer being much more concentrated.[62] The effect of polyelectrolyte dissociation is not accounted for in the calculation of phase behaviors by Flory-Huggins theory. However, the miscibility of polymers will be improved relating to the calculated value in Figure IV-11

4.2.2 Polymer Solutions

Figure IV-12 shows polymer mixtures at 21 w/o in a 1:1 weight ratio. It is clearly shown that mixtures of PMAA-PVA and PAA-PVA have two phases. During the mixing of these polymers two different phases are visually observed; one is a clear liquid phase and the other is a semi-opaque gel phase. When the mixture is allowed to sit on the table for a week, the two phases are completely separated. The fraction of semi-opaque gel phase increases with increasing PVA addition. Sodium silicate-PVA mixtures also show two phases, but the top phase is cloudy relative to other systems. Separated phases are not seen in the LS-PVA system.

The turbidity change with the ratio between PMAA and PVA at pH 9.5 is shown in Figure IV-13. Strong interactions are shown in PVA rich regions. The polymer interaction becomes significant around 21 w/o total polymer concentration. This suggests

that polymer interaction increases with the loss of solvent during drying. The highest light scattering from polymer solutions is shown at a 3:7 ratio of PMAA:PVA. Strong light scattering is also shown over narrow ranges around this ratio. It is known that two polymers interact in an equimolecular ratio.[63] The molecular weight of PMAA was measured as 19500 and that of PVA was reported as 30000-50000. Based on these molecular weights, equimolecular ratio between PMAA and PVA falls between 2.5:7.5 – 1.7:8.3, which mostly covers the region of high turbidity. The deviation seems to be caused by the wide molecular weight distribution of two polymers.

PAA-PVA also shows similar behavior as PMAA-PVA, but light scattering is lower than PMAA-PVA as shown in Figure IV-14. The bottom phase from the phase separated system was dried on a glass slide and observed under optical microscopy. Figure IV-15 shows phase separated regions with in the bottom phase, which consists of a clear PAA rich phase and an opaque PVA rich phase. Small droplets of PVA are embedded in the PAA rich phase while PAA droplets are trapped in the percolation structure of the PVA rich phase.

It is shown in Figure IV-16 that the turbidity of sodium silicate-PVA mixture increases with an increase of sodium silicate in the PVA rich area. The turbidity is lower than that of the PMAA-PVA and PAA-PVA systems. As show in Figure IV-17 sodium silicate forms homogeneous mixtures with PVA in top and bottom phases. PVA is known to form hydrogen bondings with silicate ions in solution.[14] Rodrigues and Joekes showed that sodium silicate and PVA are homogeneously mixed using FTIR, suggesting that PVA hydroxyl groups complex with the sodium silicate species.[64]

Lignosulfonate is known to have various active functional groups on the polymer chain such as hydroxyl, phenol, and carboxyl groups.[19] These are expected to be involved in the interaction with PVA. However, the turbidity of LS-PVA is very low compared to other systems. When LS is added in the PVA rich region, turbidity drops and there is no notable change with further addition of LS.

Flory pointed out that in cross-linking the larger the molecule becomes, the greater the cross linking expectancy, because of the increased number of potential cross linking units.[65] This seems to be reflected in the turbidity data. However, the way

polymers form complexes will also be important. Bel'nikevich *et al.* suggested several ways polymers could form complexes.[66] If polymers form complexes without a three-dimensional network, the effect on turbidity will be small, which might be the case for lignosulfonate-PVA mixtures. Infinite structures are only possible in systems possessing structural units, some of which are capable of joining with more than two other units. Sodium silicate might correspond to this case due to the numerous functional groups.

In the PVA gelation study it was found that the opaque gel of PVA results from non-homogeneous correlation length of the network, which corresponds to an average distance between the nearest neighboring cross-linking points. In the transparent gel the distribution of cross-linking points was homogeneous. This suggests that the opaque phase obtained from PMAA-PVA, PAA-PVA, and SS-PVA systems is induced by cross-linking between polymers, which is non-homogeneously distributed.[67]

The study of phase relations described in Section 4.2.1 is based on the assumption that the system under consideration is at equilibrium. This condition must be satisfied to develop reliable information on phase relations. However, as in the spray drying process, which is considered in this study, circumstances may not permit a condition of equilibrium to be established. The progress of a system toward its stable equilibrium state can often be frozen for kinetic reasons resulting in a phase assembly, which can persist metastably for an extended period. Hajime *et al.* showed that when two or more non-equilibrium phenomena take place simultaneously, the final phase is determined not by an equilibrium phase diagram, but by their dynamics.[68]

Dilute polymer mixtures, which correspond to the polymer concentrations of suspensions prepared for spray drying, were made and the drops of those polymer mixtures were dried on glass slides at room temperature and 100°C. Solvent quenches are expected to be inhomogeneous, leading to variations of solvent concentration within the drop due to the solvent loss at the solution-air interface. In addition, equilibrium phase compositions are constantly changing since solvent loss is continuous during drying process.[69]

The drop morphology of PMAA-PVA mixtures dried at room temperature and 100°C are shown in Figures IV-18 and IV-19, respectively. Phase separation through

spinodal decomposition is shown in both drops. However, the bicontinuous phases in a drop dried at room temperature are connected by extended branches, which are considered as PVA crystallization. The size of bicontinuous phase in a drop dried at room temperature is larger than that in a drop dried at 100°C. Droplet type phase separation is shown in the outside region of drop dried at 100°C.

As shown in Figures IV-20 and IV-21, both drops of PAA-PVA mixtures also show bicontinuous phases, which are induced by spinodal decomposition. However, the size of bicontinuous phase in a drop dried at room temperature is much larger than that in a drop dried at 100°C. In a drop dried 100°C the development of bicontinuous phase is in different state depending on the position of drop.

Figures IV-22 and IV-23 show the drop morphology of SS-PVA mixtures. In both drops no phase separation is shown. Instead, network structure is clearly shown in a drop dried at room temperature. Ring shape rim is shown outside of drop dried at 100°C.

The drops of LS-PVA mixture in Figures IV-24 and IV-25 show interesting features. No phase separation is shown in a droplet dried at room temperature, but droplet type phase separation is shown in a drop dried at 100°C. The distinct brown color of lignosulfonate is shown only on the outside of drops and the phase separation in a drop dried at 100°C coincides with this region.

The phase separation can be induced by two major mechanisms: nucleation and growth, and spinodal decomposition. Nucleation and growth occur in metastable region, implying the existence of an energy barrier and the occurrence of large composition fluctuations. The critical nuclei are a necessary condition. Spinodal decomposition takes place in unstable region under conditions in which the energy barrier is negligible, so even small fluctuations in composition grow.[37] In addition, Tanaka divided the spinodal decomposition into bicontinuous phase separation and droplet phase separation at the late stage of phase separation. For a symmetric composition bicontinuous phase separation occurs while for off-symmetric composition droplet phase separation occurs.[70] However, it is noted that whether a phase separation morphology is bicontinuous type or droplet type is likely dependent on the phase separation time and cannot be determined solely by the composition.[71]

The morphology of both drops of PMAA-PVA mixture suggests that the polymer mixtures go to the unstable region with the loss of solvent during drying. By comparing two drops it is known that the bicontinuous phase grows during drying. The coarsening mechanism for bicontinuous phase separation has been revealed to be the hydrodynamic coarsening driven by the capillary instability.[72] Therefore, compared to the drop dried at 100ºC, long lasting water phase in the drop dried at room temperature helps the growth of a bicontinuous phase. Hopkinson *et al.* showed that more rapidly dried polymer films exhibit phase separation at a higher overall water content than those dried more slowly.[69] There are many more bicontinuous phases in a drop dried at 100ºC, which are smaller in size than that in a drop dried at room temperature. This suggests that the bicontinuous phase starts to show up early during drying in a drop dried at 100ºC, but due to the loss of solvent the phase does not grow, resulting in the small phase separated domains. The droplet type phase separation on the droplet dried at 100ºC can be caused by two reasons: 1) local off symmetric composition or 2) dynamic asymmetry of components.

The drops of PAA-PVA mixture show the bicontinuous phase, but the initial stage of bicontinuous phase separation is observed in the drop dried at 100ºC. The phase separation of PAA-PVA starts at higher polymer concentrations, which corresponds to late stage of the drying process. This leads to the morphology of initial stage of phase separation with fast drying at 100ºC. It is noted that on the phase diagram the drying path is a little bit off from the unstable region, but still bicontinuous phase separation occurs.

The porous network structure in some part of SS-PVA drop dried at room temperature suggests that these two polymers form a network at certain composition and slow drying rate. The initial homogeneous solution of SS-PVA leads to the homogeneous dried film.

According to the phase diagram, at the end of drying process the LS-PVA mixture goes through an unstable region, but no bicontinuous phase separation occurs in the observed drops. Instead, droplet type phase separation is shown in some areas of drop dried at 100ºC. Droplet type phase separation can be again induced by; 1) local off symmetric composition or 2) dynamic asymmetry of components. The occurrence of brown color ring at the outside of droplet indicates the migration tendency of both

polymers. In Deegan's study on the drying of drop on a substrate, after a contact line is pinned, an outward radial fluid flow is induced when there is an evaporation at the edge of the drop. The outward flow carries the solutes and forms a ring.[43,44]

4.2.3 Binder Migration

Four systems with different dispersants are compared in Figure IV-26. The blue color reaction is most intense for the PAA-PVA system. The PMAA-PVA system shows relatively uniform blue color inside granules compared to PAA-PVA system. The sodium silicate-PVA system shows most uniform blue color throughout the granules. Due to the brownish color of sodium lignosulphonate the overall color of the image obtained from LS-PVA system turns to purple.

The polyelectrolyte, which was used as dispersants, is expected to adsorb on alumina particle surfaces. Adsorption studies of PMAA and PAA on alumina particles show that added polymers cover the particle surfaces.[8,73] From the adsorption study of lignosulfonate on kaolin it can be also assumed that the added lignosulfonate adsorbs on the alumina surfaces.[17] Sodium silicate in monosilicate or polysilicate form also adsorbs on alumina particles.[16] It was already mentioned that PVA has weak adsorption on alumina and most of added PVA exists as free polymer. No PVA adsorption occurs in the presence of the polyelectrolyte. However, the adsorption of polyelectrolyte is not affected by the presence of PVA or the polymer addition sequence.

The presence of alumina particles in suspension is not expected to interfere with the phase separation to the polymeric additive. Since PMAA and PAA have a high affinity for the alumina surface, the presence of alumina in suspension is expected to behave like a PAA or PMAA rich phase in solution. In the phase separation study of particles (GP) in binary liquid mixture (*a* and *b*) Tanaka showed that more wettable liquid (*a*) covers the particle surface (GP) and the apparent volume fraction of *a*-phase becomes *a*+GP. Then, the phase separation of a+GP and b phases was explained depending on the mobility of particles.[70]

At the beginning of drying process PAA or PMAA coated alumina particles are assumed to be homogeneously distributed in solutions with PVA. With the loss of

solvent both systems go to phase separation regions as shown in the polymer solution study. With the start of phase separation particles covered with PAA or PMAA tend to form an interconnected structure to reduce the free energy of the system. Strong attractive interaction acts between the particles to reduce the interface area with the PVA rich phase. The process to form an interconnected structure is facilitated with the shrinking of sprayed droplets. The shrinkage of PAA or PMAA rich phase will tend to expel the PVA rich phase outside of PAA or PMAA rich phases to minimize the interface areas. This process will be enhancing transportation of water to the surface area of the droplet during drying.

The phase diagram and the morphological development of polymer mixtures during drying indicate that phase separation of PAA-PVA system occurs during the later stages of the drying process compared to the PMAA-PVA system. Therefore, small domains of phase separated PVA in the PAA-PVA system migrates easily to the surface of granules during the spray drying process. Conversely, the early appearance and growth of the bicontinuous phase in PMAA-PVA system hinder the migration of the PVA rich phase.

Also, PVA, PAA, and PMAA all have strong hydrogen bonding donor and acceptor groups. It was shown that these polymers form an association in solution. Budtova also suggested that volume of polymer complex increases with the total concentration of polymer because PVA associates to already formed polymer complexes.[74] Therefore, the migration of PVA in PMAA-PVA is lower than PAA-PVA system. It is also noted that PMAA is known to form a stronger association with PVA than does PAA.[75]

The most homogeneous distribution of PVA is shown in the sodium silicate-PVA system. Sodium silicate forms a homogeneous mixture with PVA in solution. Phase behavior does not indicate any kind of phase separation between these polymers. However, sodium silicate is assumed to strongly interact with PVA due to the flexibility of low chain length and numerous functional groups on the polymer chain. PVA is known to form hydrogen bonds with silicate ions in solution.[14] This results in a network

structure between sodium silicate and PVA, leading to homogeneous distribution of PVA.

It was suggested in the polymer solution study that lignosulfonate might form a complex with PVA without the connection between other complexes. Figure IV-27 is a drop of alumina suspension with LS-PVA dried at 100°C. It is interesting that dried drops with or without alumina particles show brown ring on the outside of drops. This suggests that non-adsorbed LS in the suspension competitively migrates to the surface of granules with PVA. The competition may reduce the PVA migration.

5. Conclusions

It is shown that PVA binder migrates to the surface of granules during drying process. It is suggested that the basic reason for the migration is the incompatibility of PVA with alumina surfaces. The PVA migration is driven by the low affinity of PVA on alumina surfaces and facilitated by the capillary action during drying process.

Migration of PVA binder in the presence of another polymer is explained by the interaction and phase separation of the polymers used in the spray drying process. Phase calculation indicates phase separation in PAA-PVA, PMAA-PVA, and LS-PVA systems and homogeneous mixing in SS-PVS system. Polymer solution study by a turbidimeter reveals strong interactions in the PAA-PVA and PMAA-PVA systems and relatively weak interactions in the SS-PVA and LS-PVA systems. The morphology study of polymer drops dried at room temperature and 100°C shows that a bicontinuous type phase separation occurs in the PAA-PVA and PMAA-PVA systems, a homogeneous film is formed in SS-PVA system, and a droplet type phase separation in some regions of a drop dried at 100°C in the LS-PVA system. All these results support the binder migration behavior in spray-dried granules. The granules with PAA-PVA show the most severe PVA migration behavior due to the late occurrence of phase separation. The granules with PMAA-PVA demonstrate less PVA migration due to the growth of the bicontinuous phase, formed by early phase separation. The formation of homogenous film between SS and PVA results in the most homogenous distribution of PVA in

granules. The competitive migration behavior of LS and PVA may slow down the migration of PVA in the granules with LS and PVA.

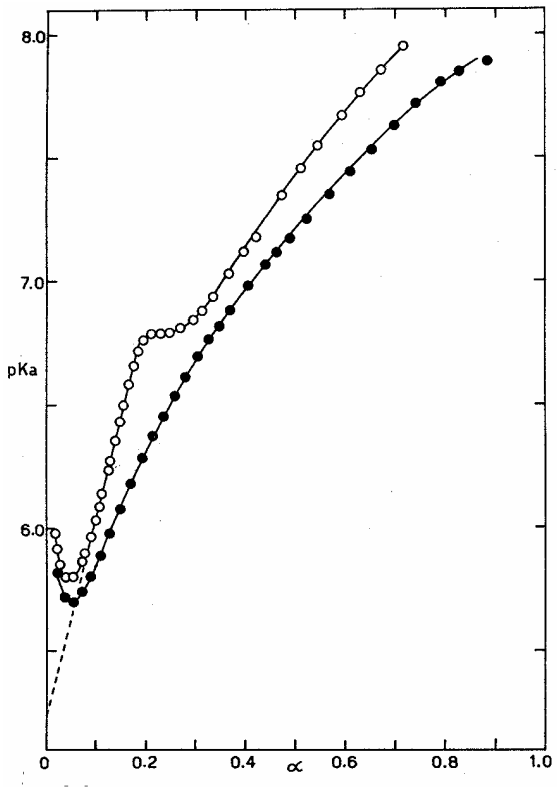

Figure IV-1. Apparent dissociation constant, pK_a, values for poly(methacrylic acid) and poly(acrylic acid) as a function of the degree of dissociation, α. Open circle is PMAA and closed circle is PAA. Polyelectrolyte concentration, $2x10^{-2}$ N; no added salts.[5] PMAA chains resist expansion before a critical charge density.

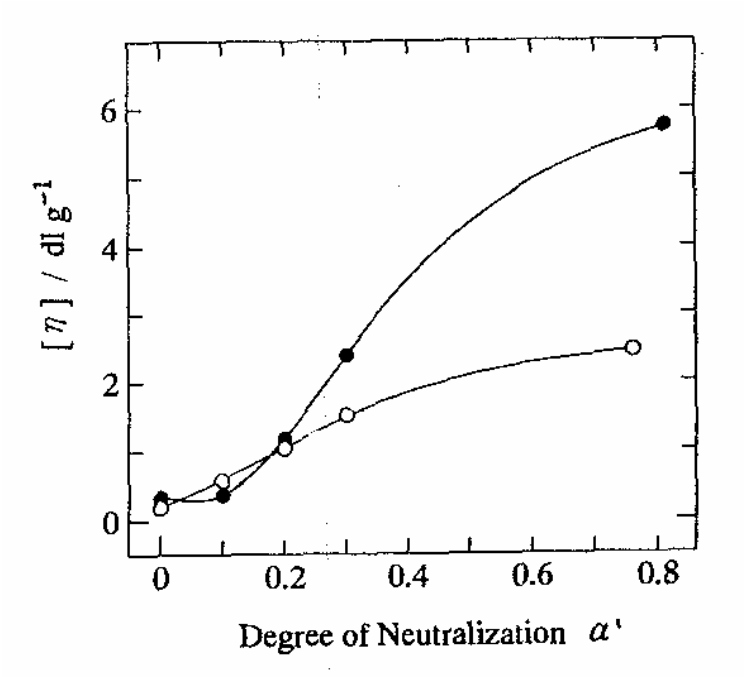

Figure IV-2. Viscosity change of polymer solutions with the degree of dissociation of polyelectrolytes.[7] Closed circle denotes PMAA and open circle denotes PAA. The intrinsic viscosity of PAA increases monotonously with increasing degree of dissociation whereas PMAA shows anomalous viscosity behavior. The viscosity behavior of PMAA is considered as one of the evidences for the chain conformation transition at a critical degree of dissociation.

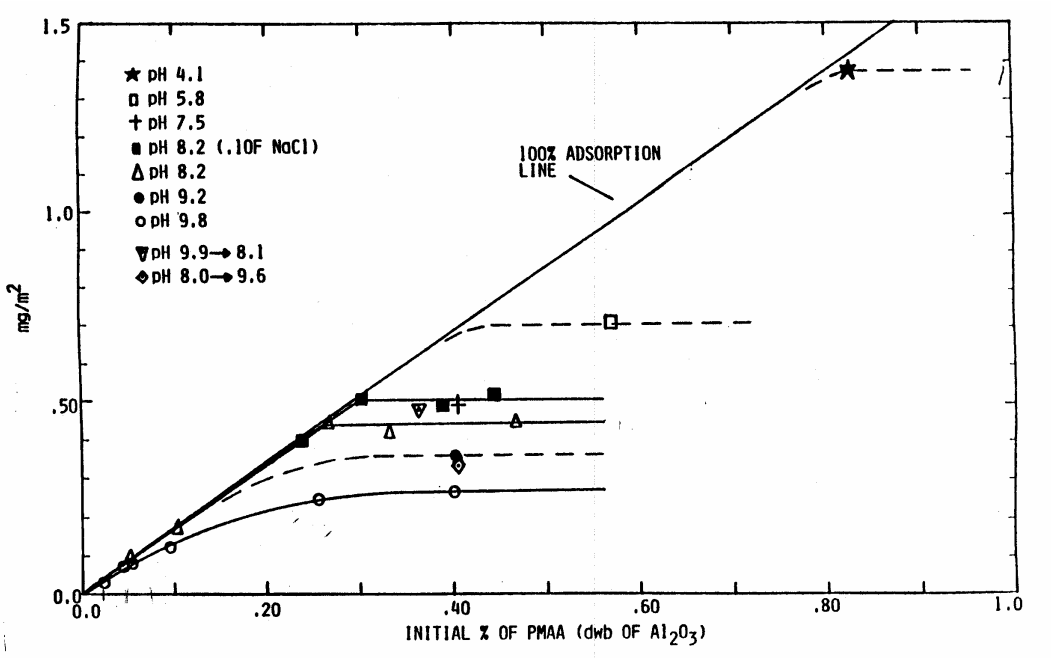

Figure IV-3. The adsorption isotherm of PMAA on alumina particles with pH change.[8] Line indicates 100% adsorption of PMAA on alumina particles. Adsorption amount decreases with the increase of suspension pH.

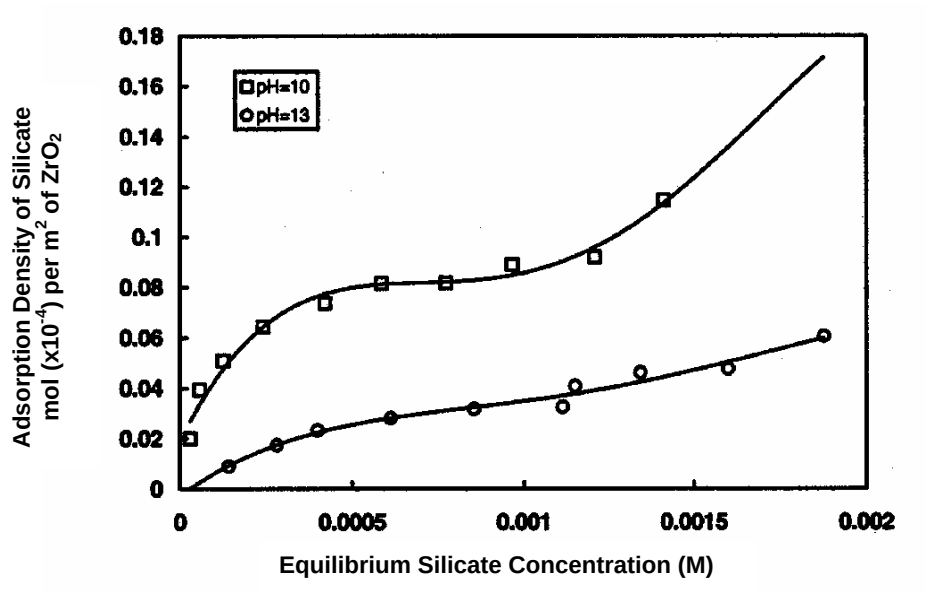

(a)

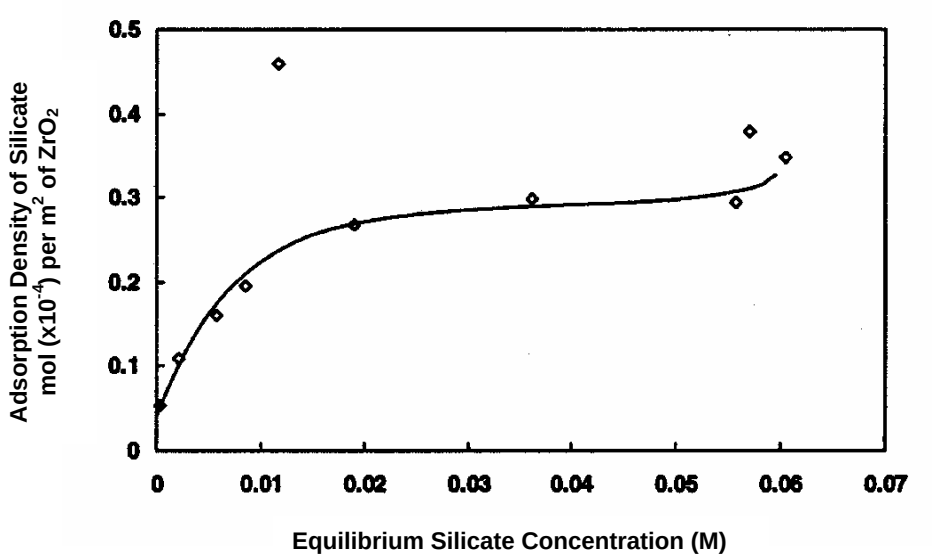

(b)

Figure IV-4. Adsorption isotherms of (a) monosilicate and (b) polysilicate on zirconia.[16]

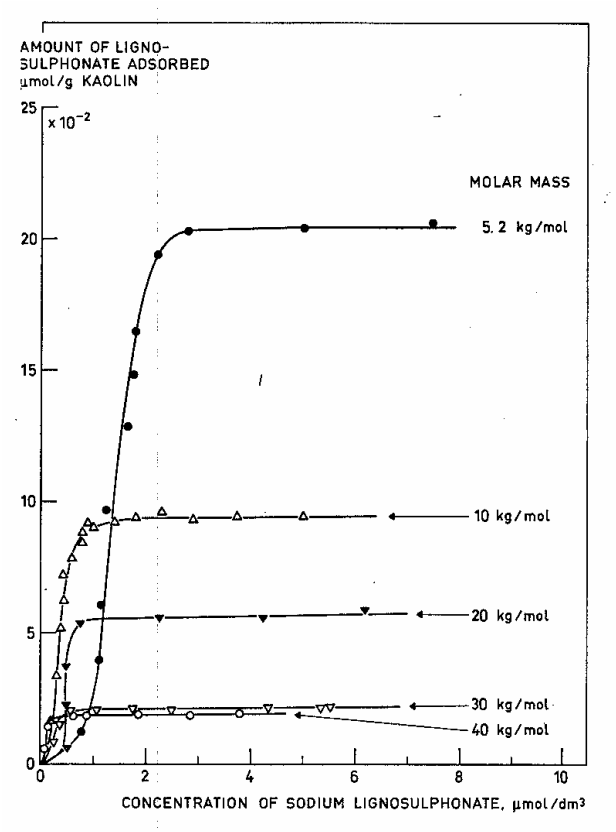

Figure IV-5. Adsorption isotherm of LS on kaolin. The adsorption amount decreases with the increase of molar mass of LS.[19]

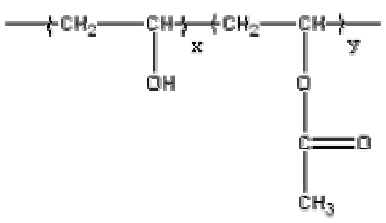

x is 88 mol% and y is 12 mol%
Poly(vinyl alcohol) [Airvol 205]
Air Products and Chemicals, Inc., Allentown, PA

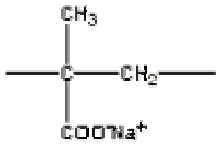

Poly (methacrylic acid) [Darvan 7]
R. T. Vanderbilt Co., Inc., Norwalk, CT

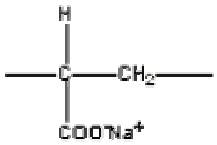

Poly (acrylic acid) [Darvan 811]
R. T. Vanderbilt Co., Inc., Norwalk, CT

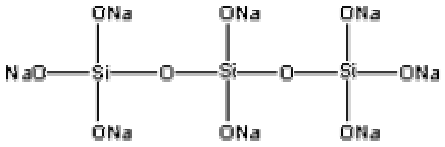

Sodium silicate
Fisher Scientific, Pittsburgh, PA
$SiO_2 : Na_2O = 3.55:1$

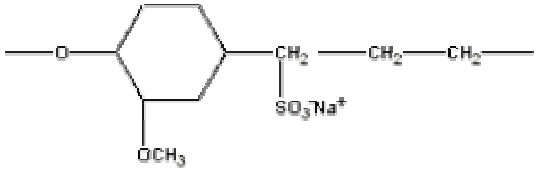

(Overly simplified) Lignosulfonate [A373]
Lignotech, Richmond, WI

Figure IV-6. Schematic illustrations of the monomer structure for the polymers used in this study. All the dispersants have ions which can be dissociated, Na.

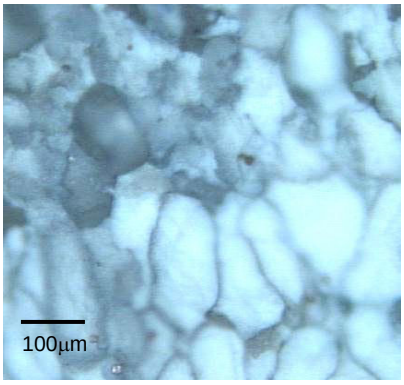

(a)

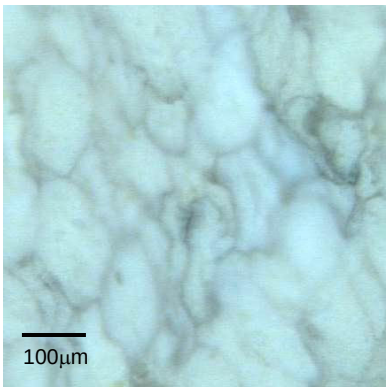

(b)

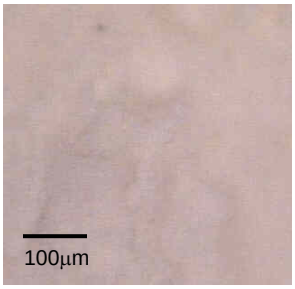

(c)

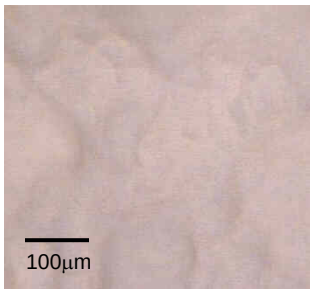

(d)

Figure IV-7. Stained fracture surface from pellets made of granules with (a) PVA, (b) PVA-PEG, (c) PMAA-PEG, and (d) PAA-PEG. Boric acid and iodine solutions were sprayed on the fracture surface. Distinct blue color reaction is shown only in pellets made of granules with PVA.

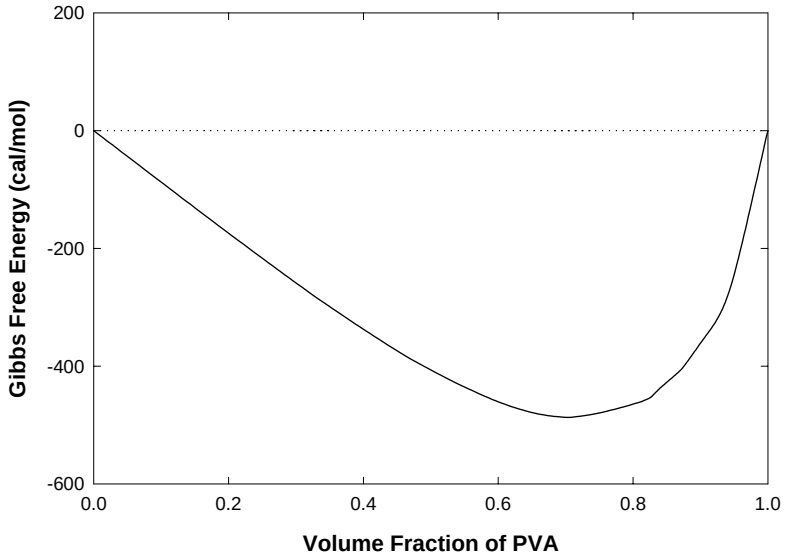

Figure IV-8. Calculated Gibbs free energy of mixing for PVA in water. The calculated Gibbs free energy indicates that the mixing is a spontaneous process over all the polymer fractions.

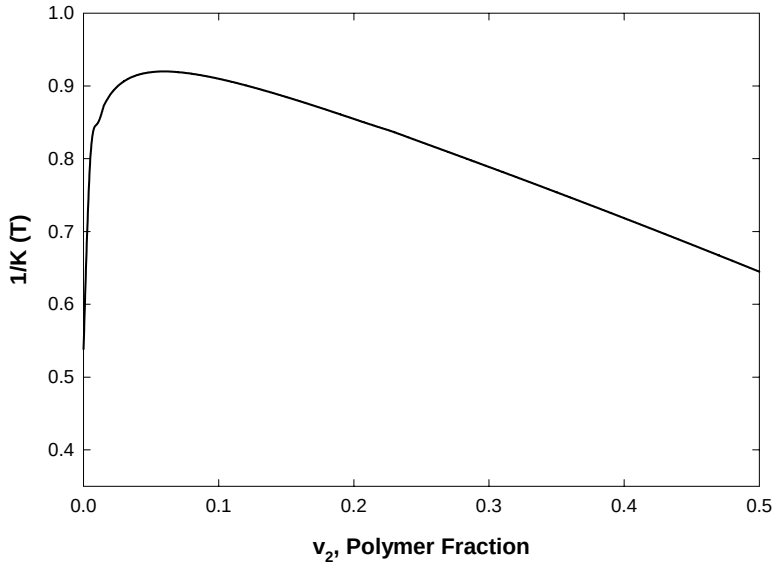

Figure IV-9. Phase composition curve calculated for a PVA solution (segment length=760). The calculation shows an unsymmetrical phase composition relationship. PVA will dissolve perceptibly in the solvent only very near the critical point.

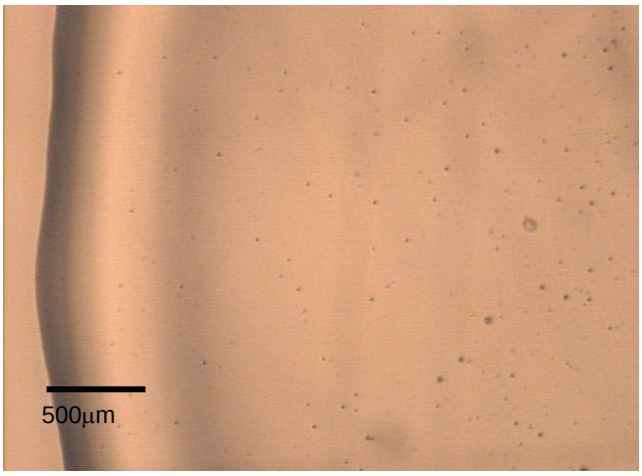

Figure IV-10. The image shows part of a dried PVA drop on glass slide. The PVA solution forms a homogeneous film after drying. The left side of image shows the edge of the drop and air bubbles are shown inside the drop.

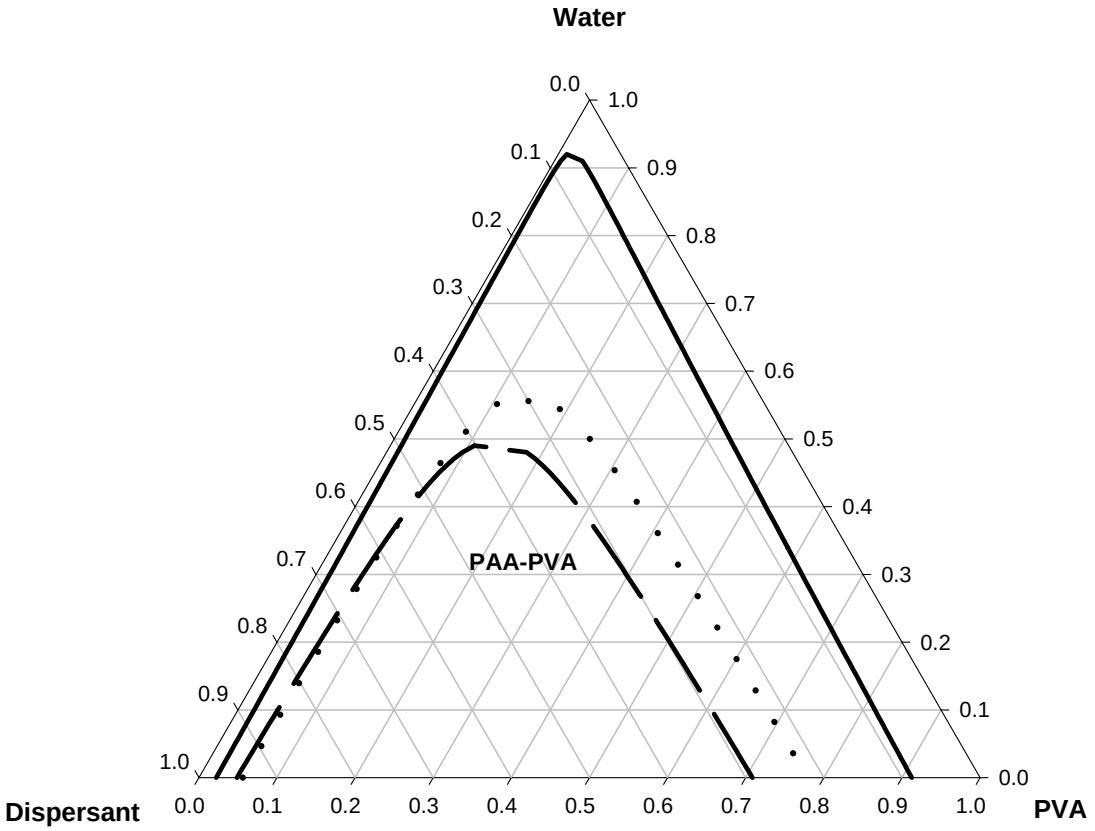

Figure IV-11. Calculated phase diagram of ternary polymer systems showing regions of predicted phase separation for the polymer systems under investigation. The lines within the phase diagram indicate the spinodal decomposition boundary, which separates the stable and metastable region from the unstable region.

Figure IV-12. Images of polymer mixtures at a 1:1 ratio for (A) PMAA-PVA, (B) PAA-PVA, (C) SS-PVA, and (D) LS-PVA. After turbidity measurement the samples were allowed to sit on a table. Two separated regions are shown in PMAA-PVA, PAA-PVA, and SS-PVA mixtures.

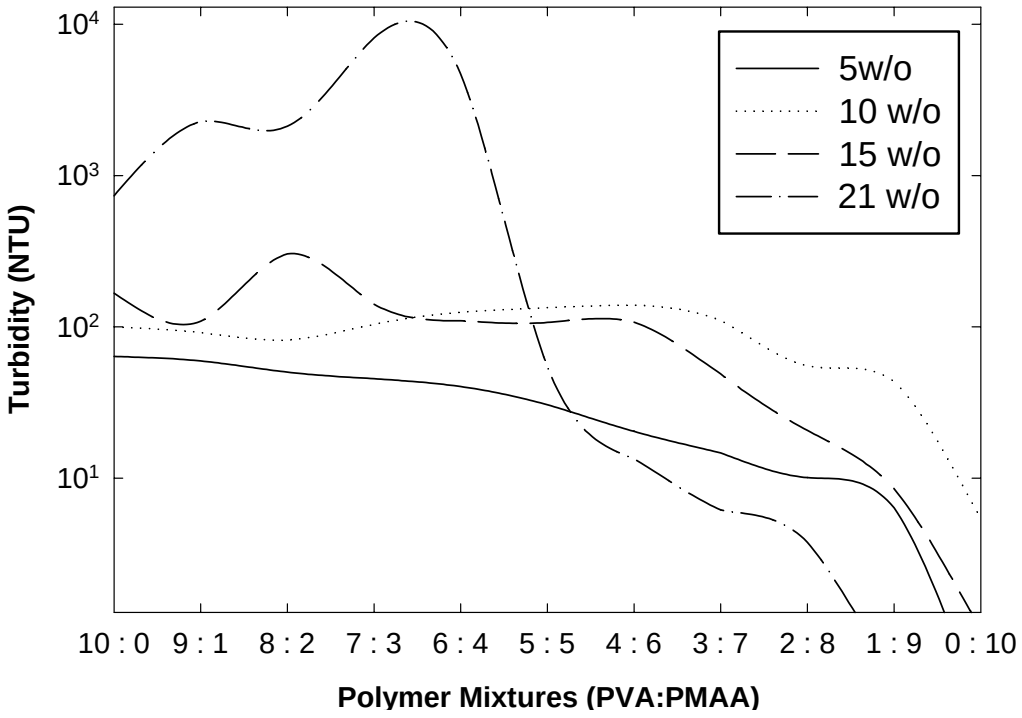

Figure IV-13. Turbidity change of PMAA and PVA mixtures for polymer solutions at various concentrations. Strong interaction between the polymers is shown in PVA rich region.

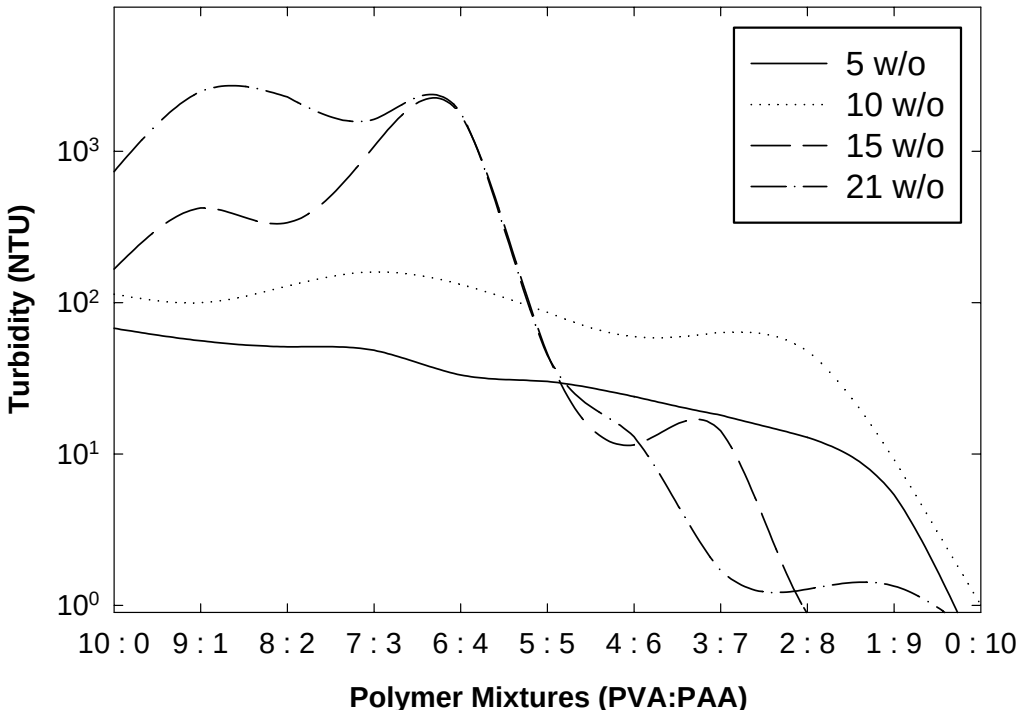

Figure IV-14. Turbidity change of PAA and PVA mixtures for polymer solutions at various concentrations.

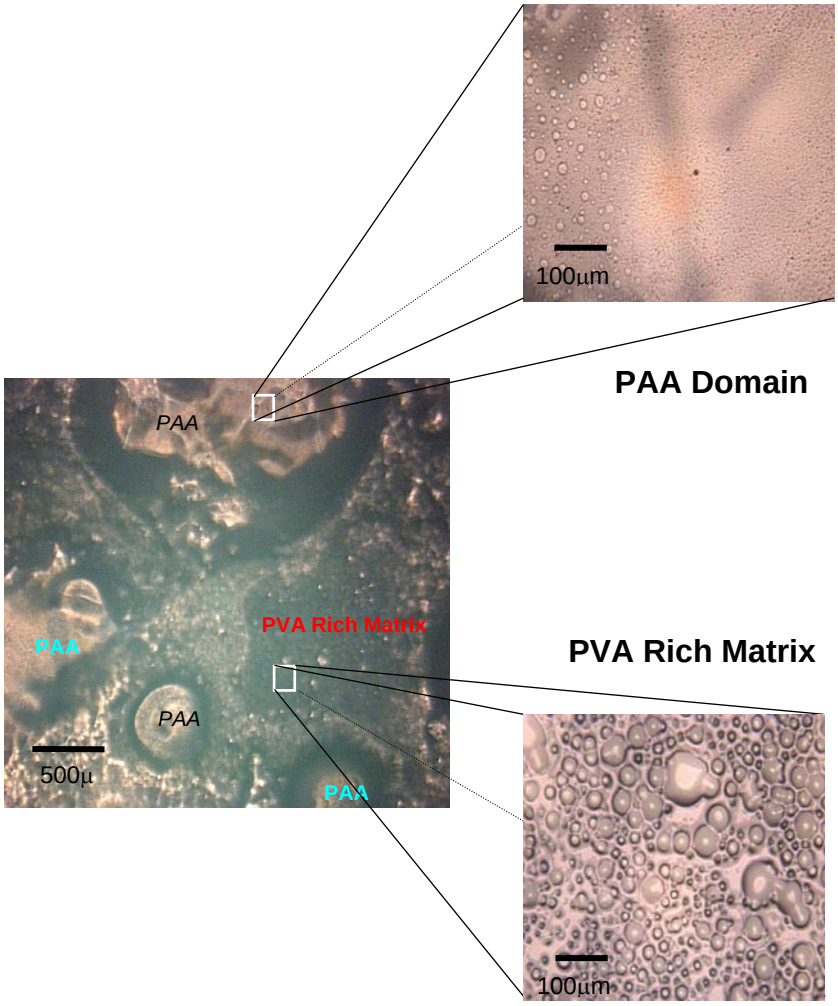

Figure IV-15. Polymer phases formed in dried PAA-PVA mixture (1:1 ratio). The settled region of PAA-PVA mixture in Figure IV-12 was dried on a glass slide. Separated phases show distinct morphology.

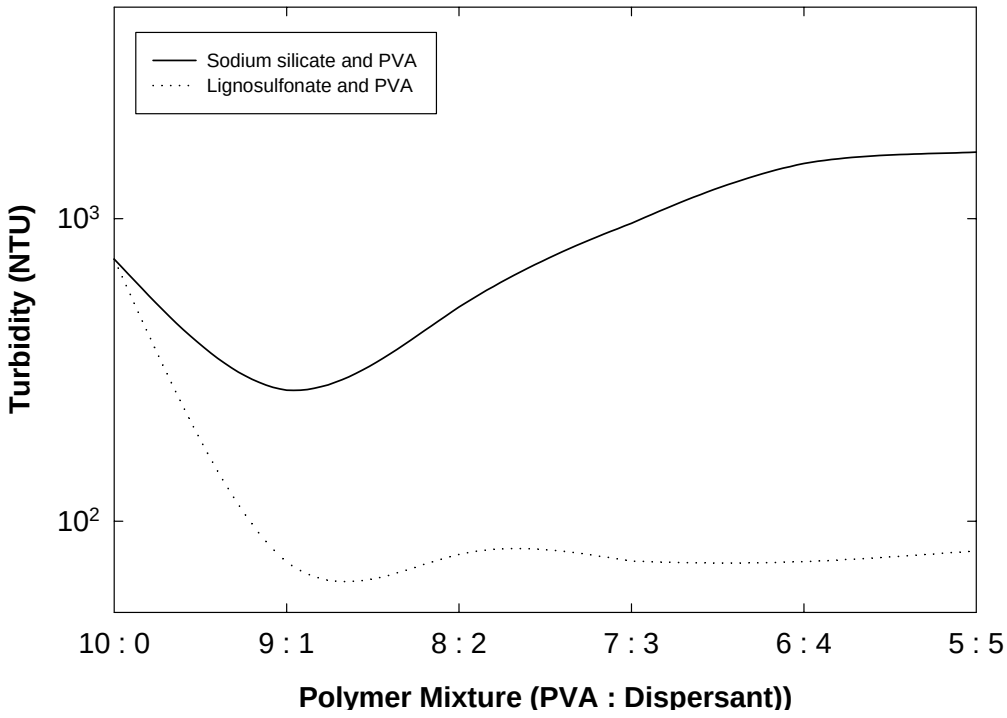

Figure IV-16. Turbidity changes of SS-PVA and LS-PVA mixtures at 21 w/o.

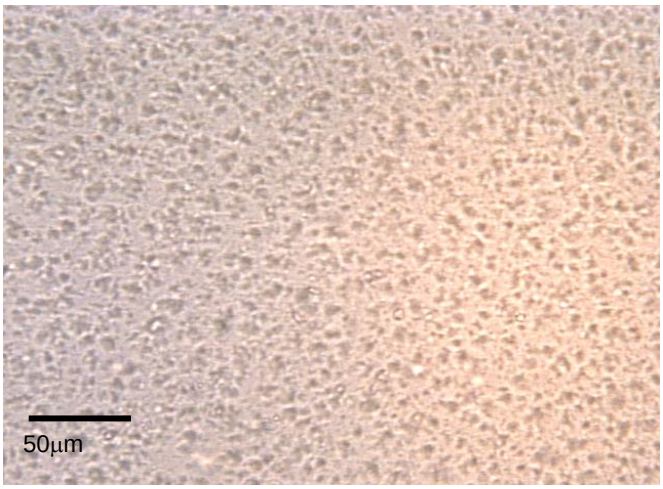

(a)

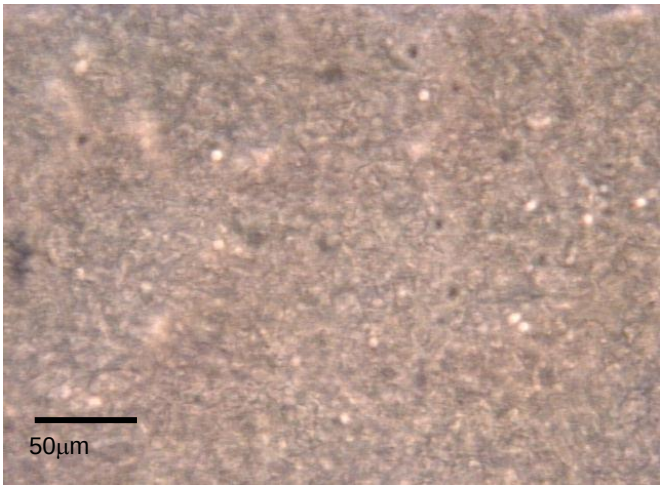

(b)

Figure IV-17. Images obtained from dried SS-PVA mixture (1:1 ratio). Images (a) and (b) are obtained from the top and bottom phases of SS-PVA mixture in Figure 13, respectively.

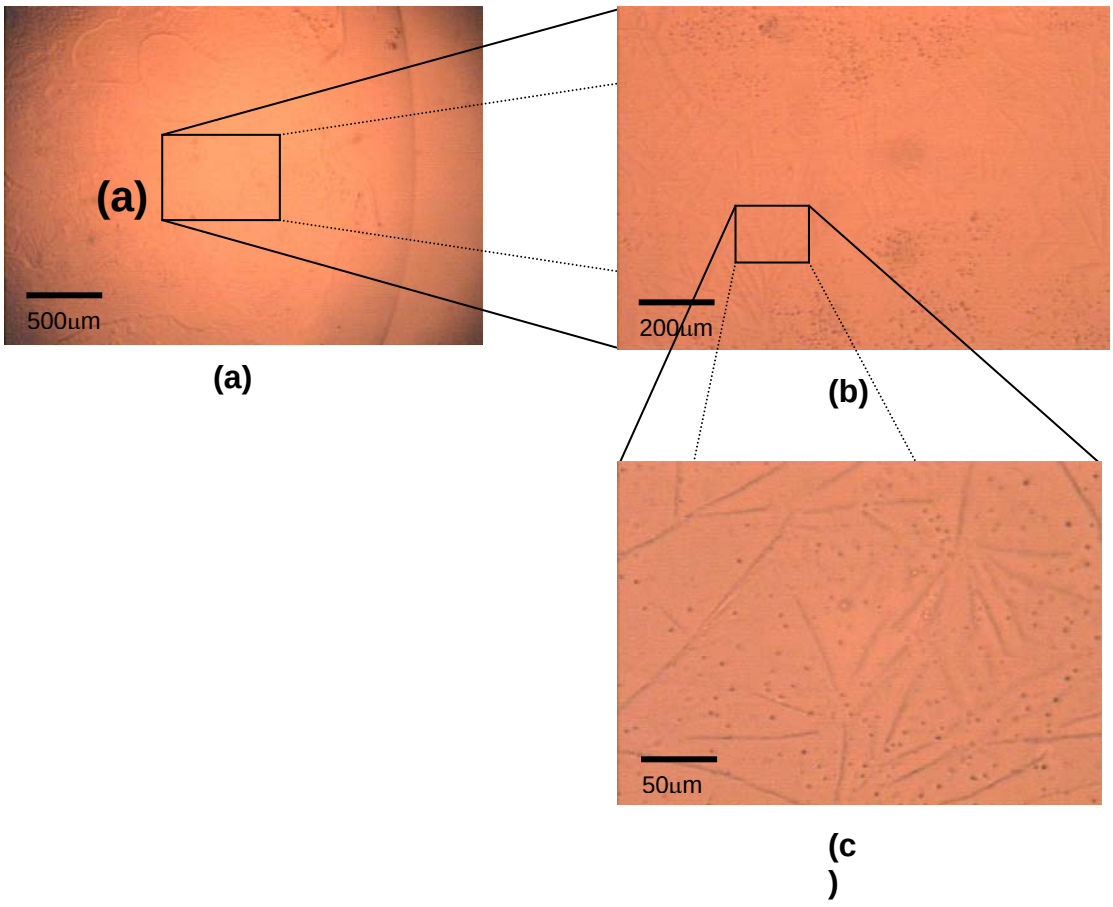

Figure IV-18. Images of a drop of the PMAA-PVA mixture dried at room temperature. Bicontinuous type phase separation is shown in images (a) and (b). Needle like morphology is shown in image (c).

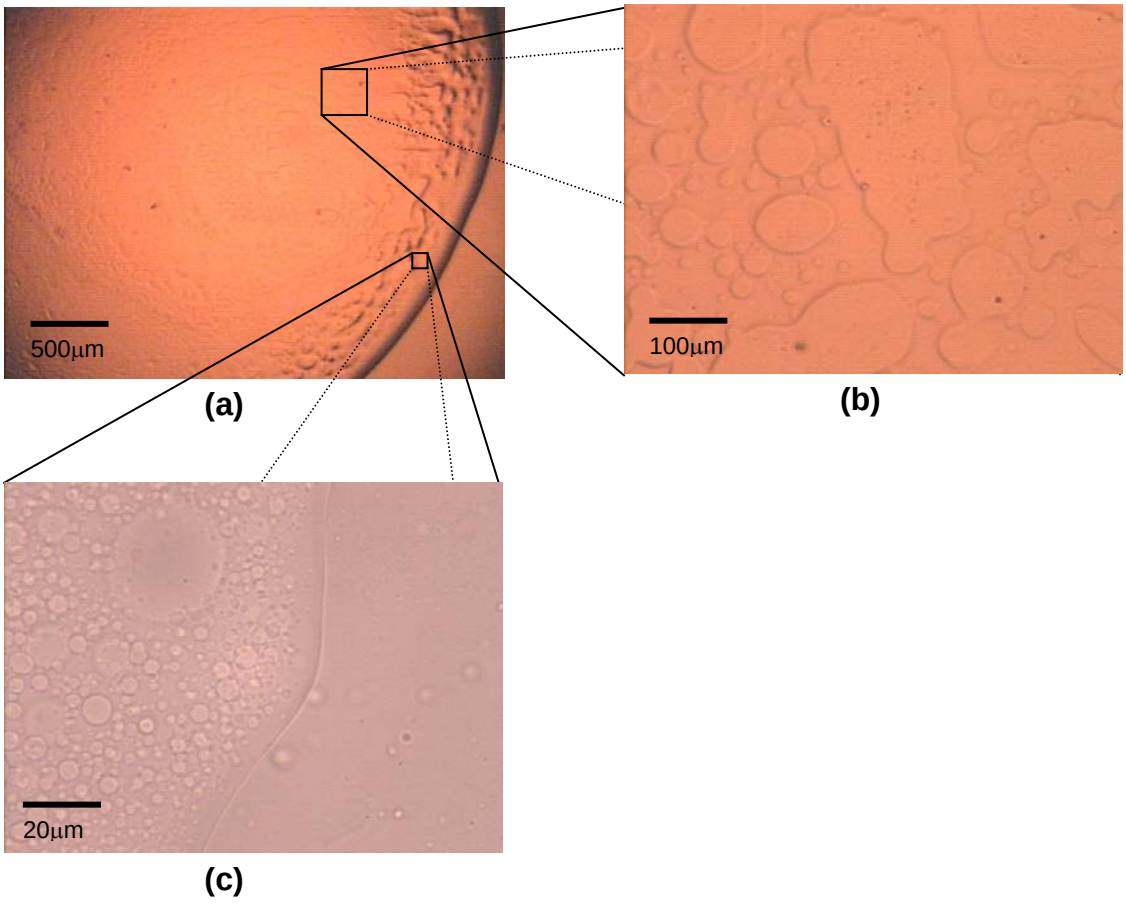

Figure IV-19. Images of a drop of the PMAA-PVA mixture dried at 100 °C. Bicontinuous and droplet type phase separation are shown in image (b) and (c), respectively.

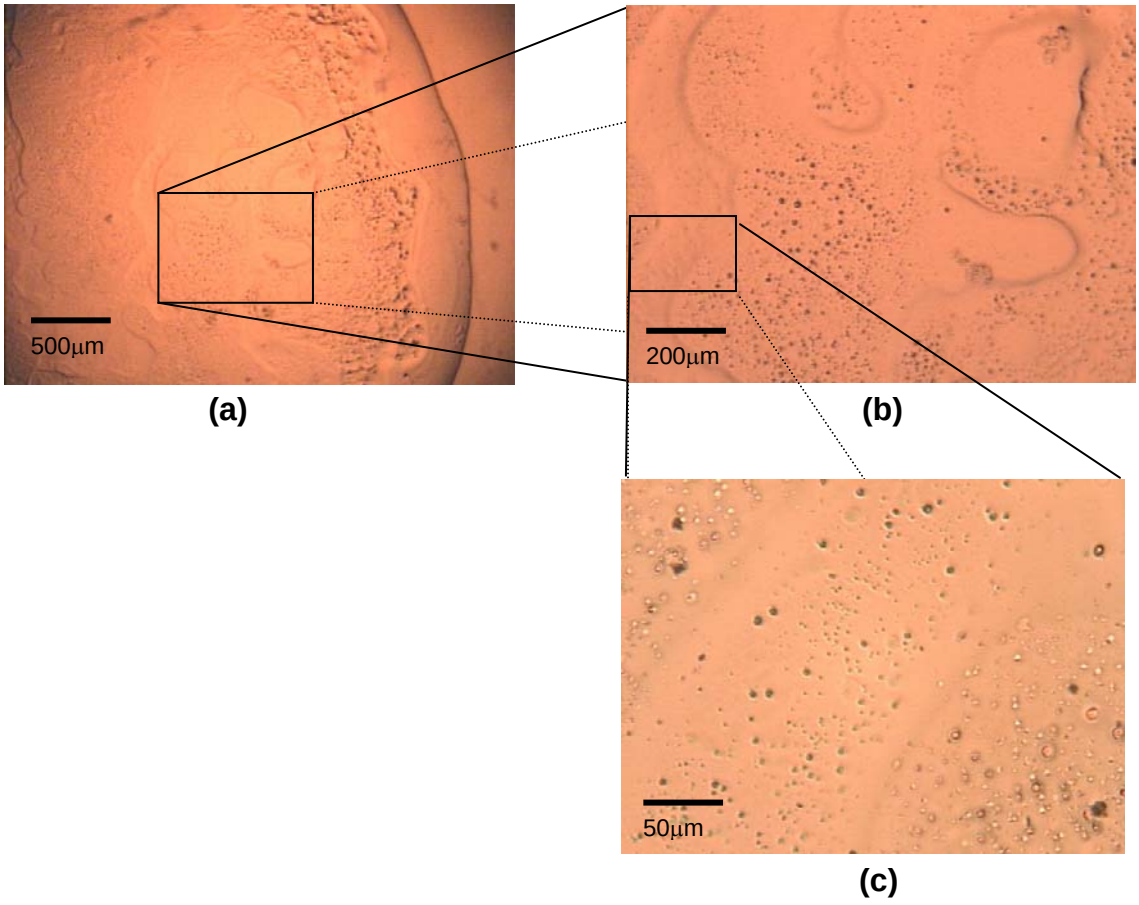

Figure IV-20. Images of a drop of the PAA-PVA mixture dried at room temperature. Well developed bicontinuous type phase separation is shown in all the images.

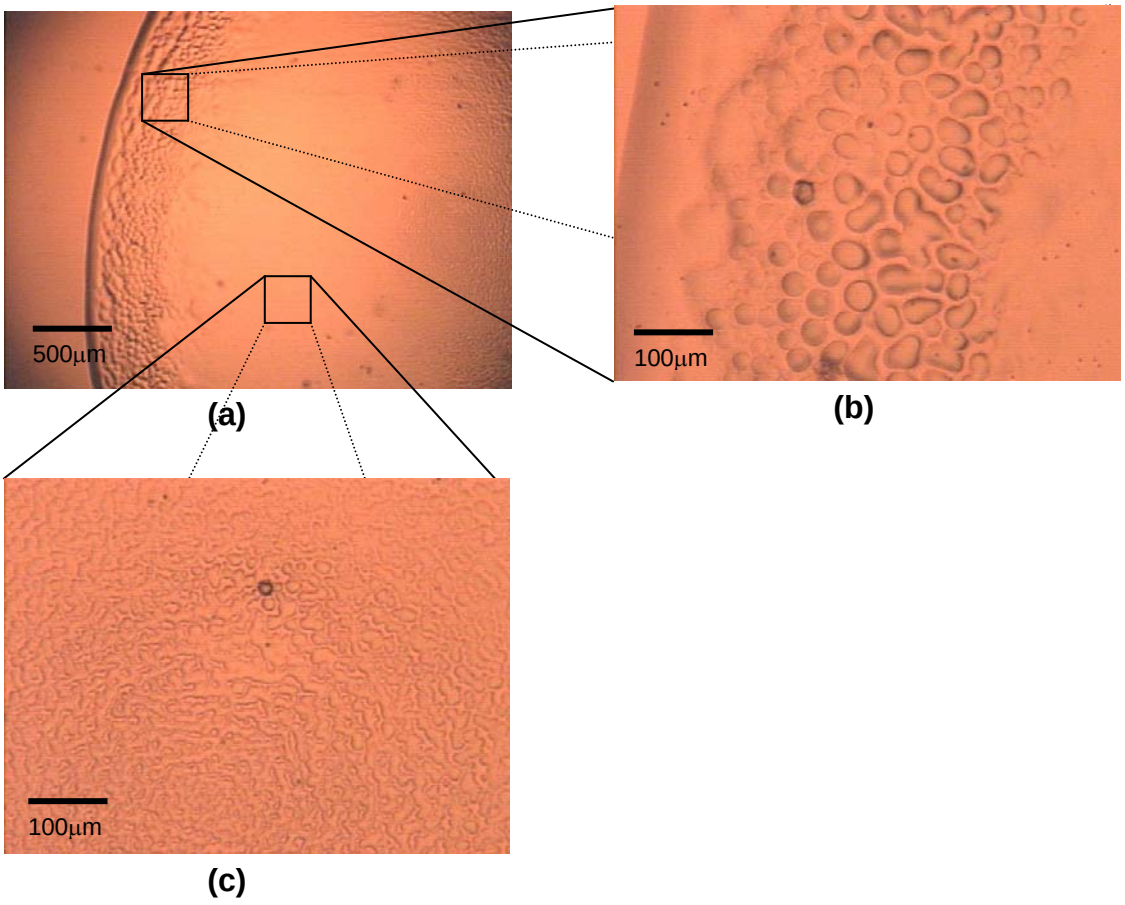

Figure IV-21. Images of a drop of the PAA-PVA mixture dried at 100 °C. Depending on the region within the drop the extent of bicontinuous type phase separation is at different period in the spinodal decomposition process.

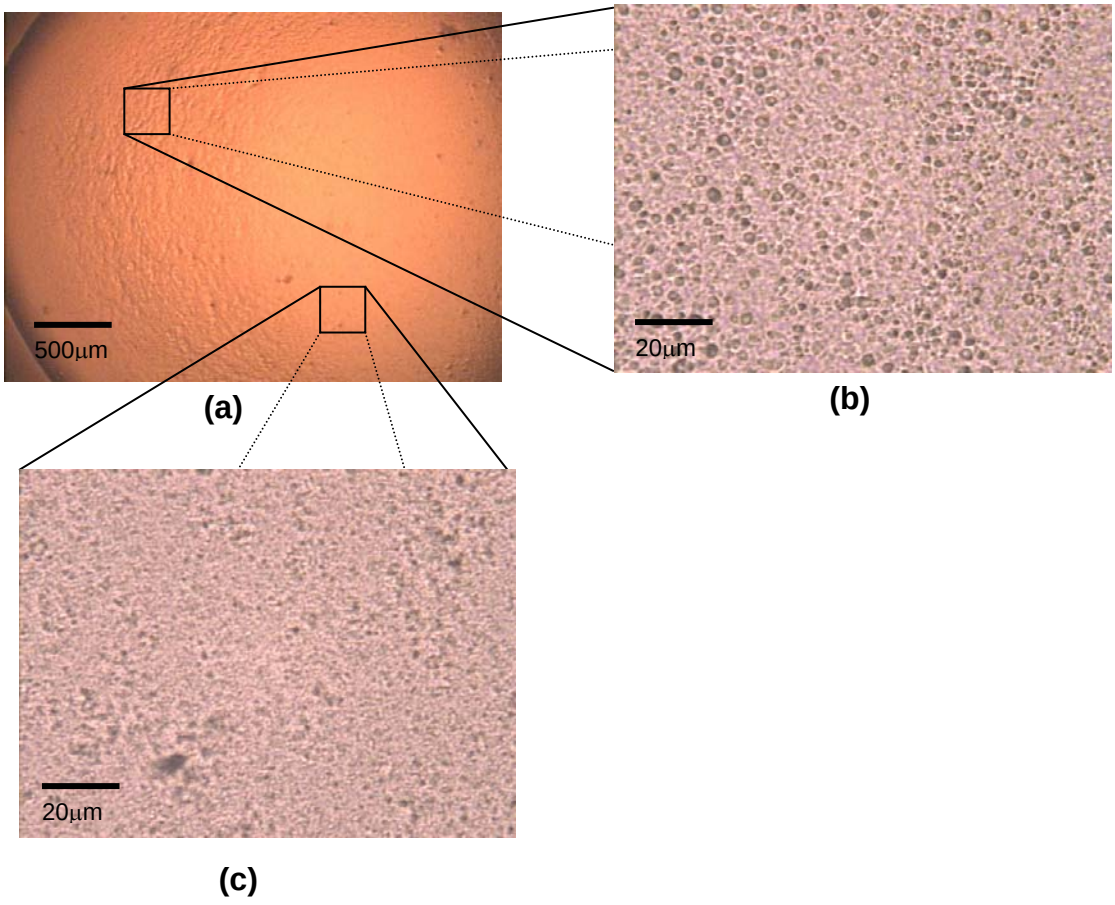

Figure IV-22. Images of a drop of the SS-PVA mixture dried at room temperature. A homogeneous film is formed from the mixture.

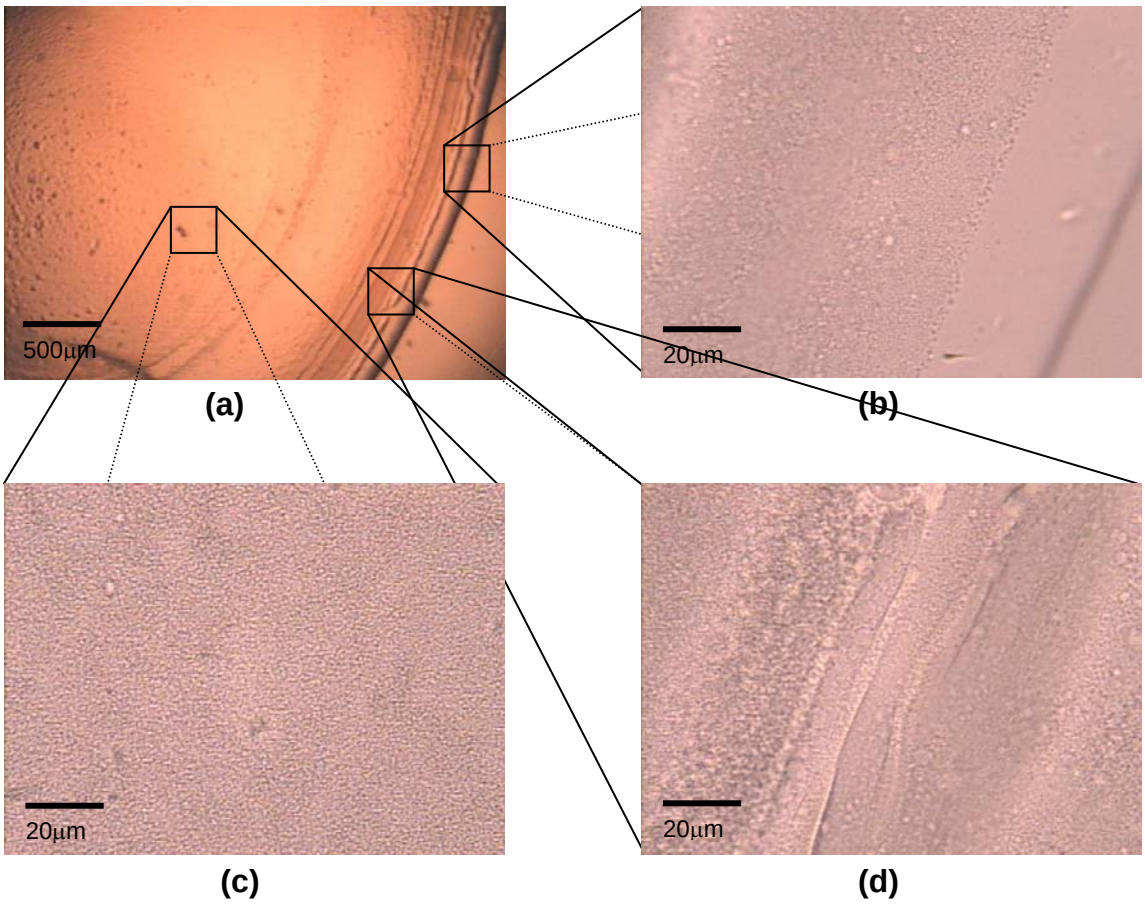

Figure IV-23. Images of a drop of the SS-PVA mixture dried at 100 °C. A homogeneous film is again formed with a distinct polymer rim on the outside of the drop.

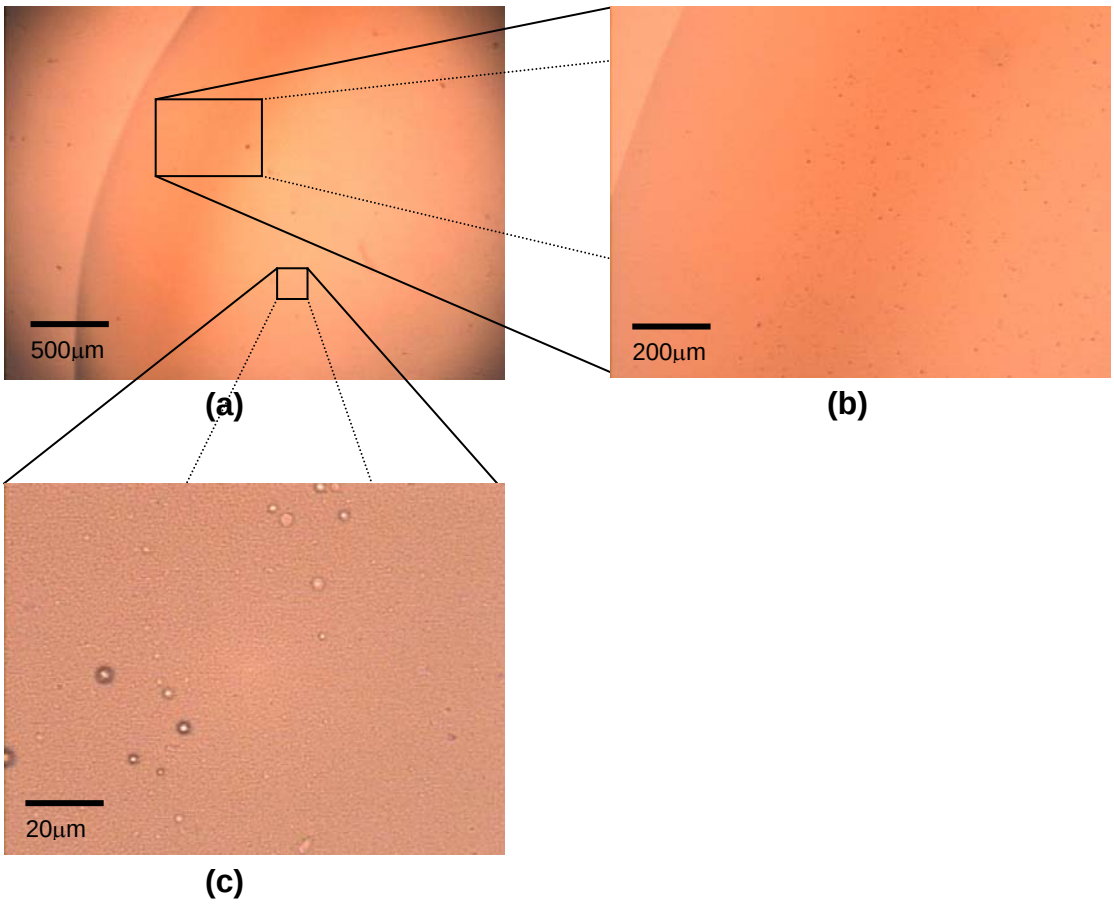

Figure IV-24. Images of a drop of the LS-PVA mixture dried at room temperature. A distinct brown ring is formed on the outside of drop from the migration of the LS during drying.

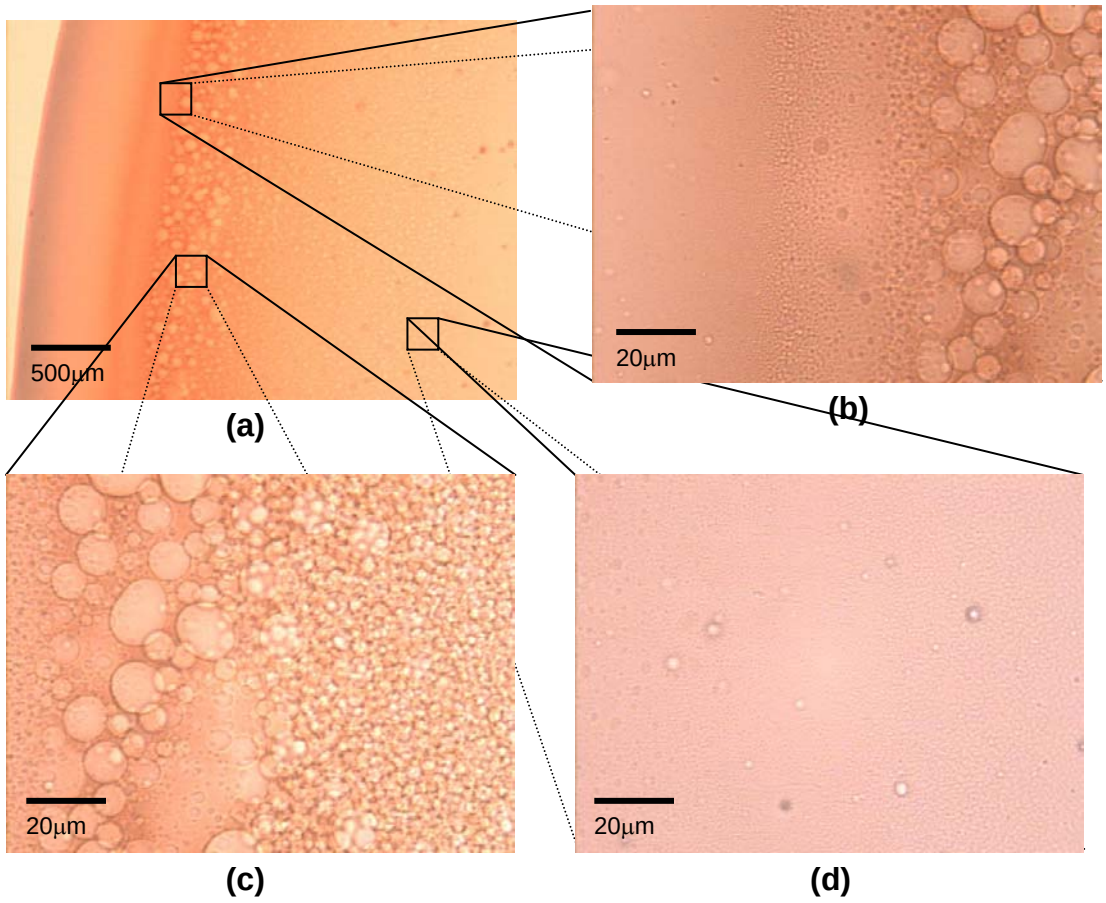

Figure IV-25. Images of a drop of the LS-PVA mixture dried at 100 °C. Brown ring is again formed on the outside of drop. Droplet type phase separation coincides with the LS rich region.

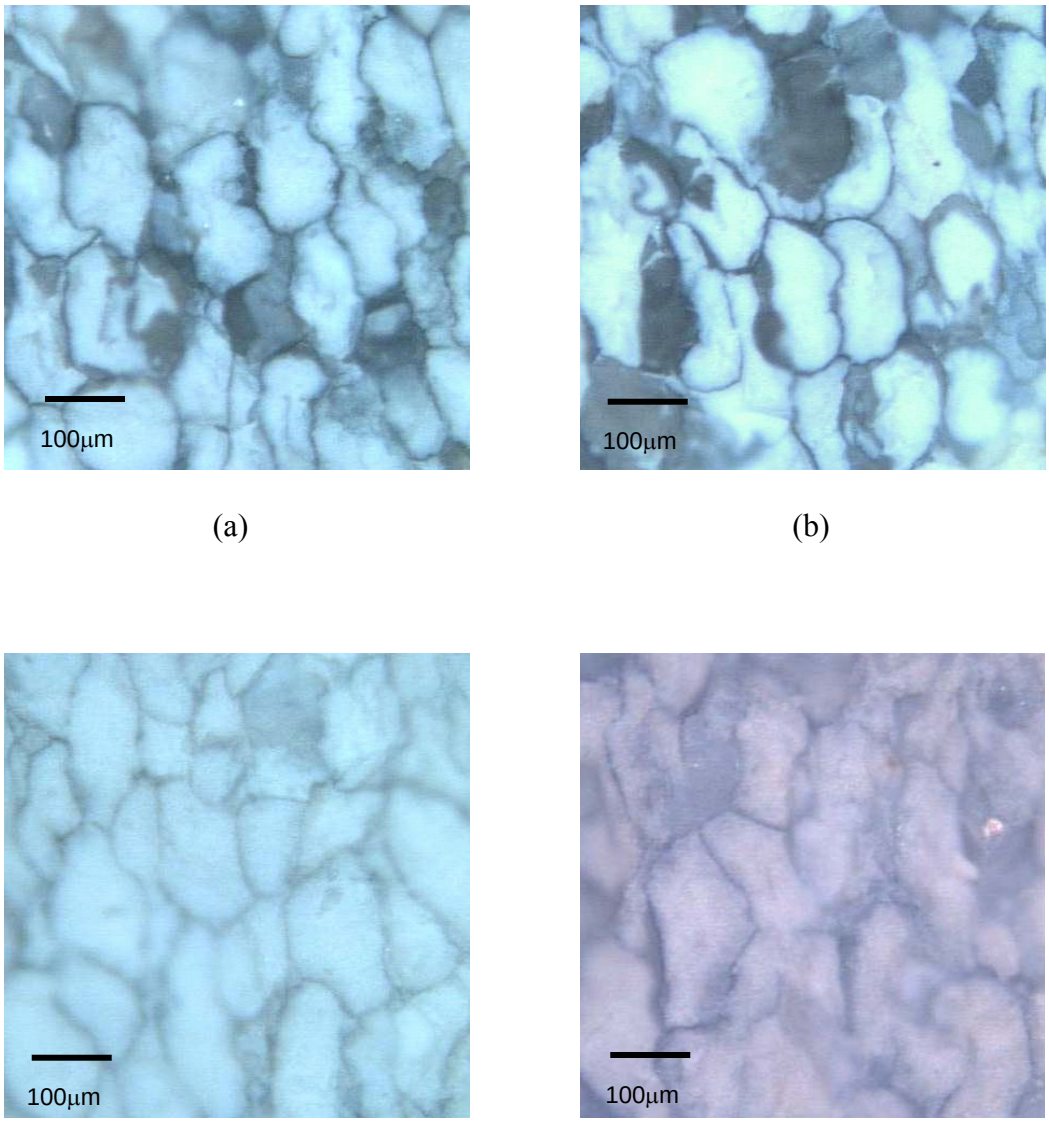

Figure IV-26. Optical microscopy images obtained from fracture surface of pellet made of granules with (a) PMAA-PVA, (b) PAA-PVA, (c) SS-PVA, and (d) LS-PVA. Granules with PAA-PVA show most severe binder migration while PVA is most homogeneously distributed in granules with SS-PVA. Due to the brown color of LS the location of PVA in granules with LS-PVA is not clearly determined.

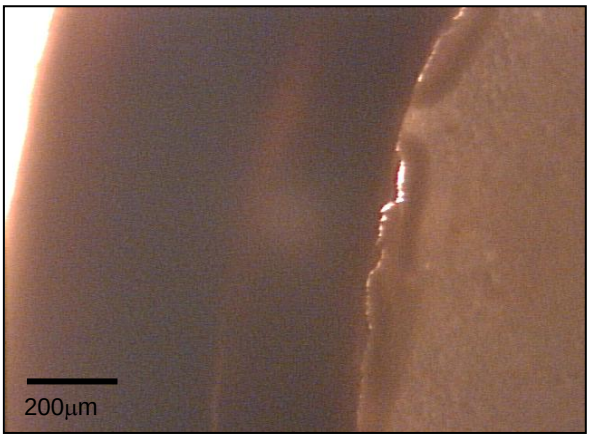

(a)

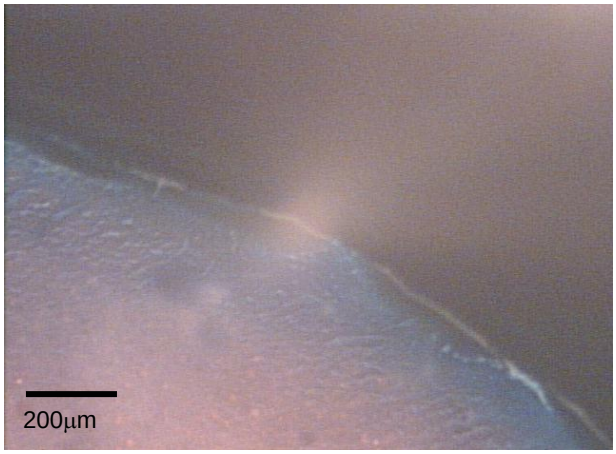

(b)

Figure IV-27. Image of dried alumina drop containing LS-PVA. Brown ring was formed on the outside of drop, which was seen in the LS-PVA solution. Stained PVA is shown within the brown ring in (b).

6. References

1. Y. Zhang, X. Tang, N. Uchida, and K. Uematsu, "Binder Surface Segregation during Spray Drying of Ceramic Slurry," *J. Mater. Res.*, **13** [7] 1881-1887 (1998).

2. Y. Zhang, X. Tang, N. Uchida, and K. Uematsu, "Mathematical Simulation for Segregation of PVA during Drying," *J. Ceram. Soc. Jpn., Int. Ed.*, **101** [2] 177-180 (1993).

3. Y. Zhang, M. Kawasaki, K. Ando, Z. Kato, N. Uchida, and K. Uematsu, "Surface Segregation of PVA during Drying of a PVA-Water-Al_2O_3 Slurry," *J. Ceram. Soc. Jpn., Int. Edition*, **100** [8] 1055-1058 (1992).

4. S. Baklouti, T. Chartier, and J. F. Baumard, "Binder Distribution in Spray-Dried Alumina Agglomerates," *J. Eur. Ceram. Soc.*, **18** [14] 2117-2121 (1998).

5. M. Liquori, G. Barone, V. Crescenzi, F. Quadrifogliop, and V. Vitagliano, "Hydrophobic Interactions in Polyelectrolyte Solutions," *J. Macromol. Chem*, **1** [2] 291-305 (1966).

6. I. Borukhov, D. Andelman, R. Borrega, M. Cloitre, L. Leibler, and H. Orland, "Polyelectrolyte Titration: Theory and Experiment," *J. Phys. Chem. B*, **104** [47] 11027–11034 (2000).

7. M. Sakurai, T. Imai, F. Yamashita, K. Nakamura, and T. Komatsu, "Temperature Dependence of Viscosities ad Potentiometric Titration Behavior of Aqueous Poly(acrylic acid) and Poly(methacrylic acid) Solutions," *Polym. J.*, **25** [12] 1247-1255 (1993).

8. J. Cesarano III, "Polyelectrolyte Adsorption on α-Alumina and Aqueous Suspension Behavior," M.S. Thesis, University of Washington, Seattle, WA, 1986.

9. F. S. Ortega, P. Sepulveda, V. C. Pandolfelli, M. M. Yokosawa, and E. Frollini, "Colloidal Stabilization of α-Alumina in Aqueous Media Using Polyelectrolyte," *Mater. Sci, Forum*, **299-300,** 104-114 (1999).

10. Fact Monster, "Sodium Silicate" (1994) In The Columbia Electronic Encyclopedia: Columbia University Press. Accessed on: September, 2002. Available at <http://www.factmonster.com/ce6/sci/A0845796.html>

11. H. Roggendorf, W. Ground, and M. Hurbanic, "Structural Characterization of Concentrated Alkaline Silicate Solutions by ^{29}Si-NMR Spectroscopy, FT-IR Spectroscopy, Light Scattering, and Electron Microscopy – Molecules, Colloids, and Dissociation Artefacts," *Glass Sci. Technol.*, **69** [7] 216-231 (1996).

12. L. S. Dent Glasser, "Silicate Species in Solution. Part 1. Experimental Observations," *J. Chem. Soc., Dalton Trans.*, [1] 393-398 (1980).

13. A. Marinangeli, M. A. Morelli, R. Simoni, and A. Bertoluzza, "A Raman and Infrared Study of Aqueous Solutions of Sodium Silicates as a Function of pH," *Can. J. Spectrosc.*, **23** [6] 173-177 (1978).

14. R. Iler, *The Chemistry of Silica*; John Wiley & Sons, New York, 1979.

15. R. V. Nauman and P. Debye, "Light Scattering Investigations of Carefully Filtered Sodium Silicate Solutions," *J. Phys. Chem.*, **55** [1] 1-9 (1951).

16. J. W. Phair, J. S. J. Van Deventer, and J. D. Smith, "Interaction of Sodium Silicate with Zirconia and Its Consequences for Polysialation," *Colloids Surf., A*, **182** [1-3] 143-159 (2001).

17. J. C. Le Bell, "The Influence of Lignosulphonate on the Colloidal Stability of Particulate Dispersions"; Ph.D. Thesis. Abo Akademi University, Abo, Finland, 1983.

18. A. Rezanowich and D. A. I. Goring, "Polyelectrolyte Expansion of a Lignin Sulfonate Microgel," *J. Colloid Sci.*, **15** [5] 452-471 (1960).

19. J. L. Bell, B. Bergroth, P Stenius, and B. Stenlund, "The Adsorption of Sodium Lignosulphonates on Kaolin," *Papper och Ta*, **56** [5] 463-466 469-471 (1974).

20. C. Browning, "Lignosulfonate Challenge," *Appl. Polym. Symp.*, **28**, 109-124 (1975).

21. S. L. Bassner and E. H. Klingenberg, "Using Poly(Vinyl Alcohol) as a Binder," *Am. Ceram. Soc, Bull.*, **77** [6] 71-75 (1998).

22. C. A. Finch, "Some Properties of Polyvinyl Alcohol and Their Possible Applications," pp. 287-306 in *Chemistry and Technology of Water Soluble Polymers*. Edited by C. A. Finch. Plenum Press, New York, NY, 1983.

23. K. Lewandowska, D. U. Staszewska, and M. Bohdanecky, "The Huggins Viscosity Coefficient of Aqueous Solution of Poly(vinyl alcohol)," *Eur. Polym. J.*, **37** [1] 25-32 (2001).

24. C. M. Ancorvati, "The Effect of Surface Chemistry on Dispersion and Binder Adsorption Aqueous Alumina Suspensions"; M.S. Thesis. Alfred University, Alfred, NY, 1993.

25. J. Zigman, "The Effect of Molecular Weight and Percent Hydrolysis on the Binding Properties of PVA"; M.S. Thesis. Alfred University, Alfred, NY, 1998.

26. G. J. Fleer, M. A. Cohen Stuart, J. M. H. M. Scheutjens, T. Cosgrove, and B. Vincent, *Polymers at Interfaces*; pp. 15-17. Chapman & Hall, London, UK, 1998.

27. P. J. Flory, *Principles of Polymer Chemistry*; pp. 495-540. Cornell University Press, Ithaca, NY, 1953.

28. H-G Elias, *An Introduction to Polymer Science*; pp. 224-227. VCH, Weinheim, Germany, 1997.

29. D. Patterson and A. Robard, "Thermodynamics of Polymer Compatibility," *Macromolecules*, **11** [4] 690-695 (1978).

30. D. Patterson, "Polymer Compatibility with and without a Solvent," *Polym. Eng. Sci.*, **22** [2] 64-73 (1982).

31. P. Molyneux, *Water-Soluble Synthetic Polymers: Properties and Behavior Volume II*; pp. 166-167. CRC Press, Boca Raton, FL, 1984.

32. A.Gustafsson, H. Wennerstrom, and F. Tjerneld, "The Nature of Phase Separation in Aqueous Two-Polymer Systems," *Polymer*, **27** [11] 1768-1770 (1986).

33. L. Zeman and D. Patterson, "Effect of the Solvent on Polymer Incompatibility in Solution," *Macromolecules*, **5** [4] 513-516 (1972).

34. C. C. Hsu and J. M. Prausnitz, "Thermodynamics of Polymer Compatibility in Ternary Systems," *Macromolecules*, **7** [3] 320-324 (1974).

35. K. Bergfeldt, L. Piculell, and P. Linse, "Segregation and Association in Mixed Polymer Solutions from Flory-Huggins Model Calculations," *J. Phys. Chem.*, **100** [9] 3680-3687 (1996).

36. J. Brandup, E.H. Immergut, and E. Grulke, *Polymer Handbook*; pp. 247-264, 675-714. Wiley, New York, 1998.

37. L. H. Sperling, *Introduction to Physical Polymer Science*; p. 71. John Wiley & Sons Inc., New York, 1992.

38. R. Scott, "The Thermodynamics of High Polymer Solutions. V. Phase Equilibria in the Ternary System: Polymer 1-Polymer 2-Solvent," *J. Phys. Chem.*, **17** [3] 279-284 (1949).

39. H. Tompa, *Polymer Solutions*; Ch. 7. Butterworths Scientific Publications, London, UK, 1956.

40. K. Kamide, *Thermodynamics of Polymer Solutions: Phase Equilibria and Critical Phenomena*; pp. 414-441. Elservier Science Publications, Amsterdam, Netherlands, 1990.

41. G. J. Fleer, M. A. Cohen, J. M. H. M. Scheutjens, T. Cosgrove, and B. Vincent, *Polymer at Interfaces*; pp. 35. Chapman and Hall, London, UK, 1998.

42. T. Nakashima, H. Mizutani, Y. Zhang, N. Uchida, and K. Uematsu, "Competitive Adsorption of PVA and PAA on Alumina Surface," *Key Eng. Mater.*, **159-160,** 151-156 (1997).

43. R. D. Deegan, O. Bakajin, T. F. Dupont, G. Huber, S. R. Nagel, and T. A. Witten, "Capillary Flow as the Cause of Ring Stains from Dried Liquid Drops," *Nature*, **389** [23] 827-829 (1997).

44. R. D. Deegan, O. Bakajin, T. F. Dupont, G. Huber, S. R. Nagel, and T. A. Witten, "Contact Line Deposits in an Evaporating Drop," *Phys. Rev. E: Stat. Nonlinear, Soft Matter Phys.*, **62** [1] 756-765 (2000).

45. S. J. Lukasiewicz, "Spray-Drying Ceramic Powders," *J. Am. Ceram. Soc.*, **72** [4] 617-624 (1989).

46. J. E. Comeforo, "Migration Characteristics of Organic Binders," *Ceram. Age*, **45** [4] 132-135 (1945).

47. M. M. Zwick, "Poly(vinyl Alcohol)-Iodine Complexes," *J. Appl. Polym. Sci.*, **9,** 2393-2424 (1965).

48. H. Noguchi, H. Jyodai, and S. Matsuzawa, "Formation of Poly(Vinyl Alcohol)-Iodine Complexes in Solution," *J. Polym. Sci., Part B: Polym. Phys.*, **35** [11] 1701-1709 (1997).

49. L. G. Tebelev, G. F. Mikul'skii, Ye. P. Korchagina, and S. A. Glikman, "Spectrophotometric Analysis of the Reaction of Iodine with Solutions of Polyvinyl Alcohol," *Vysokomol. Soedin.*, **7** [1] 123-129 (1965).

50. W. Gallay, "The Sorption of Iodine by Polyvinyl Alcohol," *Can. J. Res., Sect. B*, **14**, 105-113 (1936).

51. K. Imai and M. Matsumoto, "The Effect of Stereoregularity on the Polyvinyl Alcohol-Iodine Reaction," *J. Polym. Sci.*, **55,** 335-342 (1961).

52. A. J. Mote-Bovi, J. J. Sciarra, and V. De Paul Lynch, "Study of the Polyvinyl Alcohol-Borate-Iodine Complex III. Detection of Borates in Urine," *J. Pharm. Sci.*, **53** [10] 1278-1280 (1964).

53. T. Yoshinaga, T. Shirakata, H. Dohtsu, H. Hiratsuka, M. Hasegawa, M. Kobayashi, and T. Hoshi, "Polyvinyl Alcohol as a Useful Indicator on Iodometry: Volumetric and Spectrophotometric Studies on Iodine-PVA and Iodine-Starch Complexes," *Anal. Sci.*, **17** [2] 333-337 (2001).

54. C. D. West, "Structure-Optical Studies: II. Aqueous Dispersion of Polyvinyl Borate-Iodine and Its Heat of Formation," *J. Chem. Phys.*, **17** [12] 219 (1949).

55. Z. Kato, U. Nozomu, and K. Uematsu, and Y. Zhang, "Quantitative Analysis of a Binder Segregation in Granules," pp. 501-506 in Ceramic Transactions, Vol. 112. Edited by S. Hirano, G. L. Messing, and N. Claussen, The American Ceramic Society, Westerville, OH, 2000.

56. S. Chibowski, M. Paszkiewicz, and M Krupa, "Investigation of the Influence of the Polyvinyl Alcohol Adsorption on the Electrical Properties of Al_2O_3-Solution Interface, Thickness of the Adsorption Layers of PVA," *Powder Technol.*, **107** [3] 251-255 (2000).

57. P. J. Flory, "Thermodynamics of High Polymer Solutions," *J. Chem. Phys.*, **10** [1] 51-62 (1942).

58. E. Pines and W. Prins, **"**Structure-Property Relations of Thermoreversible Macromolecular Hydrogels," *Macromolecules*, **6** [6] 888-895 (1973).

59. M. Komatsu, T. Inoue, and K. Miyasaka, "Light Scattering Studies on the Sol-Gel Transition in Aqueous Solutions of Poly(vinyl alcohol)," *J. Polym. Sci., Polym. Phys. Ed.*, **24,** 303-311 (1986).

60. H. Takeshita, T. Kanaya, and K. Nishida, and K. Kanji, "Small-Angle Neutron Scattering Studies on Network Structure of Transparent and Opaque PVA Gels," *Phys. B (Amsterdam, Neth.)*, **311** [1-2] 78-83 (2002).

61. S. Krause, "Polymer-Polymer Compatibility," pp. 15-114 in *Polymer Blends*. Edited by D. R. Paul and S. Newman. Academic Press, New York, 1978.

62. L. Picullel and B. Lindman, "Association and Segregation in Aqueous Polymer/Polymer, Polymer/Surfactant, and Surfactant/Surfactant Mixtures: Similarities and Differences," *Adv. Colloid Interface Sci.*, **41,** 149-178 (1992).

63. I. S. Okhrimenko and E. B. D'yakonova, "Reaction of Polymethacrylic Acid with Polyvinyl Alcohol in Concentrated Aqueous Solutions," *Vysokomol. Soedin.*, **6** [10] 1891-1894 (1964).

64. F. A. Rodrigues and I. Joekes, "Macro-Defect Free Cements: A New Approach," *Cem. Concr. Res.*, **28** [6] 877-885 (1998).

65. P. J. Flory, "Introduction," *Discuss. Faraday Soc.*, **57,** 7-17 (1974).

66. N. G. Bel'nikevich, T. V. Budova, N. P. Ivanova, Ye. F. Panarin, Yu. N. Panov, and S. Ya. Frenkel, "Complex Formation in Aqueous Solutions of Mixtures of Polyacrylic Acid and Polyvinylalcool and its Copolymers," *Polym. Sci. U.S.S.R.*, **31** [8] 1859-1866 (1989).

67. H. Takeshita, T. Kanaya, and K. Nishida, and K. Kanji, "Small-Angle Neutron Scattering Studies on Network Structure of Transparent and Opaque PVA Gels," *Phys. B (Amsterdam, Neth.)*, **311** [1-2] 78-83 (2002)

68. H. Tanaka and T. Nishi, "New Types of Phase Separation Behavior during the Crystallization Process in Polymer Blends with Phase Diagram," *Phys. Rev. Lett.*, **55** [10] 1102-1105 (1985).

69. I. Hopkinson and M. Myatt, "Phase Separation in Ternary Solutions Induced by Solvent Loss," *Macromolecules*, **35** [13] 5153-5160 (2002).

70. H. Tanaka, "Viscoelastic Phase Separation," *J. Phys.: Condens. Matter*, **12** [15] R207-264 (2000).

71. H. Tanaka, "Hydrodynamic Interface Quench Effects on Spinodal Decomposition for Symmetric Binary Fluid Mixtures," *Phys. Rev. E: Stat. Nonlinear, Soft Matter Phys.*, **51** [2] 1313-1329 (1995).

72. E. D. Siggia, "Late Stage of Spinodal Decomposition in Binary Mixtures," *Phys. Rev. A: At., Mol., Opt. Phys.*, **20** [2] 595-605 (1979).

73. D. Lee, "FTIR Spectral Study of Polyacrylate Adsorption on Alumina," M.S. Thesis. Alfred University, Alfred, NY, 1994.

74. T. V. Budova, N. G. Byel'nikevich, N. P. Ivanova, V. A. Kuznetsova, Ye. F. Panarin, Yu. N. Panov, A. Ya. Sorokin, and S. Ya. Frenkel, "Dependence of the Process of the Formation of Interpolymeric Complexes in Aqueous Solutions of Blends of Polyacrylic Acid and Copolymers of Vinyl Alcohol and Vinyl Acetate on the Molecular Parameters of the Components and Their Total Concentration," *Polym. Sci.*, **33** [8] 1550-1555 (1991).

75. B. R. Sundlof, "Aqueous Processing of Alumina and Phase Behavior of Polymeric Additives," Ph.D. Thesis. Alfred University, Alfred, NY, 1999.

V. SUMMARY AND CONCLUSIONS

Polyelectrolyte Adsorption and Rheology

The adsorption study of PAA on clay particles confirms that PAA adsorption is dependent on pH, but independent on molecular weight. The surface charge of clay and the polyelectrolyte dissociation is dependent on pH and in turn directly related to the adsorption amount.

It is shown that the amount of PAA adsorbed on clay particles is not influenced by polymer molecular weight. However, the minimum viscosity of suspensions shows a dependence on the molecular weight of PAA. The degree of dissociation of PAA changes with pH, but is not dependent on the molecular weight. This suggests that adsorption amount of PAA on clay particles is determined by electrostatic. Also, both electrostatic and steric stabilization play a role in stabilizing suspensions with polyelectrolytes.

The kinetics of PAA adsorption on clay particles is influenced by the initial concentration of polymer in suspension. The adsorption plateau is quickly reached in low polymer concentration system. This suggests that the number of adsorption sites on clay particles is limited and displacement of initially adsorbed PAA occurs with time in high polymer concentration system.

The discrepancy between the concentration of adsorbed PAA and the predicted concentration of adsorbed PAA is explained by the presence of organic matter, HA and FA, in clay. The HA and FA, which are dissolved in water or adsorbed on clay particles depending on pH, interfere the PAA adsorption. The HA and FA are polyelectrolytes and complete with PAA for the clay surface. Also, dissolved HA and FA are indistinguishable from PAA during titration. Hence, the concentration in the supernatant is higher in systems with dissolved HA and FA which corresponds to a lower concentration of polymer on the powder surface.

When shear yield stress is compared to apparent viscosity, these two results show a similarity. This suggests that both results can be used to analyze the rheological property of suspensions.

Effect of Polymer Compatibility on PVA binder Migration

Phase calculation by Flory-Huggins theory qualitatively predicts phase behaviors of polymer systems in solution. It is shown that homogeneous mixing at low polymer concentration turns into phase separation as expected in Flory-Huggins calculation. However, the final phase after drying is significantly influenced by the dynamics during the drying process.

The interaction between polymeric additives during spray drying process governs the degree of PVA migration in spray dried granules. The molecular weight and functional groups of polymer determine the polymeric interaction and in turn the degree of PVA migration. Also, dynamics during drying process show strong influence on the final phase of polymers, which is directly related to PVA migration behavior.

Both PMAA-PVA and PAA-PVA systems show bicontinuous type phase separation, but the phase separation in PMAA-PVA system starts at low polymer concentration and the phase grows with time. This leads to less PVA migration in PMAA-PVA system compared to PAA-PVA system.

The homogeneous mixture of SS and PVA results in a homogenous polymer film after drying due to the hydrogen bonding. This results in the most homogeneously distributed PVA in granules with SS-PVA.

LS migrates competitively with PVA during drying process. This may reduce the migration of PVA in granules.

The phase calculation and polymer solution study can provide basic ideas for predicting polymer behaviors with ceramic particles. It is shown that the polymer behaviors observed in both studies have direct relationship with the polymer behaviors in systems where a ceramic phase is present.